UNIVERSITY
of
GLASGOW

Higgs boson masses in a Non-Minimal Supersymmetric Model

by

Alessandro Tiesi

Thesis
submitted to the
University of Glasgow
for the degree of
Doctor of Philosophy

Particle Physics Theory Group
Department of Physics and Astronomy
University of Glasgow
Glasgow, G12 8QQ.

Submitted
September 2002

"...per amore

solo per amore..."

To Petra

Acknowledgements

I would like to express my personal gratitude to my supervisors Colin Froggatt and Andrew Davies for the help and the stimulating discussions during my time as a PhD student in the Particle Physics Theory Group at the University of Glasgow. Equally my acknowledgements are expressed to the members of the group who provided extremely useful lectures, tutorial and discussions: Gordon Moorhouse, Christine Davies, David Sutherland, Ron Crawford, John McDonald, Joachim Hein and Manfred Oevers. Thanks to all the remaining members of the group for the friendly relationship through all the time spent here. My thanks are devoted to my fellow students: Lawrence, Mark, Gordon, Nektarios, Alessandro and Peter Crompton, Alan, Peter Allan, Greig, Jack and Josef. I am indebted to Paul Millar and Graeme Stuart for their useful support.

I would like to express my gratitude To Prof. J. Chapman and Prof J. Hough, for their final support. Thanks to all the friends and the people I met in the Department of Physics and Astronomy. Particular mention to my beloved friends Giulio Pellegrini and Gian Pietro Cagnoli.

My gratitude is devoted to my family, to my parents whose patience to support such a difficult son arrived to the *non plus ultra*, to my beloved brothers, their families and to my friends.

I would like to express my gratitude to the friends who shared with me private life and provided to give me support during the most difficult times: Martin and Fred, Jose Ramon and Nicola, Beatriz, Anna, Maurizio, Alejandro, Tine, Camilla, Jota, Ivor and Daniel.

Dulcis in fundo, my greatest acknowledgement is to my beloved Petra Elisabeth Maria Bechtold. This thesis is dedicated to her.

Declaration

Apart from chapter 1 which is an introductory part, this thesis and the results reported are the author's own work.

Abstract

A study of the neutral Higgs spectrum in a general Z_3-breaking *Next to Minimal Supersymmetric Standard Model (NMSSM)* is reported in several significant contexts. Particular attention has been devoted to the upper bound on lightest Higgs boson. In the CP-conserving case we show that the extra terms involved in the general Z_3-breaking superpotential do not affect the upper bound which remains unchanged: it is $\sim 136\ GeV$ when $\tan\beta = 2.7$.

The *Spontaneous CP Violation* scenario in the Z_3-breaking $NMSSM$ can occur at tree-level. When the phases of the fields are small the spectrum shows the lightest Higgs particle to be an almost singlet CP-odd. The second lightest particle, a doublet almost-CP-even state, still manifests the upper bound of the CP-conserving case. When the CP-violating phases are large the lightest particle is a doublet with no definite CP parity and its mass shows the usual upper bound at $\sim 136\ GeV$.

The large number of parameters involved in the effective potential can be significantly reduced in the *Infrared Quasi Fixed Point (IRQFP)* resulting after solving the *Renormalization Group (RG)* equations assuming universality for the soft $SUSY$ breaking masses. In the Z_3-breaking $NMSSM$, unlike the Z_3-conserving $NMSSM$, it is possible to find a Higgs spectrum which is still compatible with both experiment and universality at the unification scale. Because in the $IRQFP$ regime $\tan\beta \sim 1.8$ and the stop mixing parameter is reduced then the upper bound on the lightest Higgs boson turns out to be $\sim 121\ GeV$. This result is compatible with experimental data coming from $LEPII$ and might be one of the next predictions to be tested at hadron collider experiments.

Contents

List of Figures

List of Tables

Introduction

The *Standard Model (SM)* is the most successful known theory of high energy particle physics. In the last two decades the experimental results coming from the high energy physics laboratories have been mostly in agreement with the predictions of this theory. Despite this remarkable success in particle physics, the SM has indeed some limitations. As an example from the phenomenological point of view, it is not able to generate the CP violation necessary to produce the actual matter-antimatter asymmetry of the universe (*baryogenesis* problem). From a more theoretical point of view, in the SM troubles arise when quantum corrections to the Higgs mass are calculated. Such contributions lead to a divergent Higgs mass influencing all the SM masses, because all of these acquire mass due to the coupling with the Higgs particle; this is called the *hierarchy problem*. It is needed to extend the SM to a new wider framework capable of describing physics eventually up to very high energies.

A possible extension of the SM is represented by the *Supersymmetric theories (SUSY)*. In any of such theories there exists a transformation which transforms bosonic fields into fermionic fields and viceversa. For example if we take a scalar field A and a spinor one χ_α, then the transformation between the two is

$$\delta A = \bar{\epsilon}^{\alpha} \chi_{\alpha}$$

where $\bar{\epsilon}^{\alpha}$ must have dimension of $(\text{mass})^{-1/2}$ and be anticommuting. If we assume the transformation of χ_{α} to be linear, we get

$$\delta \chi_{\alpha} = (\gamma^{a})^{\beta} \partial_{\alpha} A \epsilon_{\beta} + \cdots$$

The term $\partial_{\alpha} A$, on the right hand side of the equation, is a space-time translation acting on A, so that we find that Poincaré transformations are necessary to close supersymmetric transformations.

In $SUSY$ theories there can be enough CP-violation to account for the observed baryon asymmetry because of complex phases of the Higgs fields violating this discrete symmetry. $SUSY$ theories can solve the technical hierarchy problem due to a very nice ultraviolet behaviour, namely that the divergences caused by high momenta in the particle loops cancel because the contributions of fermions and bosons are equal and opposite in sign; this in turn prevents the mass of any fundamental boson in the theory from becoming super-heavy due to the higher order corrections (fermions do not suffer this problem as the divergences are at most logarithmic). This in itself is a very strong argument in favour of supersymmetry as the Higgs boson, which gives mass to the fermions and vector bosons of the SM, is required to have a mass lower than $\sim 1TeV$. In all $SUSY$ models there must be at least two Higgs doublets in order to give mass through the Yukawa couplings to the *up*-type and *down*-type quark fields of each of the three quark doublets. Consequently in $SUSY$ models we have an increase in the number of Higgs bosons, i.e. at least two extra neutral Higgs bosons and a charged one, whereas in the SM we have only one Higgs doublet, and just one neutral Higgs boson. This is obviously the minimum number of Higgs doublets. One can in principle think of adding more, although several problems regarding the predictivity of such models arise.

In SUSY theories we have a very remarkable behaviour of the coupling constants, which have a common value at an energy scale of about 10^{16} GeV, the so-called unification scale. This suggests that above that scale we are dealing with a unified theory of the strong and electroweak interactions.

As supersymmetry naturally encompasses Poincaré transformations, it raises the possibility of a quantum theory of gravity. In fact we find the appearance of the graviton and its super-partner gravitino once we allow supersymmetry transformations to be local, that is to say dependent on the space-time points. However, up to the present no definitive supergravity or superstring theory exists. The reader is referred to [1]-[5] for general discussions of the theoretical and phenomenological motivations for supersymmetry.

In the present work, our attention will focus explicitly on the neutral Higgs boson spectrum, in particular on the lightest boson, as $SUSY$ provides an upper bound on its mass. After a preliminary discussion of supersymmetry in chapter 1, in chapter 2 we examine the upper bound on the lightest Higgs boson in the general Z_3-breaking $NMSSM$. Chapter 3 looks at the mass spectrum in the presence of spontaneous CP-violation. In chapter 4 renormalisation group equations are used to reduce the number of undetermined Yukawa couplings and soft $SUSY$-breaking parameters, and the implications for the Higgs spectrum are followed up in the next chapter. Chapter 6 summarizes our conclusions.

Chapter 1

Supersymmetry

1.1 MSSM

The simplest supersymmetric extension of the SM is the so called *Minimal Supersymmetric Standard Model* ($MSSM$). The most general Higgs superpotential is given by:

$$W_{MSSM} = \mu H_1 H_2 + W_{ferm} \ , \tag{1.1}$$

where

$$W_{ferm} = \bar{u}\mathbf{y_u}QH_2 - \bar{d}\mathbf{y_d}QH_1 - \bar{e}\mathbf{y_e}LH_1 \tag{1.2}$$

H_1, H_2, Q, L, $\bar{u}$, $\bar{d}$ are chiral superfields, $\mathbf{y_u}$, $\mathbf{y_d}$, $\mathbf{y_e}$ are 3×3 matrices in family space representing the dimensionless Yukawa coupling. The expression (1.2) reveals how *down*-type and *up*-type quarks aquire masses thanks to the two Higgs doublet H_1 and H_2 respectively. Since the superpotential has to be analytic in the chiral superfields, the presence of H_1^* and H_2^* is forbidden as well as the possibility for H_1 to give mass to the *up*-type quark because of gauge invariance. However there are other terms that could be added without disturbing the analyticity and the gauge invariance, but are not included because they would violate explicitly the baryon number B and the lepton number L. Indeed the superpotential manifests a new symmetry: this is called *R-parity* [7] or *matter parity* [8]. If these symmetries are preserved, then important phenomenological consequence follows: the stability of the *Lightest Supersymmetric Particle (LSP)* candidate which may solve the dark matter problem. It then follows that any sparticle should ultimately decay into a state containing at least one LSP and that sparticles can only be produced in pairs [5] [9].

In the superpotential (1.1), the term $\mu H_1 H_2$ is the well known supersymmetric μ-term, where

$$H_1 = \begin{pmatrix} H_1^0 \\ H_1^- \end{pmatrix} , \qquad H_2 = \begin{pmatrix} H_2^+ \\ H_2^0 \end{pmatrix} , \tag{1.3}$$

and we define the product

$$H_1 H_2 = H_1^i \; \varepsilon_{ij} \; H_2^j = (H_1^0 H_2^0 - H_1^- H_2^+) , \tag{1.4}$$

with ε the antisymmetric tensor

$$\varepsilon = \begin{pmatrix} 0 & 1 \\ -1 & 0 \end{pmatrix} . \tag{1.5}$$

Related to μ is the *naturalness* problem of the $MSSM$. Since μ has to satisfy phenomenology it should be of the order of the electroweak scale, but this has to be set by hand [10].

Because of the two Higgs doublets the electroweak symmetry breaking in the *MSSM* is more complicated than the one occurring in the *SM*. The classical tree-level scalar potential for the Higgs scalar fields is:

$$
\begin{aligned}
V &= (|\mu|^2 + m_{H_1}^2)(|H_1^0|^2 + |H_1^-|^2) + (|\mu|^2 + m_{H_2}^2)(|H_2^+|^2 + |H_2^0|^2) \\
&\quad + m_{12}^2(H_1^0 H_2^0 - H_1^- H_2^+) + \text{c.c.} \\
&\quad + \frac{1}{8}(g_1^2 + g_2^2)(|H_1^0|^2 + |H_1^-|^2 - |H_2^+|^2 - |H_2^0|^2)^2 \\
&\quad + \frac{1}{2} g_2^2 |H_1^- H_2^{0*} + H_1^0 H_2^{+*}|^2 \, ,
\end{aligned} \tag{1.6}
$$

where μ is the term coming from the superpotential and g_1 and g_2 are respectively the gauge coupling constants of the groups $U(1)_Y$ and $SU(2)_L$. In the potential (1.6) $m_{H_1}^2$, $m_{H_2}^2$ and m_{12}^2 are the soft *SUSY* breaking masses. One of the phenomenological aspects of supersymmetry is that it does not appear as an exact symmetry because the particles of the *SM* do not show any mass degeneracy with their superpartners[1]. Somehow the symmetry should have been broken; the soft *SUSY* breaking masses refer to this yet unclear aspect of any supersymmetric theory and they are temporarily assumed as arbitrary parameters. In Chapter 4 we will see in detail the behaviour of such parameters after studying the *Renormalisation Group (RG)* equations assuming *universality*. This analysis will exhibit the so called *radiative electroweak symmetry breaking* phenomenon, which allows us to break the electroweak symmetry in a more consistent manner than in the *SM*; the negative mass squared term in the *SM* Higgs potential has to be put by hand.

The potential (1.6) breaks the electroweak symmetry down to the *QED* gauge symmetry, when the non-symmetric minimum corresponds to the

[1] To be more precise these have not been observed yet.

Higgs fields acquiring vacuum expectation values (vevs):

$$\langle H_1^- \rangle = 0 \;, \qquad \langle H_2^+ \rangle = 0 \;, \tag{1.7}$$

for the charged fields, and

$$\langle H_1^0 \rangle = v_1 \;, \qquad \langle H_2^0 \rangle = v_2 \;, \tag{1.8}$$

for the neutral ones. These can be connected to the mass of the Z^0 boson and the electroweak gauge couplings:

$$v_1^2 + v_2^2 = \eta^2 = \frac{2\, m_Z^2}{g_1^2 + g_2^2} \approx (174\; GeV)^2 \;, \tag{1.9}$$

whereas their ratio is defined as

$$\tan\beta \equiv \frac{v_2}{v_1} \;. \tag{1.10}$$

The tree-level potential (1.6) is CP-conserving and the violation of this discrete symmetry can be triggered only when radiative corrections are involved [5] [11].

The Higgs fields consists of two complex doublets under $SU(2)$, or eight real scalar degrees of freedom. After electroweak symmetry breaking the Higgs spectrum is composed as follows:

- three Nambu-Goldstone bosons G^0 and $G^\pm$, which become the longitudinal modes of the electroweak gauge bosons Z^0 and $W^\pm$;
- one CP-odd neutral scalar A^0;
- two charged scalars $H^\pm$;
- two CP-even neutral scalars H^0 and h^0.

Expressing these eight mass eigenstate fields in terms of the original gauge-eigenstate fields, we have

$$\begin{pmatrix} G^0 \\ A^0 \end{pmatrix} = \frac{1}{\sqrt{2}} \begin{pmatrix} \sin\beta & -\cos\beta \\ \cos\beta & \sin\beta \end{pmatrix} \begin{pmatrix} Im[H_2^0] \\ Im[H_1^0] \end{pmatrix}, \tag{1.11}$$

$$\begin{pmatrix} G^+ \\ H^+ \end{pmatrix} = \begin{pmatrix} \sin\beta & -\cos\beta \\ \cos\beta & \sin\beta \end{pmatrix} \begin{pmatrix} H_2^+ \\ H_1^{-*} \end{pmatrix}, \tag{1.12}$$

where $G^- = G^{+*}$ and $H^- = H^{+*}$, and

$$\begin{pmatrix} h^0 \\ H^0 \end{pmatrix} = \begin{pmatrix} \cos\alpha & -\sin\alpha \\ \sin\alpha & \cos\alpha \end{pmatrix} \begin{pmatrix} \frac{1}{\sqrt{2}}Re[H_2^0] - v_2 \\ \frac{1}{\sqrt{2}}Re[H_1^0] - v_1 \end{pmatrix}, \tag{1.13}$$

which defines a mixing angle α. Expanding the potential around its minimum, then one can find the tree-level masses:

$$m_{A^0}^2 = \frac{2m_{12}^2}{\sin 2\beta} \tag{1.14}$$

$$m_{H^\pm}^2 = m_{A^0}^2 + m_W^2 \tag{1.15}$$

$$m_{H^0,h^0}^2 = \frac{1}{2}\left(m_{A^0}^2 + m_Z^2 \pm \sqrt{(m_{A^0}^2 + m_Z^2)^2 - 4m_Z^2 m_{A^0}^2 \cos^2 2\beta}\right). \tag{1.16}$$

It is possible from these masses to express at tree-level the mixing angle α appearing in eq.(1.13) as follows

$$\frac{\sin 2\alpha}{\sin 2\beta} = -\frac{m_{A^0}^2 + m_Z^2}{m_{H^0}^2 - m_{h^0}^2}; \qquad \frac{\cos 2\alpha}{\cos 2\beta} = -\frac{m_{A^0}^2 - m_Z^2}{m_{H^0}^2 - m_{h^0}^2}. \tag{1.17}$$

From the expressions (1.14)-(1.16) it is easy to see that the masses of A^0, $H^\pm$ and H^0 can be arbitrarily large, since they become directly proportional to the soft parameter m_{12}^2 [5]. In contrast, the mass m_{h^0} is bounded from above; from eq. (1.16) it is possible to show that [12]

$$m_{h^0}^2 < m_Z^2 \cos^2 2\beta\ . \tag{1.18}$$

This upper bound for m_{h^0} is ruled out by the experimental data because it is kinematically accessible to LEP2. However, the tree level mass formulae for m_{h^0} and all the mass eigenstates (1.14)-(1.16) are subject to significant quantum corrections. The radiative corrections to the tree-level lightest Higgs mass will be the main topic of the next chapter.

1.2 NMSSM

The simplest possible extension of the particle content of the $MSSM$ results after adding a new gauge singlet chiral supermultiplet. This is called the *Next to Minimal Supersymmetric Standard Model (NMSSM).* The strongest motivation for this extension is provided by the solution of the μ-problem in the $MSSM$. The solution to the μ-problem comes after imposing the invariance of the superpotential under the so called Z_3-symmetry, which means that each field is multiplied by a phase $e^{i\frac{2\pi}{3}}$, precluding the possibility of having terms like[2] $\mu H_1 H_2$. The superpotential then turns out to be a trilinear function in the fields H_1, H_2 and the singlet N:

$$W_{NMSSM} = \lambda N H_1 H_2 - \frac{k}{3} N^3 + W_{ferm} \,. \tag{1.19}$$

The factor λN smartly provides a substitute for μ [13] [14]. The cubic term in N is necessary to avoid a $U(1)$ symmetry, which would force the existence of a light pseudo-Goldstone mode once the symmetry is broken. The resulting $NMSSM$ scalar potential coming from eq. (1.19),

[2] To be precise, the Z_3-invariance allows the superpotential to have *only* trilinear terms, but we stress the exclusion of the bilinear μ-term because historically the $NMSSM$ has been introduced to solve this embarassment for the $MSSM$.

including the gauge and the soft part is:

$$\begin{aligned} V &= \frac{1}{2}\lambda_1(H_1^\dagger H_1)^2 + \frac{1}{2}\lambda_2(H_2^\dagger H_2)^2 \\ &+(\lambda_3+\lambda_4)(H_1^\dagger H_1)(H_2^\dagger H_2) - \lambda_4\left|H_1^\dagger H_2\right|^2 \\ &+(\lambda_5 H_1^\dagger H_1 + \lambda_6 H_2^\dagger H_2)N^\star N \\ &+(\lambda_7 H_1 H_2 N^{\star 2} + h.c.) + \lambda_8(N^\star N)^2 \\ &+m_{H_1}^2 H_1^\dagger H_1 + m_{H_2}^2 H_2^\dagger H_2 + m_N^2 N^\star N \\ &-(m_4 H_1 H_2 N + h.c.) - \frac{1}{3}(m_5 N^3 + h.c.)\ . \end{aligned} \tag{1.20}$$

where m_i are the soft $SUSY$ breaking terms of the model. It should be noted that in this tree-level potential there are three more soft terms than in the $MSSM$; one is the singlet squared scalar mass m_N^2, then there are m_4 and m_5. The latter are also named trilinear soft masses because they appear in the cubic terms of the Higgs fields. On the other hand, because of the imposed Z_3-symmetry, in the potential there is not anymore a bilinear soft mass m_{12}^2. The potential (1.20) could be explicitly CP-violating if the couplings and the soft masses are assumed to be complex. Here we assume all of these to be real. Furthermore, the potential cannot violate CP spontaneously [11]; we can have spontaneous CP violation only through radiative corrections. At the scale M_S, where supersymmetry is broken, the quartic couplings λ_i must satisfy the boundary condition

$$\begin{gathered} \lambda_1 = \lambda_2 = \frac{g_2^2+g_1^2}{4}\ , \quad \lambda_3 = \frac{g_2^2-g_1^2}{4}\ , \\ \lambda_4 = \lambda^2 - \frac{g_2^2}{2}\ , \quad \lambda_5 = \lambda_6 = \lambda^2\ , \\ \lambda_7 = -\lambda k\ , \quad \lambda_8 = k^2\ , \end{gathered} \tag{1.21}$$

where g_1 and g_2 are respectively the $U(1)$ and $SU(2)$ gauge coupling constants of the SM at that energy scale. The tree level potential can be expressed in terms of 10 scalar fields ϕ_i:

$$H_1^0 = \frac{1}{\sqrt{2}}(\phi_1 + i\phi_4) \ , \tag{1.22}$$

$$H_2^0 = \frac{1}{\sqrt{2}}(\phi_2 + i\phi_5) \ , \tag{1.23}$$

$$N = \frac{1}{\sqrt{2}}(\phi_3 + i\phi_6) \ , \tag{1.24}$$

$$H_1^- = \frac{1}{\sqrt{2}}(\phi_7 + i\phi_9) \ , \tag{1.25}$$

$$H_2^+ = \frac{1}{\sqrt{2}}(\phi_8 + i\phi_{10}) \ . \tag{1.26}$$

The full 10×10 scalar mass squared matrix $\mathcal{M}_{ij}^2$ is given by

$$\mathcal{M}_{ij}^2 = \frac{\partial^2 V}{\partial\phi_i \partial\phi_j} \ . \tag{1.27}$$

At the symmetry breaking minimum of the potential the fields get vevs:

$$\begin{aligned} \langle\phi_1\rangle &= \sqrt{2}v_1 \ , \\ \langle\phi_2\rangle &= \sqrt{2}v_2 \ , \\ \langle\phi_3\rangle &= \sqrt{2}x \ , \\ \langle\phi_i\rangle &= 0 \ , \qquad \forall i \neq 1, 2, 3 \end{aligned} \tag{1.28}$$

where v_1, v_2 are related to the Higgs vev η in the same way as in the $MSSM$ (see eq. (1.9)) and $\tan\beta$ is defined as in eq. (1.10) as well. The squared mass matrix $\mathcal{M}_{ij}^2$ decouples into one 3×3 block for the neutral CP-even particles, another 3×3 block for the neutral CP-odd, and two 2×2 blocks for the charged sector.

The tree-level CP-even mass squared matrix is

$$M^2 = \begin{pmatrix} 2\lambda_1 v_1^2 & 2(\lambda_3+\lambda_4)v_1v_2 & 2\lambda_5 x v_1 \\ 2(\lambda_3+\lambda_4)v_1v_2 & 2\lambda_2 v_2^2 & 2\lambda_6 x v_2 \\ 2\lambda_5 x v_1 & 2\lambda_6 x v_2 & 4\lambda_8 x^2 - m_5 x \end{pmatrix} \tag{1.29}$$
$$+ \begin{pmatrix} \tan\beta[m_4x-\lambda_7x^2] & -[m_4x-\lambda_7x^2] & -\frac{v_2}{x}[m_4x-2\lambda_7x^2] \\ -[m_4x-\lambda_7x^2] & \cot\beta[m_4x-\lambda_7x^2] & -\frac{v_1}{x}[m_4x-2\lambda_7x^2] \\ -\frac{v_2}{x}[m_4x-2\lambda_7x^2] & -\frac{v_1}{x}[m_4x-2\lambda_7x^2] & \frac{v_1v_2}{x^2}[m_4x] \end{pmatrix},$$

in the basis $\{Re(H_1^0), Re(H_2^0), Re(N)\}$, and the tree-level CP-odd mass squared matrix is

$$\tilde{M}^2 = \begin{pmatrix} \tan\beta[m_4x-\lambda_7x^2] & [m_4x-\lambda_7x^2] & \frac{v_2}{x}[m_4x+2\lambda_7x^2] \\ [m_4x-\lambda_7x^2] & \cot\beta[m_4x-\lambda_7x^2] & \frac{v_1}{x}[m_4x+2\lambda_7x^2] \\ \frac{v_2}{x}[m_4x+2\lambda_7x^2] & \frac{v_1}{x}[m_4x+2\lambda_7x^2] & 3m_5x+\frac{v_1v_2}{x^2}[m_4x-4\lambda_7x^2] \end{pmatrix}, \tag{1.30}$$

in the basis $\{Im(H_1^0), Im(H_2^0), Im(N)\}$. Because one of the physical eigenstates of this matrix corresponds to the neutral massless Goldstone mode, then it is possible isolate it using eq. (1.11); explicitly we have:

$$G^0 = \frac{1}{\sqrt{2}}\left[\sin\beta\ Im(H_2^0) - \cos\beta\ Im(H_1^0)\right],$$
$$A^0 = \frac{1}{\sqrt{2}}\left[\cos\beta\ Im(H_2^0) + \sin\beta\ Im(H_1^0)\right].$$

The resulting pseudoscalar matrix will contain a non-trivial 2×2 block

$$M_{PS}^2 = \begin{pmatrix} R & S \\ S & T \end{pmatrix}, \tag{1.31}$$

from which one easily obtains the analytic expressions for the masses of the eigenstates A_1^0 and A_2^0:

$$m^2_{A_1^0,A_2^0} = \frac{1}{2}(R+T) \mp \frac{1}{2}\sqrt{(R-T)^2+4S^2}, \tag{1.32}$$

where

$$
\begin{aligned}
R &= \frac{2}{\sin 2\beta}\left(m_4 x - \lambda_7 x^2\right) , \\
T &= 3m_5 x + \frac{\eta}{2x}\sin 2\beta\left(m_4 x - 4\lambda_7 x^2\right) , \\
S &= \frac{\eta}{x}\sin 2\beta\left(m_4 x + 2\lambda_7 x^2\right) .
\end{aligned}
\tag{1.33}
$$

Finally the charged Higgs boson mass is

$$
m^2_{H^\pm} = \frac{2}{\sin 2\beta}(m_4 x - \lambda_7 x^2 - \lambda_4 v_1 v_2) . \tag{1.34}
$$

Because the CP-even mass matrix (see eq. (1.29)) has the maximum rank, it is not possible to obtain any analytic expression for its eigenvalues. Nonetheless the mass of the tree-level lightest eigenstate h^0 has, in analogy with the $MSSM$, an upper limit given by [14]:

$$
m^2_{h^0} < m^2_Z \cos^2 2\beta + \lambda^2 \eta^2 \sin^2 2\beta , \tag{1.35}
$$

where $\eta = 174\ GeV$. Comparing this last upper bound with the one obtained in the $MSSM$ (i.e. eq.(1.18)), one notes the additional term $\lambda^2\eta^2\sin^2 2\beta$. In contrast to the $MSSM$, in the $NMSSM$ the maximum is reached in the region of low values of $\tan\beta$. Then the upper bound on the Higgs coupling λ involves the study of the *Renormalization Group Equations (RGE)*. In the next chapter part of the attention will focus on the value of this coupling and the consequent maximum of m_{h^0}.

1.3 The μ problem

It is worth considering a little more closely the parameter μ appearing in the superpotential (1.1) of the $MSSM$. The term $\mu H_1 H_2$ affects the mass matrices of the Higgs fermions, namely the spin $\frac{1}{2}$ supersymmetric partners of the Higgs bosons, named *charginos* and *neutralinos*. It also enters in the Higgs bosons mass matrix itself, and finally in the *slepton* and *squark* masses through the off diagonal elements of the mass matrices. Phenomenologically μ needs to be of the order of the weak scale, but it is not clear how this happens, indeed it is *naturally* expected to be of the order of the GUT scale.

Although this is considered an unclear point for the $MSSM$, from string theory it could be a well motivated clue as μ, being a mass term, would naturally vanish since all SM particles are massless modes of the theory [9]. Within string theory the value of μ can be seen as a string boundary condition. On the other hand if $\mu = 0$ then charginos and neutralinos might be so light that they would have been observed already. As far as light $SUSY$ particles are concerned, here is raised the issue of the *Lightest Supersymmetric Particle (LSP)* in connection with the *Dark Matter (DM)* problem.

As has been discussed in section 1.1, the $NMSSM$ represents an elegant solution to the μ-problem of the $MSSM$ [13]. The superpotential of eq. (1.19) is traditionally the most common in the literature, and because it is a cubic function of the chiral supermultiplets then the superpotential is Z_3-symmetry invariant. This discrete Z_3-symmetry can be the origin of a serious domain wall problem during the *Electroweak Phase Transition (EPT)*; in this way the $NMSSM$ trilinear superpotential (1.19) can be ruled out unless the Z_3 symmetry is broken explicitly [10].

Because of these considerations, we will next consider a more general $NMSSM$ superpotential without Z_3-symmetry.

1.4 The most general case of $NMSSM$

In the previous section some criticisms of the $MSSM$ and the traditional $NMSSM$ have been discussed. Here we introduce the most general $NMSSM$ superpotential [15] [16]

$$W_{NMSSM} = \mu H_1 H_2 + \lambda N H_1 H_2 - \frac{k}{3} N^3 - rN + W_{ferm} \ , \tag{1.36}$$

where we get back the μ-term of the $MSSM$ and a linear term in N, the singlet superfield. In the superpotential a term in N^2 is missing, but it can be removed after an appropriate field redefinition [17]. Other authors have introduced a superpotential without the linear term rN, in place of this a quadratic term $\mu' N^2$ is introduced [18], but the two models are equivalent.

The corresponding tree level scalar potential, expressed in the same notation as section 1.2, is

$$\begin{aligned} V \;=\; & \frac{1}{2}\lambda_1 (H_1^\dagger H_1)^2 + \frac{1}{2}\lambda_2 (H_2^\dagger H_2)^2 \\ & +(\lambda_3+\lambda_4)(H_1^\dagger H_1)(H_2^\dagger H_2) - \lambda_4 \left| H_1^\dagger H_2 \right|^2 \\ & +(\lambda_5 H_1^\dagger H_1 + \lambda_6 H_2^\dagger H_2) N^\star N + (\lambda_7 H_1 H_2 N^{\star 2} + h.c.) \\ & +\lambda_8 (N^\star N)^2 + (|\mu|^2 + (\lambda \mu^\star N + h.c.))(H_1^\dagger H_1 + H_2^\dagger H_2) \\ & +m_{H_1}^2 H_1^\dagger H_1 + m_{H_2}^2 H_2^\dagger H_2 + m_N N^\star N \\ & -(m_4 H_1 H_2 N + h.c.) - \frac{1}{3}(m_5 N^3 + h.c.) \\ & +(m_6^2 H_1 H_2 + h.c.) + (m_7^2 N^2 + h.c.) \ . \end{aligned} \tag{1.37}$$

It is easy to see that V now differs from the tree level potential (1.20) because of the reintroduction of the μ parameter and the additional soft masses m_6^2 and m_7^2. Because now the Z_3-breaking μ-term is allowed, m_6^2 is a corresponding Z_3-breaking soft mass multiplying the bilinear term $H_1 H_2$ and is the $NMSSM$ version of m_{12}^2 typical of the $MSSM$ (see eq. (1.6)). The extra soft mass m_7^2 is due to the new term rN in the superpotential (1.36). Another important difference, first noticed by Pomarol, lies in the possibility of having spontaneous CP violation already at tree-level [19]. In chapter 3 we will focus on the spontaneous CP violation in this model, including the dominant radiative corrections.

Once we have the tree level scalar potential, it is straightforward to obtain in the CP-conserving case the tree level CP-even mass squared matrix; we use the same basis $\{Re(H_1^0), Re(H_2^0), Re(N)\}$ as in section 1.2

$$M_{11}^2 = \left(M_{Z_3}^2\right)_{11} - m_6^2 \tan\beta \ , \tag{1.38}$$

$$M_{12}^2 = \left(M_{Z_3}^2\right)_{12} + m_6^2 \ , \tag{1.39}$$

$$M_{13}^2 = \left(M_{Z_3}^2\right)_{13} + 2\lambda\mu v_1 \ , \tag{1.40}$$

$$M_{22}^2 = \left(M_{Z_3}^2\right)_{22} - m_6^2 \cot\beta \ , \tag{1.41}$$

$$M_{23}^2 = \left(M_{Z_3}^2\right)_{23} + 2\lambda\mu v_2 \ , \tag{1.42}$$

$$M_{33}^2 = \left(M_{Z_3}^2\right)_{33} - \lambda\mu\frac{\eta^2}{x} \ . \tag{1.43}$$

In the basis $\{Im(H_1^0), Im(H_2^0), Im(N)\}$ we have the CP-odd squared mass matrix

$$\tilde{M}_{11}^2 = \left(\tilde{M}_{Z_3}^2\right)_{11} - m_6^2 \tan\beta \ , \tag{1.44}$$

$$\tilde{M}_{12}^2 = \left(\tilde{M}_{Z_3}^2\right)_{12} - m_6^2 \ , \tag{1.45}$$

$$\tilde{M}_{13}^2 = \left(\tilde{M}_{Z_3}^2\right)_{13} \ , \tag{1.46}$$

$$\tilde{M}_{22}^2 = \left(\tilde{M}_{Z_3}^2\right)_{22} - m_6^2 \cot\beta \ , \tag{1.47}$$

$$\tilde{M}_{23}^2 = \left(\tilde{M}_{Z_3}^2\right)_{23} \ , \tag{1.48}$$

$$\tilde{M}^2_{33} = \left(\tilde{M}^2_{Z_3}\right)_{33} - \lambda\mu\frac{\eta^2}{x} . \tag{1.49}$$

Here $\left(M^2_{Z_3}\right)_{ij}$ and $\left(\tilde{M}^2_{Z_3}\right)_{ij}$ are the matrix elements of the matrices (1.29) and (1.30) respectively. The latter notation emphasises the fact that the matrices $M^2_{Z_3}$ and $\tilde{M}^2_{Z_3}$ refer to the $NMSSM$ invariant under the Z_3 symmetry. The soft squared mass m_7^2 introduced in the tree level potential (1.37) doesn't appear in any matrix element (1.38)-(1.49) as a consequence of the CP-invariance. As in the traditional $NMSSM$, it is possible in this general model to obtain an analytical expression for the CP-odd eigenstates A_1^0 and A_2^0 adopting the general notation introduced in (1.32) where now

$$\begin{aligned} R &= \frac{2}{\sin 2\beta}\left(m_4 x - \lambda_7 x^2 - m_6^2\right) , \\ T &= 3m_5 x + \frac{\eta}{2x}\sin 2\beta\left(m_4 x - 4\lambda_7 x^2\right) - \lambda\mu\frac{\eta^2}{x} , \\ S &= \frac{\eta}{x}\sin 2\beta\left(m_4 x + 2\lambda_7 x^2\right) . \end{aligned} \tag{1.50}$$

Finally, the analytical expression for the charged Higgs boson mass is

$$m^2_{H^\pm} = \frac{2}{\sin 2\beta}(m_4 x - \lambda_7 x^2 - \lambda_4 v_1 v_2 - m_6^2) . \tag{1.51}$$

From the tree-level CP-even mass matrix we get the same upper bound on the lightest eigenvalue as before

$$m^2_{h^0} < m_Z^2\cos^2 2\beta + \lambda^2\eta^2\sin^2 2\beta . \tag{1.52}$$

At this point we should note a remarkable general result that applies to any supersymmetric theory: the supersymmetric lightest Higgs neutral boson mass is always bounded from above, no matter if extra soft terms are added to the tree-level potential [12]. In the two models so far considered it is possible to rotate each of the Higgs squared mass matrices applying a transformation

$$W M^2 W^\dagger = M'^2 , \tag{1.53}$$

giving a bound on the smallest eigenvalue

$$m^2_{h^0} < M'^2_{11} . \tag{1.54}$$

The rotation matrix is the 2×2

$$W = \begin{pmatrix} \cos\beta & \sin\beta \\ -\sin\beta & \cos\beta \end{pmatrix} , \tag{1.55}$$

in the $MSSM$, and the 3×3

$$W = \begin{pmatrix} \cos\beta & \sin\beta & 0 \\ -\sin\beta & \cos\beta & 0 \\ 0 & 0 & 1 \end{pmatrix} , \tag{1.56}$$

in the $NMSSM$. The effect of the rotation matrix in both models is to give the matrix M'^2 in a basis where the second doublet does not have any vev. The matrix element M'^2_{11} so obtained, in our case the right hand side of equations (1.18), (1.35) and (1.52), does not depend on any soft mass (see discussion in reference [20]). The same kind of rotation on the CP-odd mass matrix gives the upper bound on the lightest eigenvalue which is zero as it corresponds to the Goldstone boson.

The next chapter will be devoted to the radiative corrections to the mass of the lightest Higgs particle. The main differences between the $MSSM$ and the two $NMSSM$ versions presented above will be highlighted using the effective potential approach.

Chapter 2

The lightest Higgs boson

2.1 Introduction

The tree-level upper bounds (1.18) and (1.35) found on the lightest Higgs neutral boson m_{h^0} in the $MSSM$ and in the $NMSSM$ might induce one to think that the Supersymmetry predictions are wrong, since they are well inside the range of energy achieved at LEPII. But the question of whether or not the Supersymmetric predictions are correct cannot be answered yet. This happens because the tree-level upper bounds are affected by radiative corrections that can raise these limits above the range of energy as yet achieved by any high energy physics laboratory. The issue of discovering the Higgs boson is truly one of the most important targets of the LHC experiments.

In this chapter we will see how the lightest Higgs boson mass depends on the tree-level and radiative correction parameters. In the next section we will highlight the main differences between the behaviour of m_{h^0} in the

$MSSM$ and the traditional $NMSSM$; in both models we will show the different upper bounds obtained using analytic approximations. Then in section 2.3, we will review the methodology used in the effective potential approach. Concerning the Z_3-breaking $NMSSM$, numerical routines have been used to evaluate and to maximize the lightest CP-even Higgs particle mass m_{h^0}. The results obtained will be compared with those obtained in section 2.2.

2.2 Upper bound on the lightest Higgs boson mass

In this section we want to analyse the behaviour of m_{h^0} in the $MSSM$ and $NMSSM$ with the usual Z_3-symmetry including the radiative corrections. The differences between the upper bounds on m_{h^0} in the two models will be highlighted. This analysis will be the basis on which we will develop the numerical calculations in the following sections, having a clearer idea about the space of the parameters to use.

When radiative corrections to the lightest Higgs boson mass are considered in the $MSSM$ and $NMSSM$, the most significant contributions come from loops involving the quarks of the third generation, *top* (t) and *bottom* (b), and their supersymmetric partners, *stops* ($\tilde{t}_1, \tilde{t}_2$) and *sbottoms* ($\tilde{b}_1, \tilde{b}_2$) respectively. In particular these are driven by the top Yukawa coupling h_t and the bottom Yukawa coupling h_b [21] [22]. The top and bottom quark running masses depend on the Higgs fields as follows

$$\mathcal{M}_t^2 = h_t^2(|H_2^+|^2 + |H_2^0|^2) \ , \tag{2.1}$$

$$\mathcal{M}_b^2 = h_t^2(|H_1^0|^2 + |H_1^-|^2) \ , \tag{2.2}$$

and at the electroweak symmetry breaking minimum of the potential (see eq. (1.7) and (1.8) or (1.28)) these masses are

$$m_t^2 = h_t^2 v_2^2 \ , \tag{2.3}$$

$$m_b^2 = h_b^2 v_1^2 \ , \tag{2.4}$$

from which we evaluate the top and the bottom Yukawa couplings respectively:

$$h_t^2 = \frac{m_t^2}{v_2^2} \ , \tag{2.5}$$

$$h_b^2 = \frac{m_b^2}{v_1^2} \ . \tag{2.6}$$

Two different cases can be distinguished:

- low values of $\tan\beta$: $1 \lesssim \tan\beta \lesssim 6$ ($v_2 \gtrsim v_1$); the dominant contributions come from the top/stop loops and the bottom/sbottom ones can be neglected;

- large values of $\tan\beta$: $\tan\beta > 6$; the bottom/sbottom contributions can also be significant as now $v_2 \gg v_1$.

By looking at the tree-level upper bounds (1.18) and (1.35), we can easily see that the $MSSM$ upper bound reaches its maximum in the large $\tan\beta$ region. Concerning the $NMSSM$ one, because it depends on the additional term $\lambda^2\eta^2\sin^2\beta$, where η is the SM Higgs vev, some considerations are needed. Regarding the Higgs coupling constant λ, here we can anticipate that it has to be free of Landau poles from the electroweak scale up to the GUT scale, which means roughly $\lambda \lesssim 1$. Bearing this in mind, it is understood that the maximum of the upper bound as a function of $\tan\beta$ turns out to be in the low $\tan\beta$ region. Because one of the main interests of this work is the upper bound on the lightest Higgs boson mass in the general Z_3-breaking $NMSSM$, in the following we will focus our attention on the low $\tan\beta$ region. The reader interested in the quantum corrections in the large $\tan\beta$ region, or including the bottom/sbottom contributions, is referred to [21] ($MSSM$) and [22] ($NMSSM$).

As a starting point, we use the $MSSM$ analytic approximation for the upper bound on m_{h^0} including two-loop corrections. This has been carried out to provide an approximation to the numerical results based on the RG improved effective potential approach[1] [25] [26]. The resulting analytical approximation involves the mass of the top quark m_t and the masses of the supersymmetric partners $m_{\tilde{t}_1}$ and $m_{\tilde{t}_2}$, which are defined from the stop mass squared matrix $\mathcal{M}^2_{stop}$. Expressing it in the basis $\{\tilde{t}_L, \tilde{t}_R\}$ this is:

$$\mathcal{M}^2_{stop} = \begin{pmatrix} m_Q^2 + h_t^2|H_2^0|^2 & h_t(A_t H_2^{0*} + \mu H_1^0) \\ h_t(A_t H_2^0 + \mu H_1^{0*}) & m_T^2 + h_t^2(|H_2^0|^2 + |H_2^+|^2) \end{pmatrix} , \tag{2.7}$$

where m_Q^2, m_T^2 and A_t are the soft $SUSY$ breaking masses characterising the order of magnitude of the masses of the stops [5] [21]. The off-diagonal element A_t is involved in the mass splitting between the physical eigenstates. Also in the off-diagonal matrix elements we can see the dependence on the term $\mu H_1 H_2$ of the superpotential (1.1). Because of the lack of experimental evidence for their existence the masses of the stops are assumed to be heavy compared with the top mass m_t. So we take the soft $SUSY$ breaking masses m_T^2 and m_Q^2 to satisfy the condition

$$m_T^2, m_Q^2 \gg m_Z^2 \ . \tag{2.8}$$

[1] See also [23] [24] and references included.
For one and two-loop radiative corrections to the Higgs mass based on different approach see references [27].

Because of this the D-terms have been omitted in the squared mass matrix (2.7) as they would give negligible contributions. At the electroweak symmetry breaking the masses of the physical eigenstates $m^2_{\tilde{t}_1}$, $m^2_{\tilde{t}_2}$ are

$$m^2_{\tilde{t}_1,\tilde{t}_2} = \frac{1}{2}\left(m^2_{\tilde{Q}} + m^2_{\tilde{T}}\right) + m^2_t \pm \sqrt{\frac{1}{4}\left(m^2_{\tilde{Q}} - m^2_{\tilde{T}}\right)^2 + m^2_t(A_t + \mu\ \cot\beta)^2}\ . \tag{2.9}$$

Because A_t and μ could increase the splitting in such a way as to render $m^2_{\tilde{t}_2} \sim m^2_t$ or even negative, we supplement the condition (2.8) with the requirement that the masses satisfy the condition

$$m^2_{\tilde{t}_1} - m^2_{\tilde{t}_2} \ll m^2_{\tilde{t}_1} + m^2_{\tilde{t}_2}\ . \tag{2.10}$$

We can then approximate $m^2_{\tilde{t}_1}$ and $m^2_{\tilde{t}_2}$ by $M^2_{\tilde{S}} \sim m^2_{\tilde{Q}} \sim m^2_{\tilde{T}}$.

After the considerations made above the analytic expression for the $MSSM$ upper bound on m_{h^0} is [25]:

$$m^2_{h^0} < m^2_Z \cos^2 2\beta \left(1 - \frac{3}{8\pi^2}\frac{m^2_t}{\eta^2}\log\frac{M^2_{\tilde{S}}}{m^2_t}\right) + \frac{3}{4\pi^2}\frac{m^4_t}{\eta^2}\left[\frac{1}{2}X_t + \log\frac{M^2_{\tilde{S}}}{m^2_t}\right]$$
$$+\frac{3}{4\pi^2}\frac{m^4_t}{\eta^2}\left[\frac{1}{16\pi^2}\left(\frac{3}{2}\frac{m^2_t}{\eta^2} - 32\pi\alpha_3\right)\left(X_t\log\frac{M^2_{\tilde{S}}}{m^2_t} + \log^2\frac{M^2_{\tilde{S}}}{m^2_t}\right)\right]\ . \tag{2.11}$$

This is a good approximation to the exact numerical result provided that $M_S \lesssim 1.5\ TeV$. In eq. (2.11) $\alpha_3 = g^2_3/(4\pi)$ is the QCD coupling constant and X_t defines the mixing between the stops:

$$X_t = \frac{2(A_t + \mu\ \cot\beta)^2}{M^2_{\tilde{S}}}\left(1 - \frac{(A_t + \mu\ \cot\beta)^2}{12 M^2_{\tilde{S}}}\right)\ , \tag{2.12}$$

where $A_t + \mu\cot\beta$ comes from the off-diagonal element of the stop squared mass matrix (2.7) and is an unknown parameter. We can see that when

$$A_t + \mu\ \cot\beta = \sqrt{6}M_S \tag{2.13}$$

then X_t takes its maximum value at $X_t = 6$; this is the so-called maximum mixing case which is indeed consistent with the condition (2.10). When $X_t = 0$ then the minimum mixing case is realised.

The analytic approximation (2.11) is readily extended to approximate the upper bound to m_{h^0} in the $NMSSM$ [28], which simply by analogy is given by:

$$\begin{aligned} m_{h^0}^2 &< (m_Z^2 \cos^2 2\beta + \lambda^2\eta^2 \sin^2 2\beta) \\ &\times \left(1 - \frac{3}{8\pi^2}\frac{m_t^2}{\eta^2}\log\frac{M_S^2}{m_t^2}\right) + \frac{3}{4\pi^2}\frac{m_t^4}{\eta^2}\left[\frac{1}{2}X_t + \log\frac{M_S^2}{m_t^2}\right] \\ &+ \frac{3}{4\pi^2}\frac{m_t^4}{\eta^2}\left[\frac{1}{16\pi^2}\left(\frac{3}{2}\frac{m_t^2}{\eta^2} - 32\pi\alpha_3\right)\left(X_t \log\frac{M_S^2}{m_t^2} + \log^2\frac{M_S^2}{m_t^2}\right)\right] . \end{aligned} \tag{2.14}$$

It is easy to see that the difference between eq. (2.14) and eq. (2.11) arises from the tree-level contribution $\lambda^2\eta^2\sin^2 2\beta$. The difference in the quantum corrections lies in the usual substitution

$$\mu \to \lambda x \tag{2.15}$$

in eq. (2.12), occurring when we pass from the $MSSM$ to the $NMSSM$.

Because we are interested in the upper bound on m_{h^0} in the $NMSSM$, we need to find the value of λ such that the tree-level contribution is maximal. It is possible to find constraints on the coupling constants λ from the *Renormalization Group (RG)* equations. The complete set of *RG* equations can be found in Appendix A. For the gauge couplings g_1, g_2 and g_3, the coupling constants λ and k, and the top Yukawa coupling h_t, at one-loop level and in the low $\tan\beta$ scenario, we have [28]

$$16\pi^2\frac{dk}{dt} = 6k(k^2 + \lambda^2) ,$$

$$16\pi^2\frac{d\lambda}{dt} = \lambda(2k^2 + 4\lambda^2 + 3h_t^2 - \frac{3}{5}g_1^2 - 3g_2^2) ,$$

$$16\pi^2\frac{dh_t}{dt} = h_t(6h_t^2 + \lambda^2 - \frac{13}{15}g_1^2 - 3g_2^2 - \frac{16}{3}g_3^2) \ ,$$
$$16\pi^2\frac{dg_i}{dt} = -c_i g_i^3 \ , \quad i = 1, 2, 3 \ ; \tag{2.16}$$

where $c_1 = -\frac{33}{5}$ (in a *GUT* normalization), $c_2 = -1$, $c_3 = 3$, and t is defined as

$$t = \frac{1}{2}\log\frac{Q^2}{m_Z^2} \ . \tag{2.17}$$

Here we neglect the effect of supersymmetric particle mass thresholds, considering these *RG* equations valid from the electroweak breaking scale $Q \sim M_Z$, up to the unification scale $Q \sim 10^{16}$ GeV. For any scale Q we impose the constraints:

$$\lambda^2(Q^2) < 4\pi \ , \quad k^2(Q^2) < 4\pi \ , \quad h_t^2(Q^2) < 4\pi \ . \tag{2.18}$$

The boundary conditions on the gauge couplings come from the experimental values at the electroweak scale[2] [29]:

$$g_1(M_Z) \approx 0.46 \ , \quad g_2(M_Z) \approx 0.65 \ , \quad g_3(M_Z) \approx 1.22 \ . \tag{2.19}$$

We need to calculate the value of the top Yukawa coupling at the electroweak scale from the top quark pole mass

$$m_t^{pole} = (173.8 \pm 5.2) \ GeV \ . \tag{2.20}$$

We transform this into the running top quark mass using the relation:

$$m_t(m_t) = \frac{m_t^{pole}}{1 + \frac{g_3^2}{3\pi^2}} = (165 \pm 5) \ GeV \ . \tag{2.21}$$

[2]A more extensive analysis of the *RG*-equations for λ, k and h_t and the relationships between these Yukawa couplings is contained in chapter 4.

After this transformation (using the relation (2.5)) we get the value of $h_t(m_t)$.

After using the RG equations, we find the value of λ such that the mass m_{h^0} reaches its maximum. In figure 2.1 we show the upper bound on λ, called λ_{max}, as a function of $\tan\beta$. In our range of study, i.e. for $\tan\beta \lesssim 6$ and $k = 0$, we find $\lambda_{max} \simeq 0.7$. The dependence on k is better shown in figure 2.2, where λ is plotted versus $\tan\beta$ and k is assumed to be a parameter at the scale m_t. In order to get the maximum value for λ we fix the running mass of the top quark $m_t = 160\ GeV$.

Once we have fixed the value of the coupling λ, we can calculate the upper bound on m_{h^0} in the $NMSSM$. In figure 2.3 we can see the plot of equations (2.11) and (2.14) as a function of $\tan\beta$ in the minimal mixing scenario ($X_t = 0$). In figure 2.4 we can see the same plot in the maximal mixing scenario ($X_t = \sqrt{6}$). In both cases, the stop masses have been identified with a $SUSY$ breaking scale of $M_S = 1\ TeV$. The behaviour of the upper bounds in the two supersymmetric models are significantly different. In the $MSSM$ the upper bound reaches its maximum for large values of $\tan\beta$. However in the $NMSSM$ the upper bound reaches its maximum already for low values of $\tan\beta$ ($2 \lesssim \tan\beta \lesssim 3$), and then it decreases for $\tan\beta \gg 1$, where the $MSSM$ and $NMSSM$ upper bounds approach each other. Comparing the figures 2.3 and 2.4 we can appreciate how the upper bound on m_{h^0} increases with the mixing. Using the definition (2.12), and the substitution (2.15), it is useful to define the parameter $\tilde{A}_t$ in the $MSSM$

$$\tilde{A}_t^{MSSM} = A_t + \mu \cot\beta \tag{2.22}$$

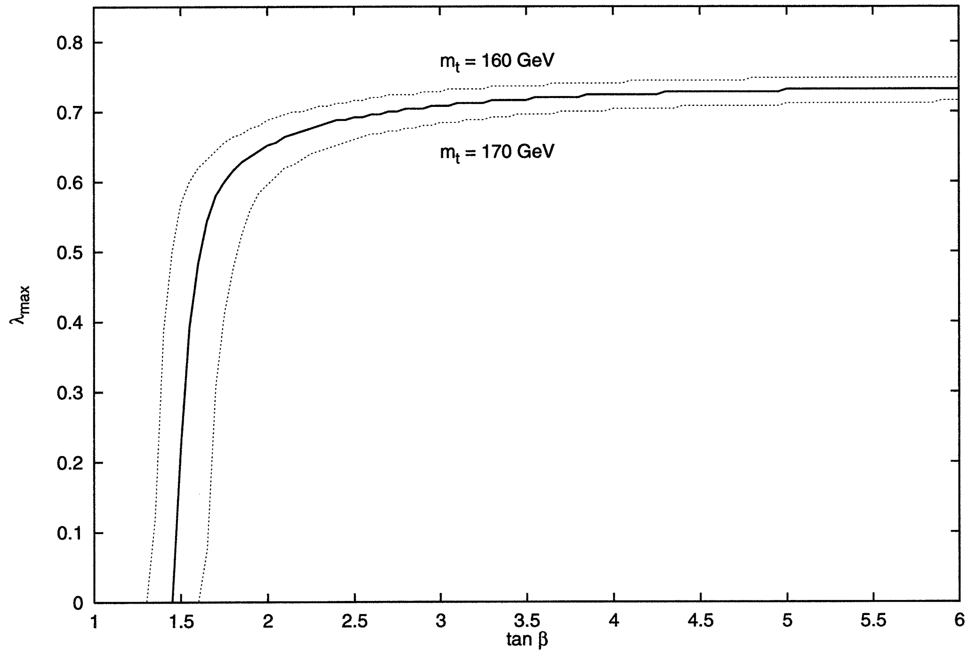

Figure 2.1: *Upper bound on* $|\lambda(m_t)|$ (λ_{max}) *as a function of* $\tan\beta$ *for* $k(m_t) = 0$. *The dotted lines take account of the error on the running top quark mass.*

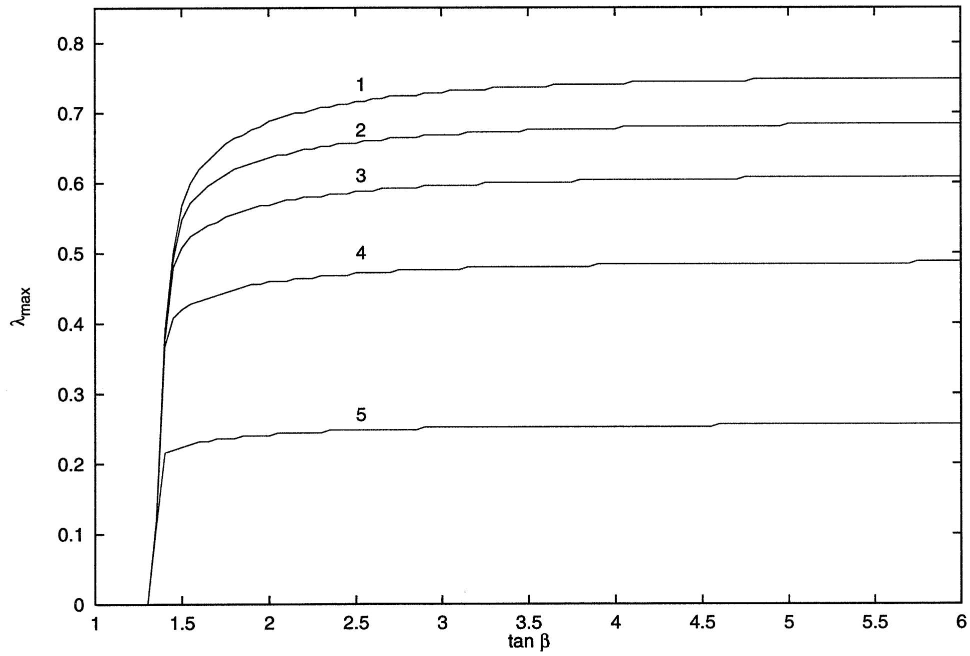

Figure 2.2: *Upper bound on* $|\lambda(m_t)|$ (λ_{max}) *as a function of* $\tan\beta$ *for* $m_t = 160$ *GeV and* $k(m_t) = 0;\ 0.3;\ 0.4;\ 0.5;\ 0.6$ *(lines 1, 2, 3, 4, 5 respectively).*

and in the $NMSSM$

$$\tilde{A}_t^{NMSSM} = A_t + \lambda x \cot\beta \ . \tag{2.23}$$

From figures 2.5 and 2.6 we can see how the radiative corrections to m_{h^0} vary as a function of the parameter $\tilde{A}_t$. Once we fix the value of $\tan\beta$ we see that, in any case, the maximum contribution to the lightest Higgs boson mass occurs when $\tilde{A}_t = \sqrt{6}M_S$, as anticipated in eq. (2.13). The choice of $\tan\beta$ in these two figures corresponds to two different cases: $\tan\beta = 2.5$ is in the region where the $NMSSM$ upper limit reaches its maximum, $m_{h^0} \simeq 133\ GeV$, it is also clear that in this region ($2 \lesssim \tan\beta \lesssim 3$) the two upper bounds in the different $SUSY$ models have the maximal difference:

$$m_{h^0}^{NMSSM} - m_{h^0}^{MSSM} \simeq 25\ GeV \ . \tag{2.24}$$

In figure 2.6 the choice of $\tan\beta = 6$ corresponds to the region in which the upper bounds in both models start to be significantly closer compared to the case shown in figure 2.5[3].

[3]Although here we neglected the effect of the radiative corrections due to the bottom/sbottom contributions, it has been proved that including the radiative effect of such particles for large values of $\tan\beta$ the two upper bounds continue to approach each other [20].

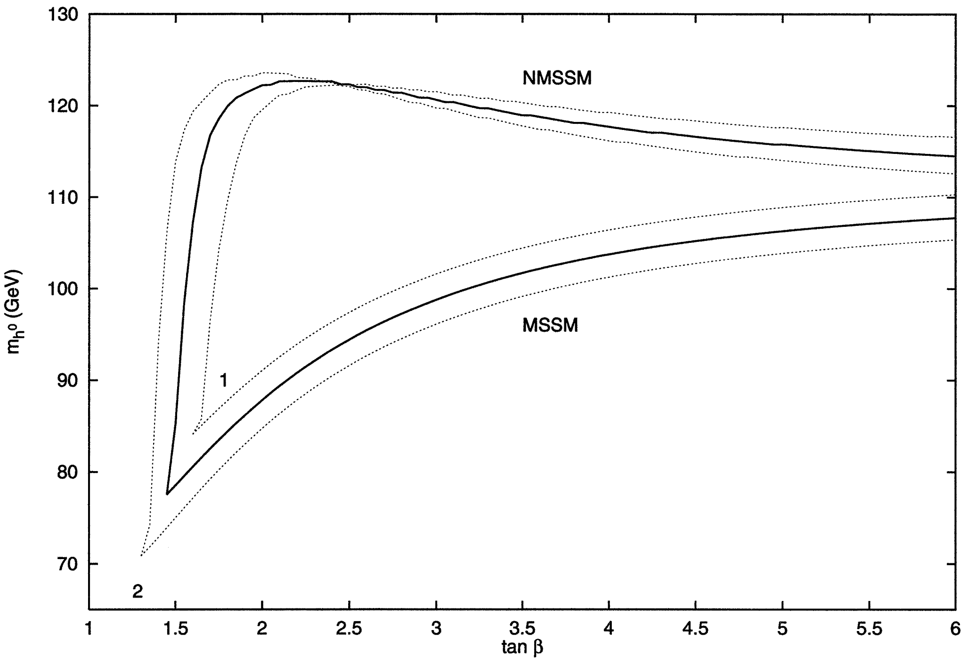

Figure 2.3: *Upper bound on m_{h^0} in the MSSM and the NMSSM for $X_t = 0$ (minimal mixing). The results are derived for $m_t = 170\,GeV$ (dotted lines matching at the point 1), $m_t = 165\ GeV$ (solid lines) and for $m_t = 160\ GeV$ (dotted lines matching at the point 2) and $M_S = 1\ TeV$.*

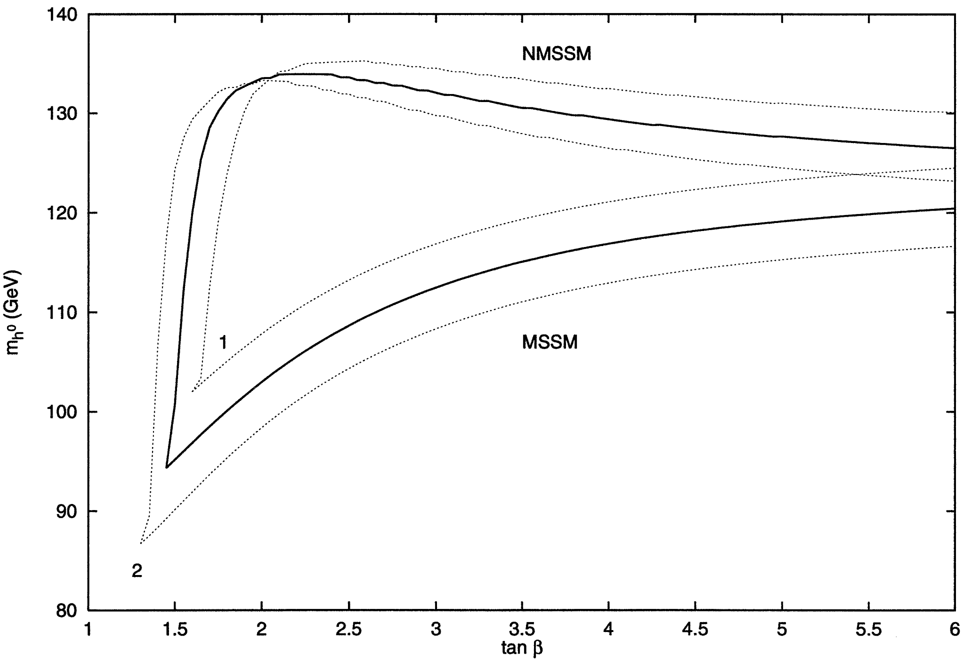

Figure 2.4: *Upper bound on m_{h^0} in the MSSM and the NMSSM for $X_t = 6$ (maximal mixing). The results are derived for $m_t = 170\,GeV$ (dotted lines matching at the point 1), $m_t = 165\ GeV$ (solid lines) and for $m_t = 160\ GeV$ (dotted lines matching at the point 2) and $M_S = 1\ TeV$.*

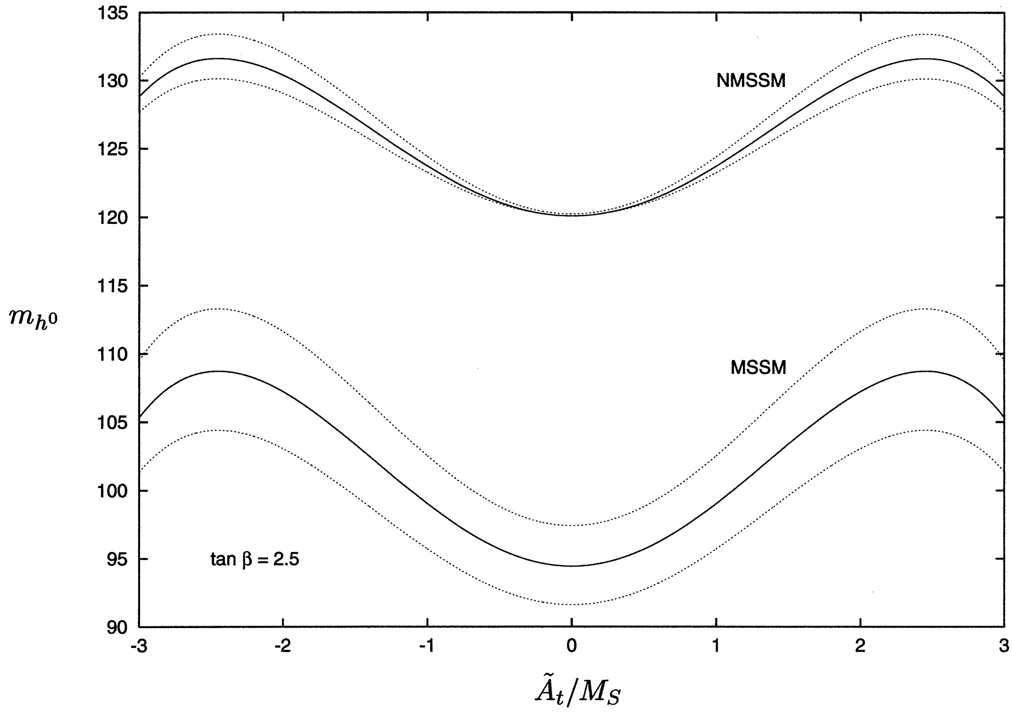

Figure 2.5: *Upper bound on m_{h^0} in the MSSM and the NMSSM versus $\tilde{A}_t/M_S$ fixing $\tan\beta = 2.5$ and $M_S = 1$ TeV. The dotted lines reflect the error on the top mass.*

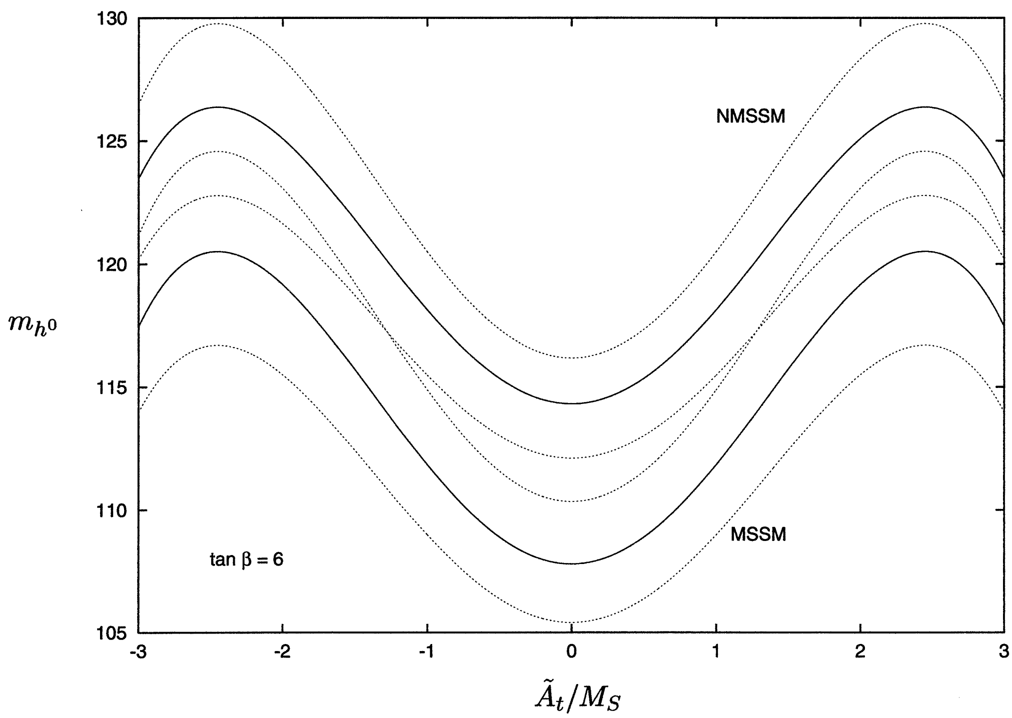

Figure 2.6: *Upper bound on m_{h^0} in the MSSM and the NMSSM versus $\tilde{A}_t/M_S$ fixing $\tan\beta = 6$ and $M_S = 1$ TeV. The dotted lines reflect the error on the top mass.*

2.3 The effective potential approach

In the previous section we have been looking at the two-loop analytic approximation to the upper bound on the lightest Higgs boson mass. In this section we will use an effective potential approach in the Z_3-breaking $NMSSM$. One and two loop corrections will be added to the tree-level neutral Higgs potential (1.37) to give the two-loop corrected effective potential. Then, we will present the methodology used to handle the many free parameters, and the upper bound on m_{h^0} will be obtained numerically from the corrected Higgs squared mass matrix. The numerical results obtained will be briefly compared with the results shown in the previous section, and an interesting comparison will be made with the results of reference [30] which inspired the present analysis.

2.3.1 The effective potential

The effective potential V_{eff} is defined as

$$V_{eff} = V^{(0)} + V^{(1)} + V^{(2)} + ... \tag{2.25}$$

where $V^{(0)}$ is the potential of eq. (1.37) and $V^{(1)}$ and $V^{(2)}$ are respectively the one-loop and two-loop radiative corrections[4] to $V^{(0)}$. Assuming the case of electroweak symmetry breaking vevs for the fields (eq.(1.28)), the tree-level potential can be written as

$$\begin{aligned} V &= \frac{1}{8}(g_1^2 + g_2^2)(v_1^2 - v_2^2)^2 + \lambda^2 x^2 (v_1^2 + v_2^2) + \lambda^2 v_1^2 v_2^2 \\ &\quad -2\lambda k v_1 v_2 x^2 + k^2 x^4 + (|\mu|^2 + 2\lambda\mu x)(v_1^2 + v_2^2) \end{aligned}$$

[4]In the analysis we are going to show, we are not going further than the dominant two-loop radiative corrections.

$$+m_{H_1}^2 v_1^2 + m_{H_2}^2 v_2^2 + m_N^2 x^2$$

$$-2m_4 v_1 v_2 x + \frac{2}{3} m_5 x^3 + 2m_6^2 v_1 v_2 + 2m_7^2 x^2 \ . \tag{2.26}$$

Let us first consider the one-loop radiative corrections to the effective potential, which takes the form:

$$V^{(1)} = \frac{1}{64\pi^2} STr\mathcal{M}^4 \Big[ln\Big(\frac{\mathcal{M}^2}{Q^2}\Big) - \frac{3}{2}\Big] \ , \tag{2.27}$$

where Q is the renormalisation scale. The supertrace is a trace over all fields which couple through the mass matrix and includes a factor $(-1)^{2J}(2J+1)$ so that a Weyl fermion acquires a factor -2, a real scalar a factor 1, and there are appropriate colour and flavour factors. $\mathcal{M}^2$ is the field dependent mass squared matrix for the particles. Here we will consider the contributions coming from the top quark, whose field dependent squared mass is expressed in eq. (2.1), and from its superpartners $\tilde{t}_1$ and $\tilde{t}_2$. The field dependent squared mass matrix for the scalar top quarks can be generalised from eq. (2.7) by simply including contribution from the terms $\mu H_1 H_2$ and $\lambda N H_1 H_2$ in the superpotential (1.36); in the basis $\{\tilde{t}_L, \tilde{t}_R\}$ we have:

$$\mathcal{M}^2_{stop} = \begin{pmatrix} m_Q^2 + h_t^2 |H_2^0|^2 & h_t[A_t H_2^{0*} + (\lambda N + \mu) H_1^0] \\ h_t[A_t H_2^0 + (\lambda N^* + \mu^*) H_1^{0*}] & m_T^2 + h_t^2(|H_2^0|^2 + |H_2^+|^2) \end{pmatrix} . \tag{2.28}$$

The physical mass eigenvalues are formally identical to those of eq. (2.9). It turns out useful to rearrange them as

$$m^2_{\tilde{t}_1, \tilde{t}_2} = M_S^2 + m_t^2 \pm \sqrt{\delta^2 M_S^4 + m_t^2 \tilde{A}_t^2} \ , \tag{2.29}$$

in which M_S is defined as follows

$$M_S^2 \equiv \frac{1}{2}(m_Q^2 + m_T^2) \ , \tag{2.30}$$

and

$$\delta \equiv \left| \frac{m_Q^2 - m_T^2}{m_Q^2 + m_T^2} \right| . \tag{2.31}$$

From the assumption stated in eq. (2.8), it turns out that $M_S \gg m_Z$. The off-diagonal matrix elements of eq. (2.28) define the new mixing parameter $\tilde{A}_t$ as:

$$\tilde{A}_t = A_t + (\lambda x + \mu) \cot\beta , \tag{2.32}$$

and finally the one-loop radiative corrections to the effective potential can be written in terms of the top/stop squared mass eigenvalues:

$$V^{(1)} = \frac{3}{32\pi^2} \left[m_{\tilde{t}_1}^4 \left(ln\frac{m_{\tilde{t}_1}^2}{Q^2} - \frac{3}{2} \right) + m_{\tilde{t}_2}^4 \left(ln\frac{m_{\tilde{t}_2}^2}{Q^2} - \frac{3}{2} \right) - 2m_t^4 \left(ln\frac{m_t^2}{Q^2} - \frac{3}{2} \right) \right] . \tag{2.33}$$

Next let us consider the dominant two loop radiative corrections to the effective potential. These are the terms coming from the leading logs quadratic in t, where

$$t \equiv \ln \left(\frac{M_S^2 + m_t^2}{m_t^2} \right) , \tag{2.34}$$

multiplied by terms $\sim h_t^6$ and $\sim \alpha_s h_t^4$, with α_s the strong coupling constant. The two loop radiative correction to the effective potential then reads [30]

$$V_{LL}^{(2)} = 3 \left(\frac{h_t^2}{16\pi^2} \right)^2 v_2^4 \left(32\pi\alpha_s - \frac{3}{2} h_t^2 \right) t^2 . \tag{2.35}$$

Finally let us consider the quantum corrections to the Higgs boson kinetic terms. Because of these, there is a wave function renormalization factor Z_{H_2} in front of the $D_\mu H_2 D^\mu H_2$ term given, to order h_t^2, by [30]

$$Z_{H_2} = 1 + 3\frac{h_t^2}{16\pi^2} t^2 . \tag{2.36}$$

Then the top quark Yukawa coupling $h_t(m_t)$, including the quantum corrections to order h_t^2 and α_s, is

$$h_t(m_t) = h_t(Q)\left[1 + \frac{1}{32\pi^2}\left(32\pi\alpha_s - \frac{9}{2}h_t^2\right)t\right] , \tag{2.37}$$

where the running top quark mass is

$$m_t(m_t) = h_t(m_t) Z_{H_2}^{1/2} v_2 , \tag{2.38}$$

and it is related to the pole quark mass, to order α_s, through the relation (2.20).

2.3.2 Implementing the upper bound on m_{h^0}

So far we have determined the two-loop effective potential, and now we need to work out the CP-even Higgs squared mass matrix applying eq.(1.27) as follows[5]

$$\mathcal{M}_{ij}^2 = \frac{\partial^2 V}{\partial\phi_i \partial\phi_j} , \quad i,j = 1,3 .$$

Once the squared mass matrix is determined, we need to use the first derivative minimization conditions

$$\frac{\partial V_{eff}}{\partial v_1} = 0 , \quad \frac{\partial V_{eff}}{\partial v_2} = 0 , \quad \frac{\partial V_{eff}}{\partial x} = 0 . \tag{2.39}$$

If the effective potential derivatives satisfy such conditions, then the effective potential itself, satisfying eq. (1.9) and (1.10), has a stationary point. If the scalar masses are positive, then the potential has a local

[5]We could extend our study to the whole Higgs spectrum as we did in chapter 1, but the main focus of this chapter is the upper bound on m_{h^0}. A review of the complete Higgs spectrum in the $NMSSM$, including radiative corrections can be found in reference [22]. In chapter 3 we will report the complete neutral Higgs spectrum in the Z_3-breaking $NMSSM$ with and without spontaneous CP-violation.

mimimum. The conditions (2.39) allow us to eliminate respectively the soft masses $m^2_{H_1}$, $m^2_{H_2}$ and m^2_N from eq.(2.26), and replace them by vevs v_1, v_2 and x. Using eq. (1.27), and after considerable algebra, we get the full dominant two-loop CP-even squared mass matrix in the basis $\{H_1, H_2, N\}$:

$$\mathcal{M}^2 = M^2 + \Delta M^2 + \delta M^2 \ , \tag{2.40}$$

where M^2 is the tree-level matrix introduced in section (1.4) and here explicitly expressed:

$$\begin{aligned}
M^2_{11} &= 2\lambda_1 v_1^2 + \tan\beta \left(m_4 x - \lambda_7 x^2 - m_6^2\right) \\
M^2_{12} &= 2(\lambda_3 + \lambda_4) v_1 v_2 - \left(m_4 x - \lambda_7 x^2 - m_6^2\right) \\
M^2_{13} &= 2\lambda_5 x v_1 - \frac{v_2}{x} \left(m_4 x - 2\lambda_7 x^2 - 2\lambda\mu x \cot\beta\right) \\
M^2_{22} &= 2\lambda_2 v_2^2 + \cot\beta \left(m_4 x - \lambda_7 x^2 - m_6^2\right) \\
M^2_{23} &= 2\lambda_6 x v_2 - \frac{v_1}{x} \left(m_4 x - 2\lambda_7 x^2 - 2\lambda\mu x \tan\beta\right) \\
M^2_{33} &= 4\lambda_8 x^2 - m_5 x + m_4 \frac{v_1 v_2}{x} - \lambda\mu \frac{\eta^2}{x}
\end{aligned} \tag{2.41}$$

ΔM^2 is the one-loop correction

$$\Delta M^2 = \begin{pmatrix} \Delta^2_{11} & \Delta^2_{12} & \Delta^2_{13} \\ \Delta^2_{12} & \Delta^2_{22} & \Delta^2_{23} \\ \Delta^2_{13} & \Delta^2_{23} & \Delta^2_{33} \end{pmatrix} + \begin{pmatrix} \tan\beta & -1 & -\frac{v_2}{x} \\ -1 & \cot\beta & -\frac{v_1}{x} \\ -\frac{v_2}{x} & -\frac{v_1}{x} & \frac{v_1 v_2}{x^2} \end{pmatrix} \Delta^2. \tag{2.42}$$

The explicit matrix elements of the two-loop corrected CP-even mass matrix, including Δ^2 and the Δ^2_{ij} can be found in appendix B.

Finally, in eq.(2.40), δM^2 is the two-loop correction where

$$\delta M^2_{ij} = 0 \quad i,\ j \neq 2\ , \tag{2.43}$$

and the only contribution comes from

$$\begin{aligned}\delta M_{22}^2 &= 12\left(\frac{h_t^2}{16\pi^2}\right)^2\left(32\pi\alpha_s-\frac{3}{2}h_t^2\right)v_2^2 \\ &\times\left[t^2-t\frac{M_S^2}{M_S^2+m_t^2}\left(3+\frac{m_t^2}{M_S^2+m_t^2}\right)+\left(\frac{M_S^2}{M_S^2+m_t^2}\right)^2\right] . \qquad (2.44)\end{aligned}$$

In the matrix $\mathcal{M}^2$, v_1 and v_2 are related to the physical Z^0-boson mass through the the relation

$$m_Z^2=\frac{1}{2}(g_1^2+g_2^2)(v_1^2+Z_{H_2}v_2^2) \qquad (2.45)$$

where the correction factor Z_{H_2} has been defined in eq.(2.36). Finally, the correct 3×3 symmetric squared mass matrix is related to the matrix of second derivatives of the Higgs potential at the minimum after dividing $\mathcal{M}_{12}^2$ and $\mathcal{M}_{13}^2$ by $Z_{H_1}^{1/2}$, and $\mathcal{M}_{22}^2$ by Z_{H_1}.

2.3.3 Parameter discussion and numerical results

After finding the two-loop dominant CP-even mass squared matrix, the remaining task is to diagonalise numerically the 3×3 matrix obtained and maximize the lightest eigenvalue $m_{h^0}^2$. The first problem we have to face is the large number of parameters involved in the mass matrix. In particular $m_{h^0}^2$ depends on nine tree-level parameters and four others appearing only through the radiative corrections. Resuming, these are:

- the couplings λ and k;
- the variables defined from the electroweak symmetry breaking Higgs fields x and $\tan\beta$;
- the soft $SUSY$ breaking parameters m_4, m_5, m_6^2 and m_7^2;

- the parameter μ

and continuing in the radiative corrections:

- the $SUSY$ breaking scale M_S;
- the mixing parameters $\tilde{A}_t$ which involves the soft term A_t and the tree-level parameters x, $\tan\beta$ and μ;
- the top Yukawa coupling h_t;
- the parameter δ representing the splitting of the soft $SUSY$ breaking masses m_Q^2 and m_T^2 (see eq. (2.31)).

We start tackling the problem by looking at the results shown in the previous section. The first parameter choice to be made can be inferred by looking at figures 2.1 and 2.2, obtained after solving the RG equations and imposing the condition that λ and k are free of Landau poles below the GUT scale. We obtain the upper limits on m_{h^0} when $\lambda = \lambda_{max} \sim 0.7$ and $k \sim 0$. Then combining together the plots of figures 2.3-2.6 we can fix $\tan\beta$ and $\tilde{A}_t$. It turns out that the maximun upper bound on m_{h^0} occurs when $\tan\beta \simeq 2.5$ and, according to eq. (2.13), $\tilde{A}_t = \sqrt{6}M_S$. Finally it is useful to fix $m_Q = m_T = M_S$, and then from eq. (2.31) $\delta = 0$. This choice is essential for obtaining the maximal mixing scenario[6] and allows us to handle the masses of the stops in an easier way as the splitting between them then only depends on the mixing parameter $\tilde{A}_t$. Concerning the supersymmetry breaking scale M_S, it will be fixed to 1 TeV, consistent with the assumption (2.8). Finally, because we assume CP-invariance,

[6]This will be explicitly shown in chapter 5.

the Higgs mass squared matrix does not depend on m_7^2; this advantage will be lost once we impose the spontaneous CP-violation scenario in the next chapter[7]. At the end we are still left with five free parameters:

$$x \ , \ \mu \ , \ m_4 \ , \ m_5 \ , \ m_6^2 \ . \tag{2.46}$$

The task is to find the maximum possible value for the Higgs mass m_{h^0} using numerical routines. Performing the calculations we disregarded any issue related to the naturalness of the parameters involved, as the aim is to simply show that the upper bound does not depend on any soft parameter[8]. At this point it is straightforward to calculate the lightest eigenvalue from the mass matrix (2.40). Because the conditions (2.39) do not guarantee a minimum of the effective potential, only a stationary point, our task is now to find the set of free parameters such that all the eigenvalues of the mass squared matrix (2.40) are positive. Our procedure was first to set up a grid of over 10^6 points in the space of the parameters (2.46) and select only the sets for which eigenvalues were positive. Starting from each of these selected points in the 5-dimensional parameters space, we then varied the parameters, using a hill-climbing routine, to maximise the lightest eigenvalue. At the end of the task we obtain the maximum calculated eigenvalue corresponding to the upper bound on the lightest Higgs boson. Here we comment on the results found.

In figure 2.7 is shown the dependence of the upper bound as a function of $\tan\beta$. The absolute upper bound, $m_{h^0} \simeq 136$ GeV, occurs when $\tan\beta \sim 2.7$. This result is in good agreement with the Z_3-symmetric $NMSSM$ upper bound shown in figure 2.4. Comparing the two results,

[7]Although this seems a complication, there will be the possibility to deal with this, as will be discussed in chapter 3.

[8]Finding a set of low energy soft $SUSY$ breaking parameters resulting from an appropriate RG analysis will be the issue of chapters 4 and 5.

it is important to remark that these are obtained following different approaches[9].

Another numerical analysis gives as an outcome the plot shown in figure 2.8, where the absolute upper limit on m_{h^0} is plotted versus M_S. In this figure $m_t^{pole} = 173.8\ GeV$. Concerning this graph, when $M_S = 1\ TeV$ the upper limit is $m_{h^0} \lesssim 136\ GeV$. In the range $1\ TeV \lesssim M_S \lesssim 3\ TeV$, M_S weakly affects the upper bound on m_{h^0}, which increases only by a few GeV due to the negative contribution of the two-loop corrections. In the region where $M_S \lesssim 1\ TeV$, the dependence of m_{h^0} is much stronger. From eq.(2.9), and setting $\delta = 0$, one can see that the assumption of maximal stop mixing (i.e. $\tilde{A}_t = \sqrt{6} M_S$) cannot be kept for M_S in the range

$$\frac{\sqrt{6}-\sqrt{2}}{2} m_t < M_S < \frac{\sqrt{6}+\sqrt{2}}{2} m_t \ , \tag{2.47}$$

because otherwise the squared mass of the lightest stop $m^2_{\tilde{t}_2}$ becomes negative. To avoid this, in this range of M_S it is enough to choose $\tilde{A}_t$ such that $m^2_{\tilde{t}_2}$ remains positive. On the other hand, because of the choice of our parameters, the region of small M_S would contradict the negative results on sparticle searches. For example, in the maximal mixing scenario $M_S \sim m_t$ would give the contradictory result of the lightest scalar top with a mass lower than the experimental lower bound $86.4\ GeV$ $(CL = 95\%)$ [29].

As previously mentioned, the analysis performed has been inspired by that of reference [30], which is based on the traditional $NMSSM$. It is natural then to compare the results shown in figures 2.7 and 2.8, with those of the cited paper. Because of the Z_3-symmetry imposed in the superpotential (1.19), the number of free parameters can be reduced by

[9] This can be seen in the $MSSM$ comparing references [21], [23] and [27]. Concerning the $NMSSM$ the reader can compare the results of references [20] and [24]

three in the effective potential; these are μ, m_6^2 and m_7^2. The calculations in the limit of the traditional $NMSSM$ have been performed by setting to zero μ and m_6^2 in the Higgs mass squared matrix; the results are shown in figures 2.9 and 2.10. To allow a comparison between the results for the two models, the parameters of the Z_3-symmetric $NMSSM$ in common with the general one have been kept unchanged. This means that in figure 2.7, where the upper bound on m_{h^0} is plotted versus $\tan\beta$, $m_t^{pole} = 173.8\ GeV$ and $M_S = 1\ TeV$. In figure 2.8, where the upper bound on m_{h^0} is expressed as a function of M_S, we set $\tan\beta = 2.7$. The two plots show an excellent agreement with plots in figures 2.9 and 2.10, confirming at two-loop-leading-log-level the equality obtained in the tree-level results (1.35) and (1.52).

A final remark has to be made concerning the results shown in figures 2.4 and 2.7. The former, obtained from the analytic approximation (2.14), reveals a maximum in the curve when $\tan\beta \simeq 2.5$; the latter, obtained using the numerical effective potential approach, shows a maximum in the upper bound for m_{h_0} when $\tan\beta \simeq 2.7$. This could lead to the tempting conclusion that one of the two plots is wrong. However this is not correct, since the expression (2.14) represents, although accurate, always an approximation. On the other hand because it has been introduced in the context of the $MSSM$, and only adapted to the $NMSSM$ case in reference [28] with the aim of highlighting the differences between the two supersymmetric models, the level of accuracy of eq. (2.14) in the $NMSSM$ is not completely reliable. To support this comment we recall the results of reference [25]: already in the $MSSM$ and adopting the parameters as specified in section 2.2, eq. (2.14) provides an approximation for the m_{h^0} upper bound with a discrepancy which in the worst case is

2 GeV. Then similarly in the $NMSSM$ we accept the results of figure 2.4 as just a good hint to help us find more accurate results based on the numerical approach. We note, however, that this plot confirms the analysis of reference [28] and figure 2.7 agrees with the results of reference [30].

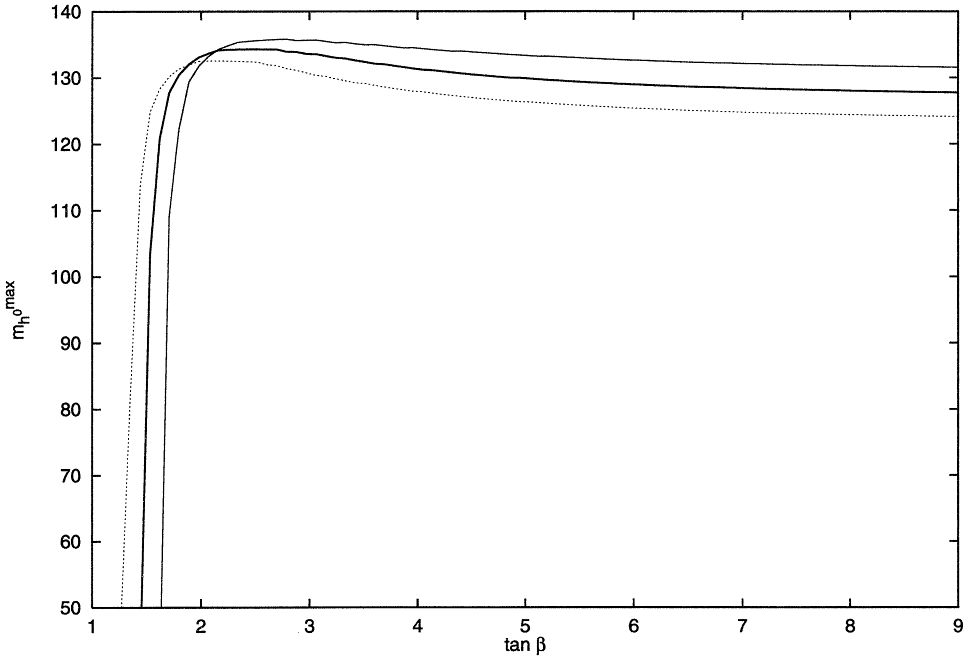

Figure 2.7: *Z_3-breaking $NMSSM$ upper bound on the mass of the lightest CP-even Higgs boson m_{h^0} versus $\tan\beta$ with $m_t^{pole} = (173.8 \pm 5.2)$ GeV and fixing $M_S = 1$ TeV. The dotted lines refer to the error on m_t^{pole}.*

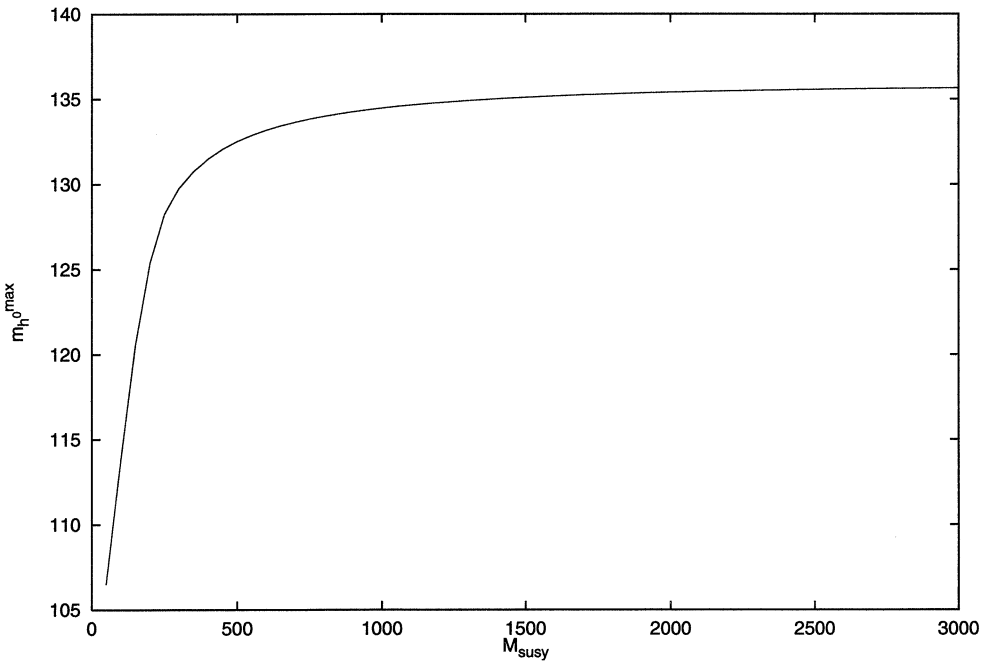

Figure 2.8: *Z_3-breaking $NMSSM$ upper bound on the mass of the lightest CP-even Higgs boson m_{h^0} versus M_S fixing $m_t^{pole} =$ 173.8 GeV and $\tan\beta = 2.7$.*

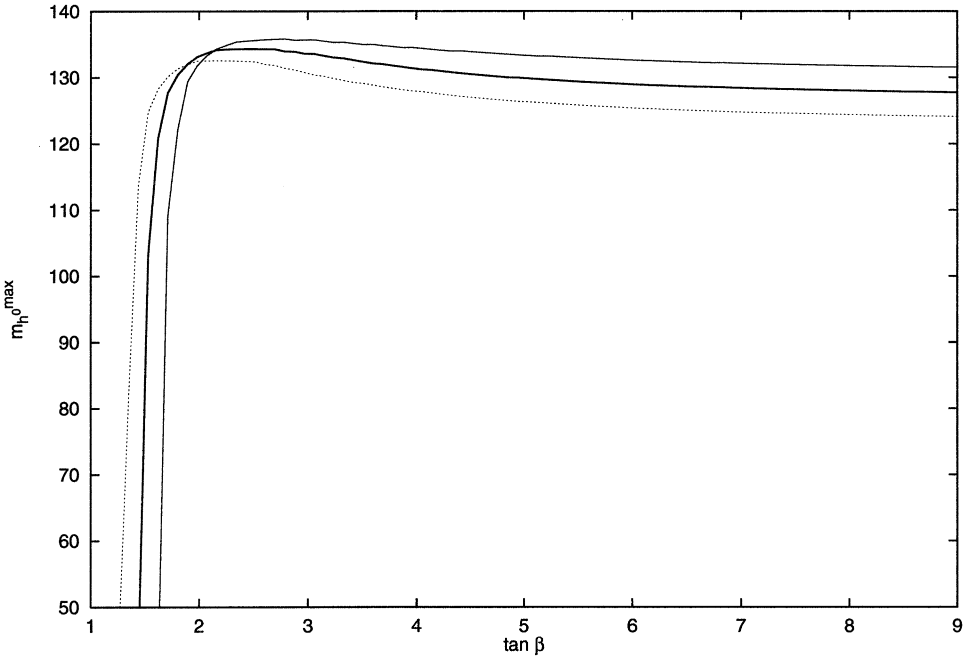

Figure 2.9: *Upper bound on the mass of the lightest CP-even Higgs boson m_{h^0} versus $\tan\beta$ with $m_t^{pole} = (173.8 \pm 5.2)$ GeV and fixing $M_S = 1\,TeV$. This figure, obtained in the traditional $NMSSM$, is the analogue of figure 2.7. The dotted lines are referred to the error on the top quark mass.*

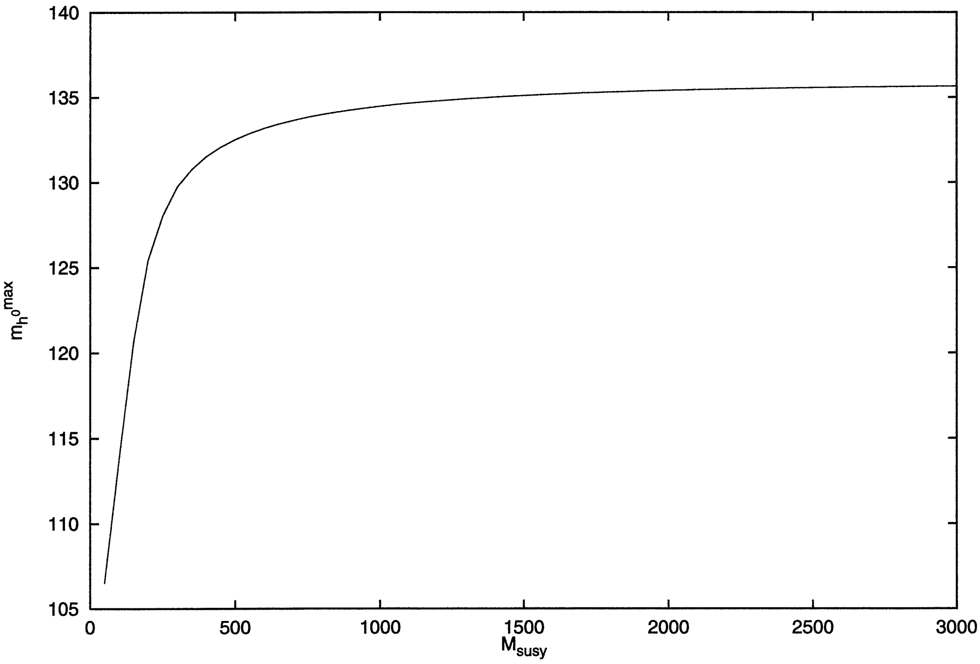

Figure 2.10: *Upper bound on the mass of the lightest CP-even Higgs boson m_{h^0} versus M_S fixing m_t^{pole} = 173.8 GeV and $\tan\beta$ = 2.7. This is the calculated upper bound in the traditional $NMSSM$. Compare with figure 2.8.*

Chapter 3

Spontaneous CP Violation

3.1 Introduction

The origin of CP violation is one of the open questions in particle physics. In the Standard Model CP symmetry is explicitly broken by the complex Yukawa couplings in the Lagrangian; these give rise to the complex CP-violating phase in the Cabibbo-Kobayashi-Maskawa matrix. Although this phase can give an account of the CP-violation observed in the neutral kaon sector, it is insufficient to generate the matter-antimatter asymmetry in the universe.

In Supersymmetric theories there are more possibilities for finding sources of CP violation. In Supersymmetry the Lagrangian can violate CP through the complex Yukawa couplings as in the Standard Model and also through the complex soft terms. Another possibility is spontaneous CP violation, where the CP symmetry is preserved by the Lagrangian, assuming all the coupling constants to be real, but it is violated by the vacuum.

In the $SUSY$ models revisited in the previous chapters, the "traditional" $MSSM$ and $NMSSM$, spontaneous CP violation by means of the vevs of the Higgs fields occurs only when we consider radiative corrections to the effective potential [11]. Both models predict the existence of a very light Higgs boson in accordance with the Georgi-Pais theorem [31], but this is ruled out in the $MSSM$ because of the lack of any experimental evidence [32]. On the other hand, such a possibility in the $NMSSM$ is allowed because here a singlet Higgs field is introduced [19].

It is our intention in this chapter to explore in detail the CP-violation due to the vacuum in the most general $NMSSM$. Within such a Z_3-breaking model, according to the result of reference [19], it is possible to achieve CP violation already at tree-level. Then we want to study the Higgs spectrum and eventually see if the lightest Higgs boson has an upper bound as well as in the CP conserving case.

3.2 CP-violating phases and the effective potential

Let us recall that the Higgs complex scalar fields N, H_1 and H_2 can be expressed in terms of the real scalar fields $\phi_1, \ldots, \phi_{10}$ as in equations (1.22-1.26). At the non-trivial minimum of the potential (1.37) we can have

$$\langle \phi_i \rangle \neq 0 \ , \quad \text{with } i = 1, \ldots, 6 \ .$$

These assumptions, generalising the assumptions (1.28), take into account a complex phase on each field vev:

$$\langle H_1^0 \rangle = v_1 e^{i\theta_1} \ , \quad \langle H_2^0 \rangle = v_2 e^{i\theta_2} \ , \quad \langle N \rangle = x e^{i\theta_3} \ . \tag{3.1}$$

With these three phases the Lagrangian still remains explicitly CP-symmetric, but the vacuum is not anymore: this is what is known as *Spontaneous CP Violation (SCPV)*. Then expressing the tree-level potential (1.37) in terms of the vevs (3.1) we have:

$$\begin{aligned} V_0 &= \frac{1}{2}\left(\lambda_1 v_1^4 + \lambda_2 v_2^4\right) + \left(\lambda_3 + \lambda_4\right) v_1^2 v_2^2 + \left(\lambda_5 v_1^2 + \lambda_6 v_2^2\right) x^2 \\ &\quad + 2\lambda_7 v_1 v_2 x^2 \cos\theta_M + \lambda_8 x^4 + \left(\mu^2 + 2\lambda\mu x \cos\theta_3\right)\left(v_1^2 + v_2^2\right) \\ &\quad + m_{H_1}^2 v_1^2 + m_{H_2}^2 v_2^2 + m_N^2 x^2 - 2m_4 v_1 v_2 x \cos\theta_P \\ &\quad - \frac{2}{3} m_5 x^3 \cos 3\theta_3 + 2m_6^2 v_1 v_2 \cos\theta_{12} + 2m_7^2 x^2 \cos 2\theta_3 \ , \end{aligned} \tag{3.2}$$

where the the phases θ_1, θ_2 and θ_3 appear in the linear combinations:

$$\begin{aligned} \theta_M &= \theta_1 + \theta_2 - 2\theta_3 \ , \\ \theta_P &= \theta_1 + \theta_2 + \theta_3 \ , \\ \theta_{12} &= \theta_1 + \theta_2 \ . \end{aligned} \tag{3.3}$$

Here we recall the boundary conditions to be satisfied by the λ_i (with $i = 1, \ldots, 8$) at the scale M_S:

$$\begin{aligned} \lambda_1 = \lambda_2 = \frac{g_2^2 + g_1^2}{4} \quad &, \quad \lambda_3 = \frac{g_2^2 - g_1^2}{4} \ , \\ \lambda_4 = \lambda^2 - \frac{g_2^2}{2} \quad &, \quad \lambda_5 = \lambda_6 = \lambda^2 \ , \\ \lambda_7 = -\lambda k \quad &, \quad \lambda_8 = k^2 \ . \end{aligned}$$

The complex phases in the Higgs field vevs affect the masses of the scalar tops as well. These enter in the one-loop correction to the effective potential (see eqs. (2.25) and (2.33)). By looking at the squared mass matrix of the stops (2.28), we see that the complex phases affect the mixing parameter $\tilde{A}_t$. Then, using the vevs (3.1), we obtain

$$\tilde{A}_t = A_t + \left(\mu + \lambda x \ e^{i\theta_3}\right) \cot\beta \ e^{i(\theta_1 + \theta_2)} \ . \tag{3.4}$$

When the phases $\theta_1 = \theta_2 = \theta_3 = 0$, we obtain eq. (2.32) of the CP-conserving case.

Concerning the further correction to the effective potential, the field dependence of $V_{LL}^{(2)}$ (see eq. (2.35)) is such that the phase θ_2 doesn't affect the two-loop correction. Finally, not surprisingly the kinetic correction considered at the end of section 2.3.1 (see eq. (2.36)) is not affected by the CP-violating phases; this is in agreement with the concept of $SCPV$ because the Yukawa coupling of the top quark is real.

3.3 Neutral Higgs spectrum

After having considered the effect of the phases θ_i (with $i = 1, 2, 3$) on the effective potential, we want to see what happens to the Higgs scalar mass matrix after imposing the $SCPV$. In the CP-conserving case we know this matrix splits into two 3×3 blocks: one CP-even or scalar (S), and another CP-odd or pseudoscalar (PS). Because of the phases, now the off diagonal blocks of our matrix are non-zero so that it is impossibile to split it into submatrices with different and definite CP eigenstates:

$$\mathcal{M}^2 = \begin{pmatrix} S & 0 \\ 0 & PS \end{pmatrix} \xrightarrow{\theta_i \neq 0} \begin{pmatrix} A & X \\ X & B \end{pmatrix},$$

where the off-diagonal block X contains factors $\sin\theta_i$ and A and B involve factors $\cos\theta_i$. As a consequence any eigenvalue obtained from the 6×6 Higgs matrix represents a hybrid state between CP-even and CP-odd.

Despite such a complication in the Higgs mass matrix, we can obtain more constraints compared to the CP-conserving case: one for each introduced phase on the Higgs fields vevs. In simple words, if before we had three minimization conditions, now we have two additional ones. Because of the identical dependence of the effective potential on the phases θ_1 and θ_2, we have two additional minimization conditions instead of three, and without loss of generality we can fix $\theta_2 = 0$. Calculating the first derivative of the effective potential we get five minimization conditions, the first three are the ones already mentioned in section 2.3.2

$$\frac{\partial V_{eff}}{\partial v_1} = 0 \ , \qquad \frac{\partial V_{eff}}{\partial v_2} = 0 \ , \qquad \frac{\partial V_{eff}}{\partial x} = 0 \ , \tag{3.5}$$

and to these we add

$$\frac{\partial V_{eff}}{\partial \theta_1} = 0 \ , \qquad \frac{\partial V_{eff}}{\partial \theta_3} = 0 \ . \tag{3.6}$$

These five minimization conditions will allow us to eliminate from the tree-level potential (3.2) five soft masses

$$m_{H_1}^2, m_{H_2}^2, m_N^2, m_6^2, m_7^2 \ ,$$

and for these the corresponding conditions are given in equations (C.7)-(C.11). The conditions on the first derivatives of V_{eff}, together with the condition of having positive eigenvalues, are enough to ensure a local minimum of the effective potential. After eliminating the five soft masses we are left with seven other tree-level free parameters:

$$\lambda, k, x, \tan\beta, m_4, m_5, \mu$$

and with another four at one-loop level:

$$M_S, \tilde{A}_t, h_t, \delta \ .$$

As already discussed in the previous chapter (see section 2.3.3), we can restrict most of the free parameters as we are interested in finding the upper bound on the lightest neutral Higgs boson. We can apply these constraints by fixing some of the parameters and deducing some others. Here we summarize:

- FIXED PARAMETERS
  - $\lambda = \lambda_{max} \simeq 0.7\ ,\quad k \simeq 0\ ,\quad \tan\beta = 2.7\ ;$
  - $M_S = 1\ TeV\ ,\quad |\tilde{A}_t| = \sqrt{6}M_S\ ,\quad m_Q = m_T = M_S\ .$
- OTHER DEDUCED PARAMETERS
  - once $|\tilde{A}_t|$ is fixed, then from eq. (3.4) we can express A_t in terms of it together with the still free parameters x and μ;
  - we determine the Yukawa coupling h_t using eq. (2.37).

At this stage we are left with four free parameters: the tree-level trilinear soft masses m_4 and m_5, the modulus of the singlet vev x and the reappeared μ parameter typical of our general model.

We can use the expression for the mass of the charged Higgs particle $m_{H^\pm}$ to eliminate m_4:

$$m^2_{H^\pm} = \frac{2}{\sin 2\beta}(m_4 x - \lambda_7 x^2 - \lambda_4 v_1 v_2 - m_6^2)\ , \tag{3.7}$$

Here we observe that elimination of m_4 doesn't mean a reduction in the number of unknown parameters, because in this way we introduce another parameter $m_{H^\pm}$. The real advantage of this substitution lies in the fact that we can express the neutral Higgs spectrum as a function of the charged Higgs particle mass, and when we try to maximise m_{h^0} we perform the task effectively eliminating another free parameter. Summarising we are left with three parameters:

$$x,\ m_5\ ,\mu\ . \tag{3.8}$$

The complete neutral Higgs mass matrix inclusive of the dominant two-loop contribution is given in appendix C.

The most natural thing to do at this point is to see what happens to the eigenvalues of the Higgs mass matrix when we vary the phases θ_1 and θ_3 from small to large values. Evaluating the Higgs spectrum it is necessary to recall that the CP-violating phases are constrained by the *Electric Dipole Moment (EDM)* of the electron, the neutron and the mercury atom [33]. To suppress EDMs in $SUSY$ models then it is necessary for the CP-violating phases to be $\lesssim 10^{-2}$ [34]. Nonetheless studies of the CP-violation in the Z_3-breaking $NMSSM$ requires large CP-vilolating phases to give an account of ϵ_k for the decay of the neutral kaon [35] [36] [37]. Aware of these facts, in the next section our results will range from small to large CP-violating phases, as the main issue of this chapter is the study of the mathematical features of the matrix giving the full spectrum of the neutral Higgs bosons and its eigenvectors.

3.4 Analysis and results: the lightest Higgs bosons

Let us start this section with some interesting theoretical remarks about the lightest Higgs boson. As previously mentioned in the Z_3-symmetric $NMSSM$ the $SCPV$ cannot be achieved unless radiative corrections are involved and, according to the Georgi-Pais theorem [31], with the consequence that a light particle characterises the Higgs spectrum. In the Z_3-breaking $NMSSM$ the $SCPV$ occurs already at tree-level because of the non-trilinear terms in the superpotential (1.36) and a light particle is only predicted in the limit of small CP-violating phases [38]. The latter result depends on a different argument and is not a consequence of the Georgi-Pais theorem. In the small phase limit from eq. (3.1) we have

$$\begin{aligned} v_1 e^{\pm i\theta_1} &\simeq v_1 \pm i\theta_1 v_1 \ , \\ v_2 e^{\pm i\theta_2} &\simeq v_2 \pm i\theta_2 v_2 \ , \\ x e^{\pm i\theta_3} &\simeq x \pm i\theta_3 x \ . \end{aligned} \tag{3.9}$$

It follows that the effective potential has two CP-conjugate minima at the points

$$\underline{\varepsilon}_1 = (v_1, v_2, x, v_1\theta_1, v_2\theta_2, x\theta_3), \tag{3.10}$$

$$\underline{\varepsilon}_2 = (v_1, v_2, x, -v_1\theta_1, -v_2\theta_2, -x\theta_3) \ , \tag{3.11}$$

where the two vectors are expressed in the basis $\{\phi_1, \phi_2, \phi_3, \phi_4, \phi_5, \phi_6\}$ for the neutral scalar fields. In a small neighbourhood of radius δ of the 6-dimensional point $\underline{\varepsilon}_1$ such that $\delta > |\underline{\varepsilon}_1 - \underline{\varepsilon}_2| > 0$, we can always expand the first derivative of the potential

$$\frac{\partial V}{\partial \phi_i} \simeq \left.\frac{\partial V}{\partial \phi_i}\right|_{\underline{\varepsilon}_1} + (\underline{\phi} - \underline{\varepsilon}_1)_j \left.\frac{\partial^2 V}{\partial \phi_j \partial \phi_i}\right|_{\underline{\varepsilon}_1} \simeq 0 \ , \tag{3.12}$$

where $|\underline{\phi} - \underline{\varepsilon}_1| < \delta$. Now in the case $\underline{\phi} = \underline{\varepsilon}_2$ the right hand side of eq. (3.12) is identically equal to zero, and we can write:

$$(\underline{\varepsilon}_2 - \underline{\varepsilon}_1)_j \left.\frac{\partial^2 V}{\partial \phi_j \partial \phi_i}\right|_{\underline{\varepsilon}_1} \approx \left.\frac{\partial V}{\partial \phi_i}\right|_{\underline{\varepsilon}_2} - \left.\frac{\partial V}{\partial \phi_i}\right|_{\underline{\varepsilon}_1} = 0 - 0 \ . \tag{3.13}$$

In the case when the phases tend to zero, this expression represents a solution of the eigenvalue equation: one eigenvalue zero at the leading order with eigenvector along the direction $\underline{\varepsilon}_2 - \underline{\varepsilon}_1$. When $\theta_i \neq 0$, but small, then we have a light particle. Because $(\underline{\varepsilon}_2 - \underline{\varepsilon}_1)$ contains just the imaginary parts of the Higgs fields, this particle is purely CP-odd in the limit of small phases. To this remarkable result it is necessary to add another important consideration based on the experimental signatures. Because of the lack of evidence for the existence of a light CP-odd doublet, we will not study the case $\theta_1 \gg \theta_3 \sim 0$. In that case the nature of the eigenvector would be predominantly doublet in contradiction with the experimental results.

In figures 3.1-3.4 we can see the plots of the upper bound on the lightest Higgs neutral boson m_{h^0} obtained by fixing θ_1 and scanning versus θ_3 in the range $0 \lesssim \theta_3 \lesssim 2\theta_1$. The numerical analysis has been performed after setting $\theta_2 = 0$, this does not affect the generality of the results. Concerning the remaining free parameters we started the scan for them in the ranges:

$$\begin{aligned} 10\ GeV \lesssim &\ x \lesssim 1\ TeV\ , \\ -500\ GeV \lesssim &\ m_5 \lesssim 500\ GeV\ , \\ -2\ TeV \lesssim &\ \mu \lesssim 2\ TeV\ , \end{aligned}$$

and for the mass of the charged Higgs boson

$$80\ GeV \lesssim m_{H^\pm} \lesssim 2\ TeV\ .$$

m_4 has been determined, for a given $m_{H^\pm}$, using eq. (3.7). m_6^2 plays a significant role after being fixed automatically by one of the the minimization conditions (3.6).

Figure 3.1 shows the plot of the upper bound on m_{h^0} for the smallest values of the phases, with $\theta_1 = 10^{-3}\ rad$ and θ_3 ranging up to $3\times10^{-3}\ rad$. As θ_3 grows the calculated upper limit approaches the limit $m_{h^0} \lesssim 1.5\ GeV$ when $\theta_3 \simeq 2\theta_1$. Plots in figures 3.2 and 3.3 show the same behaviour of the lightest Higgs boson mass as in figure 3.1, with the only difference that the upper bound m_{h^0} saturates to different upper limits: $m_{h^0} \lesssim 15\ GeV$ in figure 3.2, and $m_{h^0} \lesssim 130\ GeV$ in figure 3.3. Finally, from figure 3.4, we can see that when $\theta_1 \sim 1\ rad$, then the lightest eigenvalue of the Higgs mass matrix shows an upper bound. This upper bound on m_{h^0} turns out to be $\sim 136\ GeV$, in good agreement with the upper bound on the lightest eigenvalue of the CP-even Higgs mass matrix obtained in the previous chapter for the CP-conserving case.

The behaviour of the two lightest Higgs boson masses[1] $m_{h_1^0}$ and $m_{h_2^0}$ changes remarkably as the phases θ_i increase. In figure 3.5 the plots show the upper bound on the two masses versus the phase $\theta = \theta_1 = \theta_3$. In the small phase region the upper bound on the lightest eigenvalue $m_{h_1^0}$ is less than a few GeV, and the upper bound on the next lightest turns out to be $m_{h_2^0} \simeq 136\ GeV$. The plot of figure 3.6 shows the percentage of the singlet field in the eigenvectors corresponding to $m_{h_1^0}$ and $m_{h_2^0}$. Concerning the nature of these bosons, in the region of small CP-violating phases, the analysis of the eigenvectors reveals that the lightest Higgs boson is predominantly singlet due to large values[2] of x. For small phases and from eqs. (3.10) and (3.11) the percentage of the singlet field contained in the eigenstate $(\underline{\varepsilon}_2 - \underline{\varepsilon}_1)$ of h_1^0 is approximately

$$N_{\%} = \frac{x^2\theta_3^2}{\eta^2\cos^2\beta\theta_1^2 + x^2\theta_3^2}\ 100\ . \tag{3.14}$$

The second lightest h_2^0 is instead predominantly doublet for small phases. For larger phases $\theta_1, \theta_3 \sim 1\ rad$, the upper bound on the lightest Higgs boson $m_{h_1^0} \simeq 136\ GeV$, and the second lightest satisfies $m_{h_2^0} \lesssim 1\ TeV$.

[1]In the rest of the chapter, when we will deal with the neutral Higgs spectrum, we will identify $m_{h_1^0}$ with m_{h^0}. We will swap from one notation to another without creating too many problems for the reader. In general we shall use $m_{h_i^0}$ $(i = 1, \ldots, 5)$ to denote the masses of the neutral Higgs bosons in increasing order.

[2]The singlet percentage depends also on the value of $\tan\beta$, as we will see later.

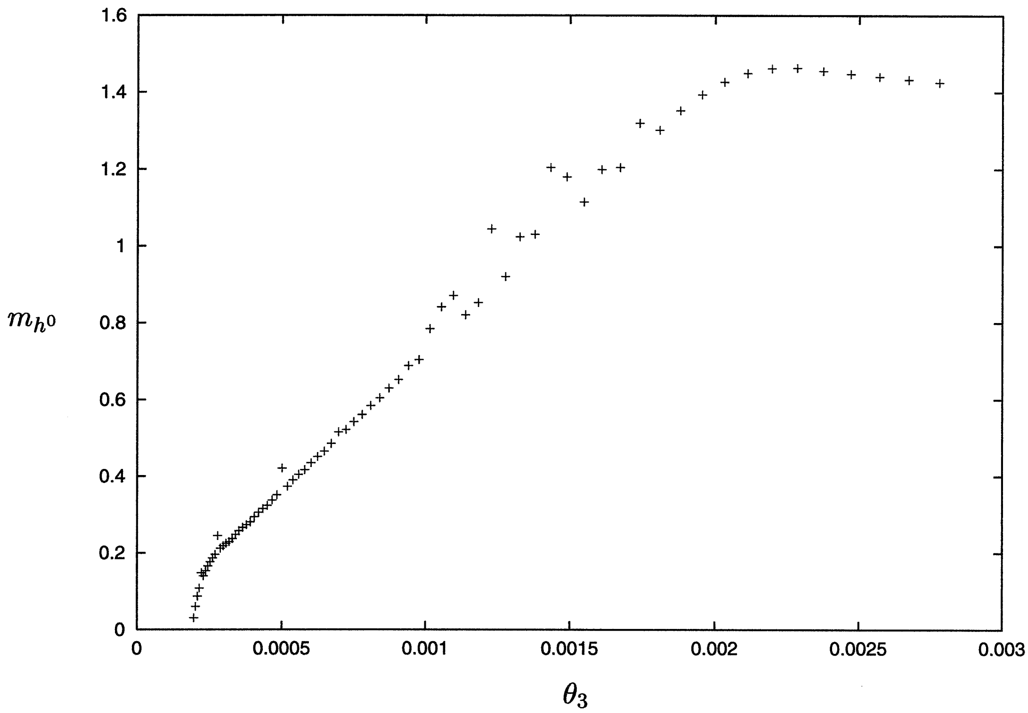

Figure 3.1: *Plot showing the upper bound on the lightest Higgs boson mass m_{h^0} versus the CP-violating phase θ_3 in the Z_3-breaking $NMSSM$. In the plot we fixed $\theta_1 = 10^{-3}$ rad and $M_S = 1$ TeV.*

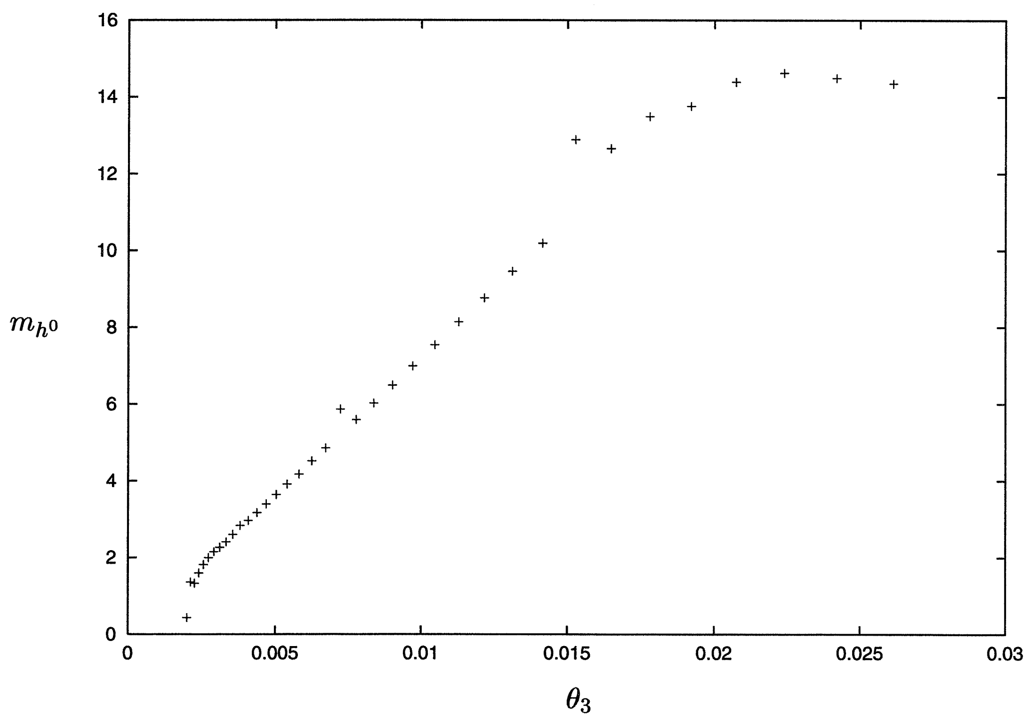

Figure 3.2: *Same plot as the one shown in figure 3.1 with $\theta_1 = 10^{-2}$.*

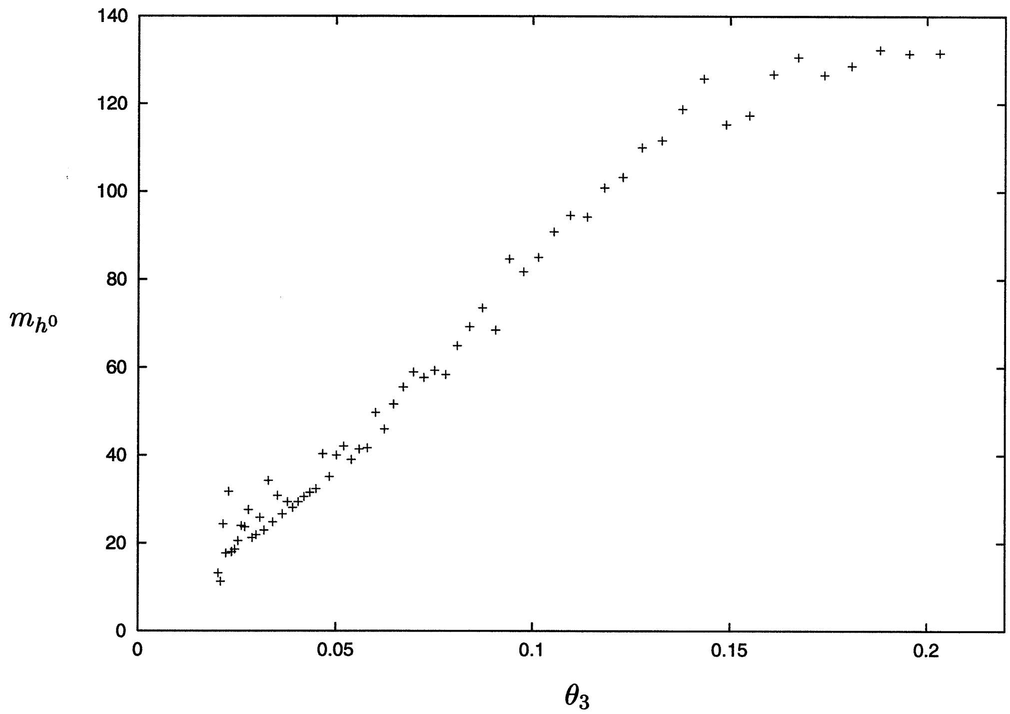

Figure 3.3: *Same plot as the one shown in figure 3.1 with* $\theta_1 = 0.1$.

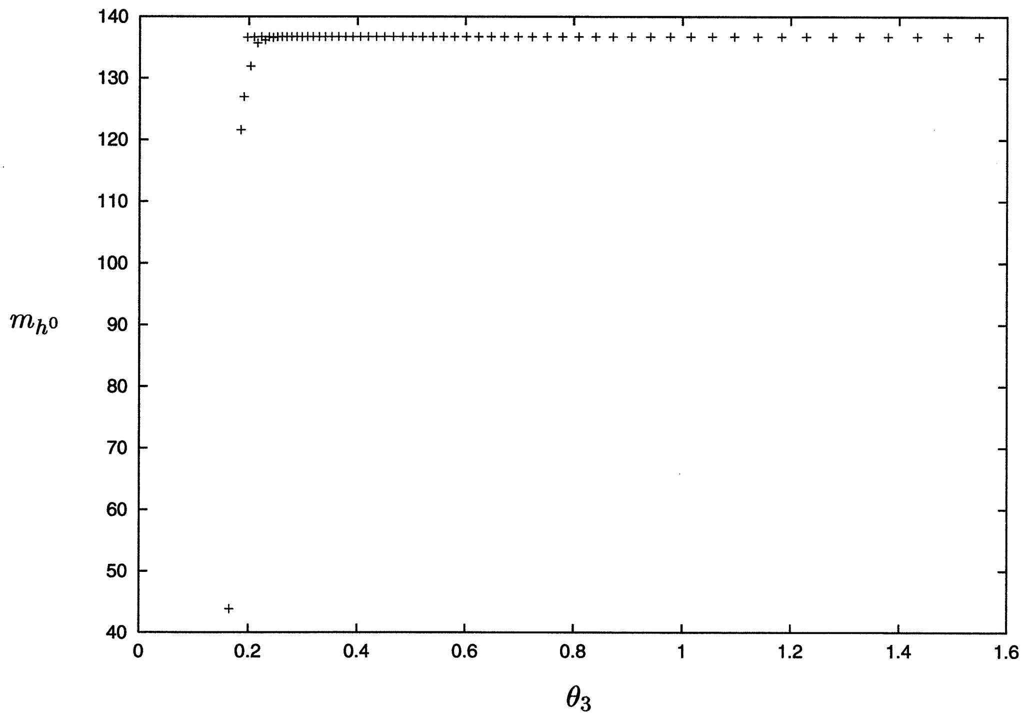

Figure 3.4: *Same plot as the one shown in figure 3.1 with* $\theta_1 = 1$.

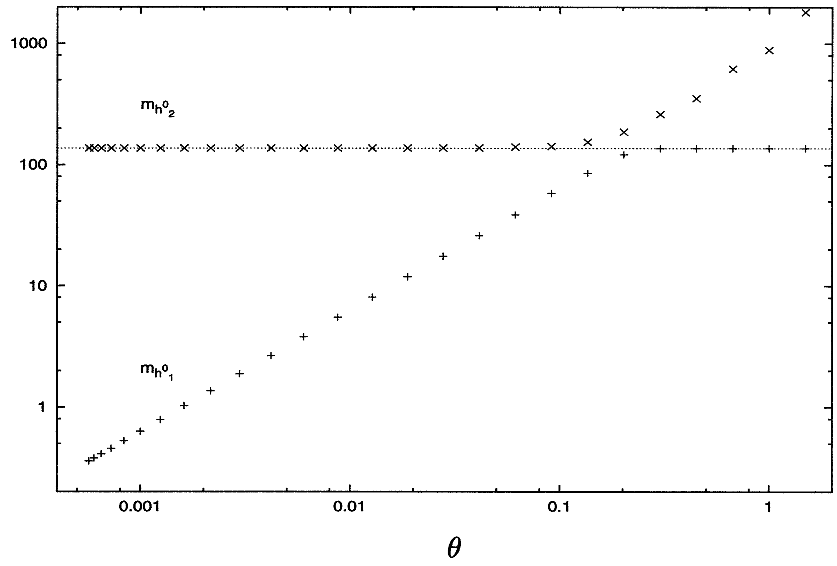

Figure 3.5: *Plots of the upper bounds on the two lightest Higgs boson masses $m_{h_1^0}$ and $m_{h_1^0}$ versus $\theta = \theta_1 = \theta_3$. The SUSY breaking scale $M_S = 1\ TeV$ and the dotted line represents the limit 136 GeV.*

Now the situation concerning the nature of the two upper limits is reversed as the eigenvector of h_1^0 shows a small percentage of singlet field, and h_2^0 is almost exclusively singlet. In figure 3.5 the dotted line highlights the limit $\simeq 136\ GeV$. An additional consideration relates to the number of upper bounds. Although in the region of large θ_1 and θ_3 the second lightest eigenvalue doesn't shown any sign of saturation, when the two phases are small the presence of the light $m_{h_1^0}$ and the upper bound on $m_{h_2^0}$ reveal that the two lightest eigenvalues of the Higgs mass matrix both have upper bounds. This is a special feature of the general $NMSSM$ in the $SCPV$ case.

From figures 3.5 and 3.6, the region where $\theta \sim 0.2\ rad$ shows an interesting crossover. As the CP-violating phases approach this region the upper bound on $m_{h_2^0}$ starts to increase above the line at $\sim 136\ GeV$, and

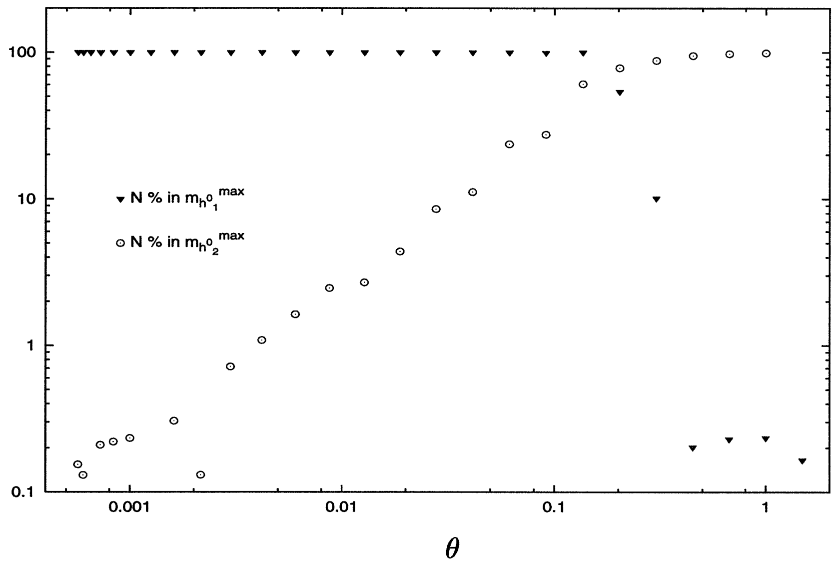

Figure 3.6: *Plots showing the singlet percentage of the two lightest Higgs bosons as a function of* $\theta = \theta_1 = \theta_3$ *. The plots refer to the masses of figure 3.5.*

it continues to increase when $\theta \gtrsim 0.2$ *rad*. At the same time the content of singlet field in its eigenstate changes as before mentioned, as in this region the eigenstate evaluated for different values of the phases ceases to be exclusively doublet dominated. Concerning the lightest Higgs boson h^0_1, the eigenvector analysis show the opposite tendency. It remains in any case the lightest physical eigenstate as in this cross-over region its mass flattens out as a function of θ and the upper bound on $m_{h^0_1}$ becomes the usual $\sim 136\ GeV$. From the overall point of view, in the region where $\theta \sim 0.2$ *rad* the two lightest eigenstates clearly swap roles and this regime is the only one where the limit $136\ GeV$ represents an upper bound for neither of them.

Figures 3.7-3.10 can help us to understand the situation better. The plots show the singlet component in the eigenvector analysis of the light-

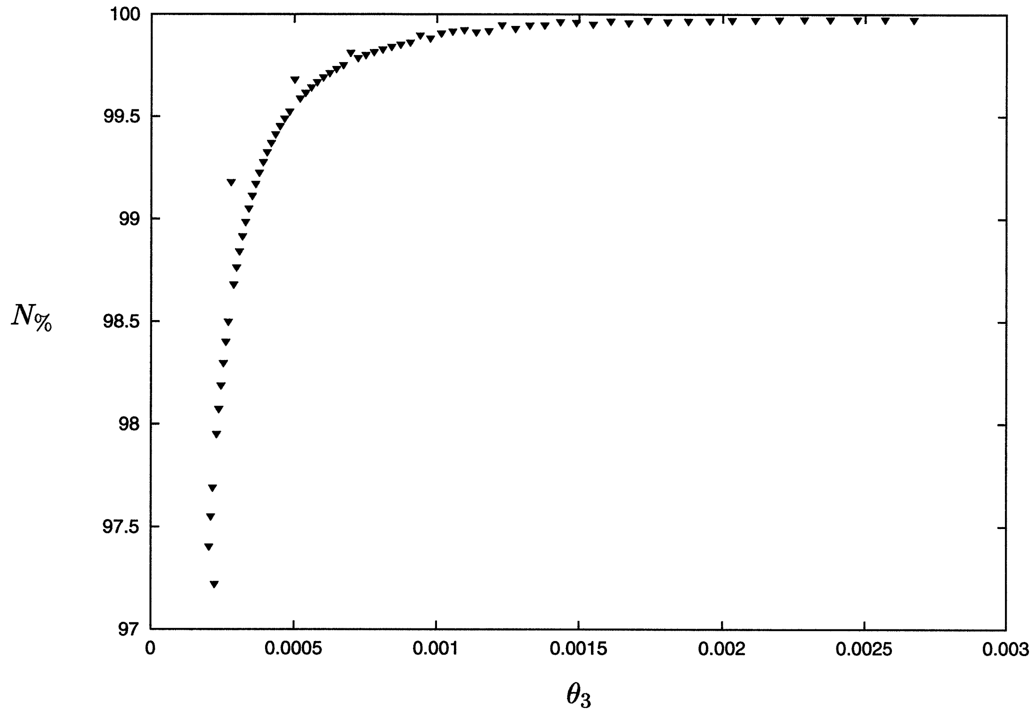

Figure 3.7: *Plot showing the percentage of the singlet fields contained in the eigenvector of the lightest Higgs boson versus* θ_3. *We fixed* $\theta_1 = 10^{-3}$ *rad and* $M_S = 1$ *TeV.*

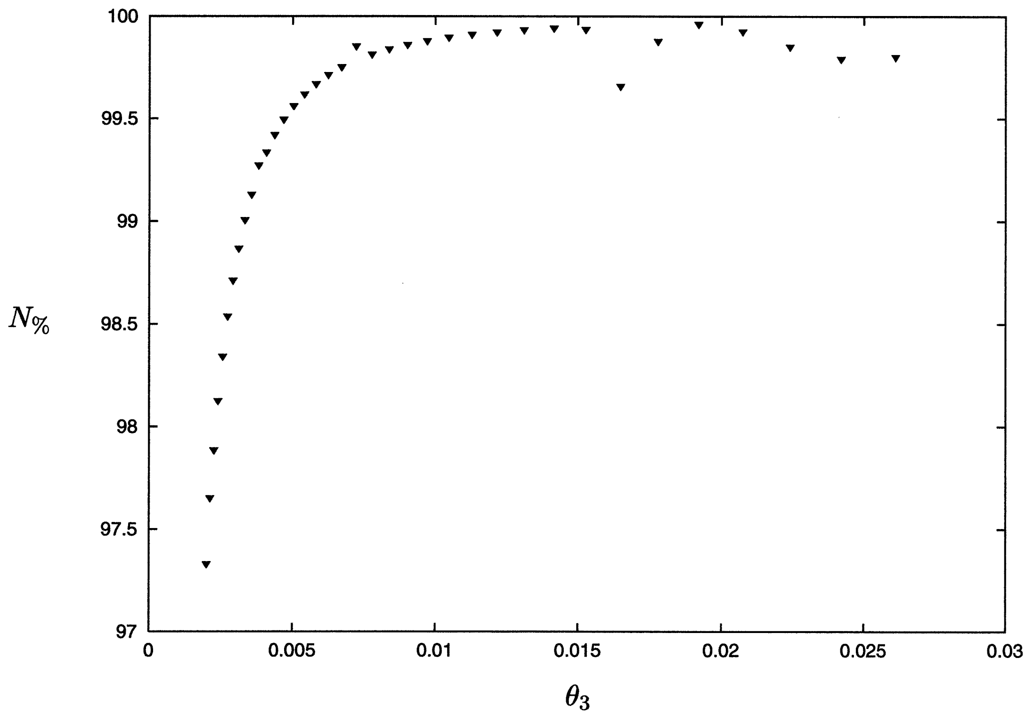

Figure 3.8: *Same plot as the one shown in figure 3.7 with* $\theta_1 = 10^{-2}$.

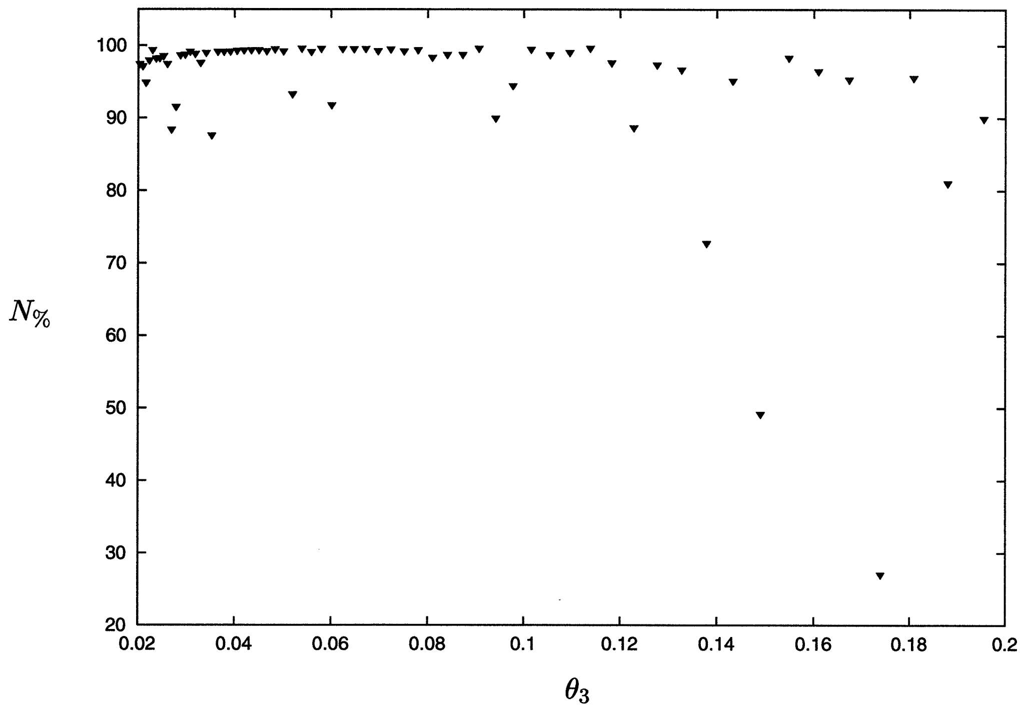

Figure 3.9: *Same plot as the one shown in figure 3.7 with* $\theta_1 = 0.1$.

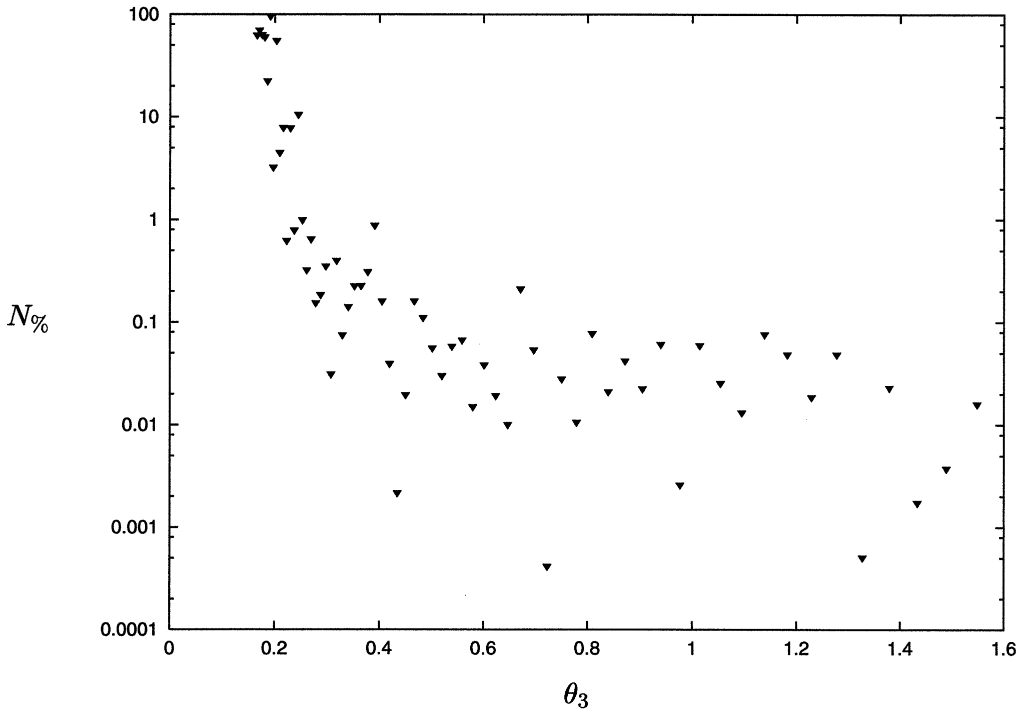

Figure 3.10: *Same plot as the one shown in figure 3.7 with* $\theta_1 = 1$.

est Higgs boson for the plots shown in figures 3.1-3.4 respectively. In the first two of these, where θ_1 is fixed to 10^{-3} and 10^{-2} rad respectively, the eigenvector analysis show the high dominance of the singlet part. In the plot of figure 3.9 we can see the singlet percentage in the cross-over region previously mentioned, and here the singlet dominance starts to decline. Eventually when $\theta_1, \theta_3 \sim 1$ rad, as shown in figure 3.10, the eigenvector of the lightest eigenvalue has the lowest singlet component, corresponding to an eigenvector strongly dominated by the doublet fields.

At this point it is worth discussing on the differences between the results just shown and those of reference [38]. There the upper bound on the lightest Higgs boson mass for small CP-violating phases is given by

$$m_{h^0} \simeq \frac{min(\theta_1, \theta_3)}{0.01} 5\ GeV\ , \tag{3.15}$$

whereas we obtain larger masses. Figure 3.2 shows masses up to $\sim 14\ GeV$ for $\theta_1 = \theta_3 = 0.01$, not $\sim 5\ GeV$ as in reference [38]. The difference can be explained as follows. The result of the mentioned reference was obtained calculating the one-loop radiative corrections to the dimensionless coupling constants of the tree-level Higgs potential using the RG approach. Besides assuming $M_S = 1\ TeV$, the parameters in the cited paper were randomly chosen in the following ranges, which are narrower than ours, described previously in this section:

$$\begin{aligned} 2 \leq & \quad \tan\beta & \leq 3\ , \\ 10\ GeV \leq & \quad x & \leq 510\ GeV\ , \\ -500\ GeV \leq & \quad m_5 & \leq 500\ GeV\ , \\ -500\ GeV \leq & \quad \mu & \leq 500\ GeV\ , \\ 55\ GeV \leq & \quad m_{H^\pm} & \leq 800\ GeV\ , \end{aligned}$$

and the Yukawa-like coupling λ and k were fixed differently:

$$\lambda = k \quad = \quad 0.5\ .$$

An additional important difference is that reference [38] assumed the minimum mixing. As discussed in section 2.2, this means degeneracy in the masses of the scalar tops $m_{\tilde{t}_1}$ and $m_{\tilde{t}_2}$ and translates to $X_t = 0$ (see eq. (2.12)). Adopting this scenario and restricting the parameters range as in reference [38] we performed an analysis of the lightest Higgs boson mass and the results are reported in figures 3.11-3.14. In the small CP-violation regime they roughly follow the evolution stated in eq. (3.15), provided we substitute 4.5 GeV for the factor 5 GeV. The discrepancy is due to the effect of the two-loop contributions to the effective potential and to the correction to the top Yukawa coupling h_t left in our calculations. Figure 3.14 finally shows the large CP-violating regime and we see that when θ_3 approaches $\sim$ 0.3 rad then the upper bound saturates to an upper limit of $\sim$ 118 GeV. Comparing this with the 136 GeV shown in figure 3.4, we can once more appreciate the important contribution to the raising of the upper bound on m_{h^0} coming from the mixing regime between the stops. This confirms what was found in Chapter 2 where we analysed the upper limit in the CP-conserving case.

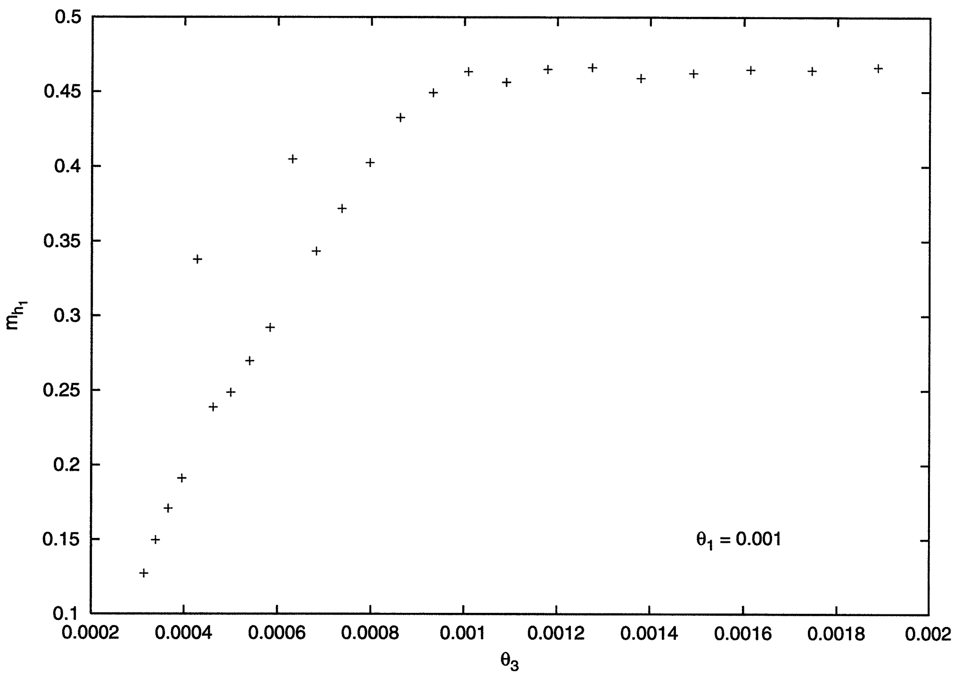

θ_3

Figure 3.11: *Plot showing the upper bound on the lightest Higgs boson mass m_{h^0} versus θ_3. We fixed $\theta_1 = 10^{-3}$ rad and $M_S = 1\ TeV$ and adopted the parameters as in reference [38].*

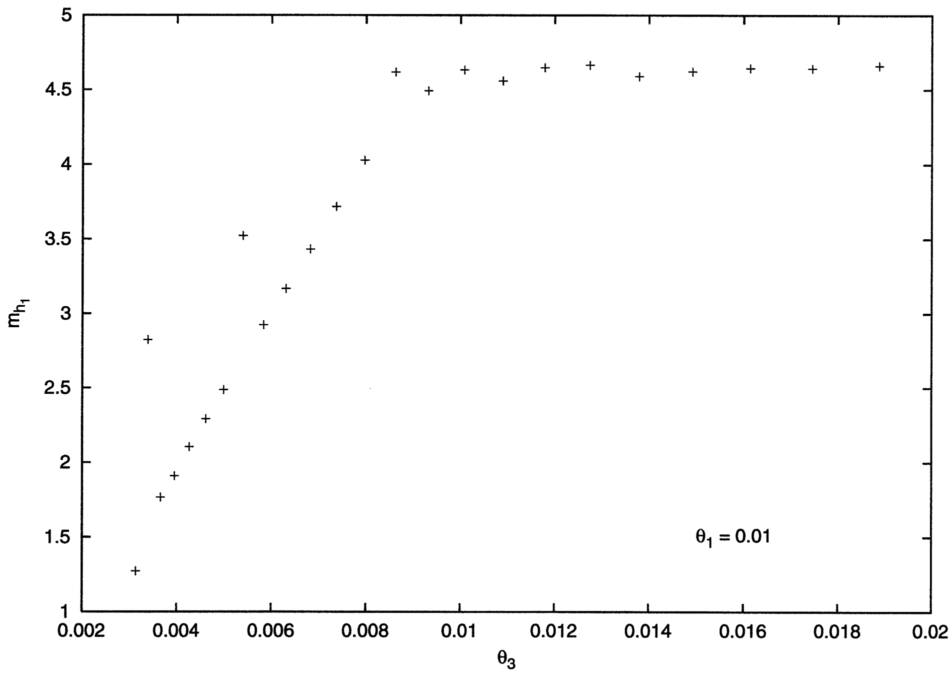

θ_3

Figure 3.12: *Same plot as the one shown in figure 3.11 with $\theta_1 = 10^{-2}$.*

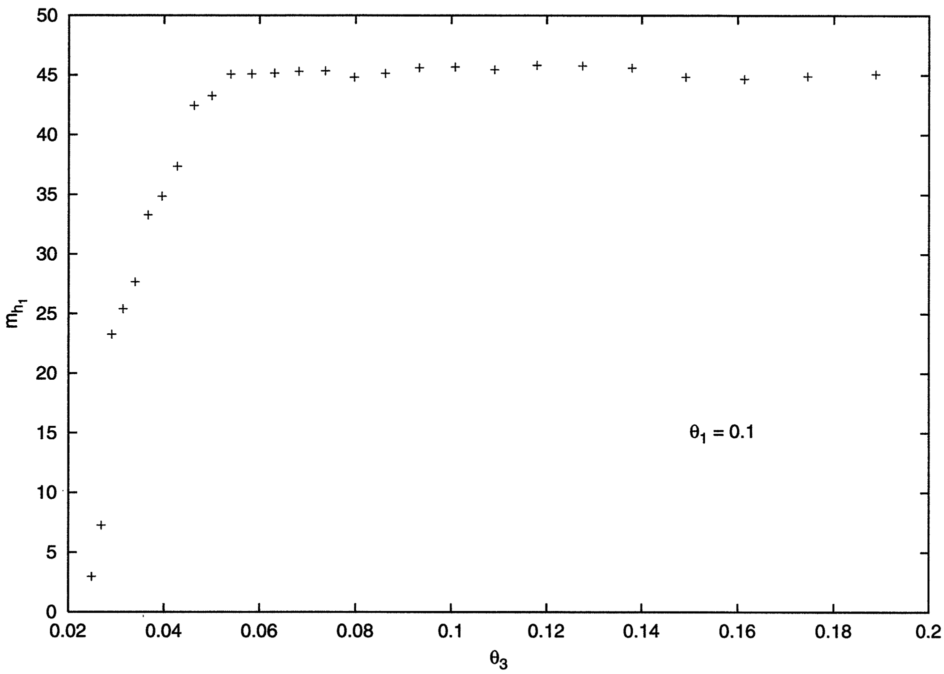

θ_3

Figure 3.13: *Same plot as the one shown in figure 3.11 with* $\theta_1 = 0.1$.

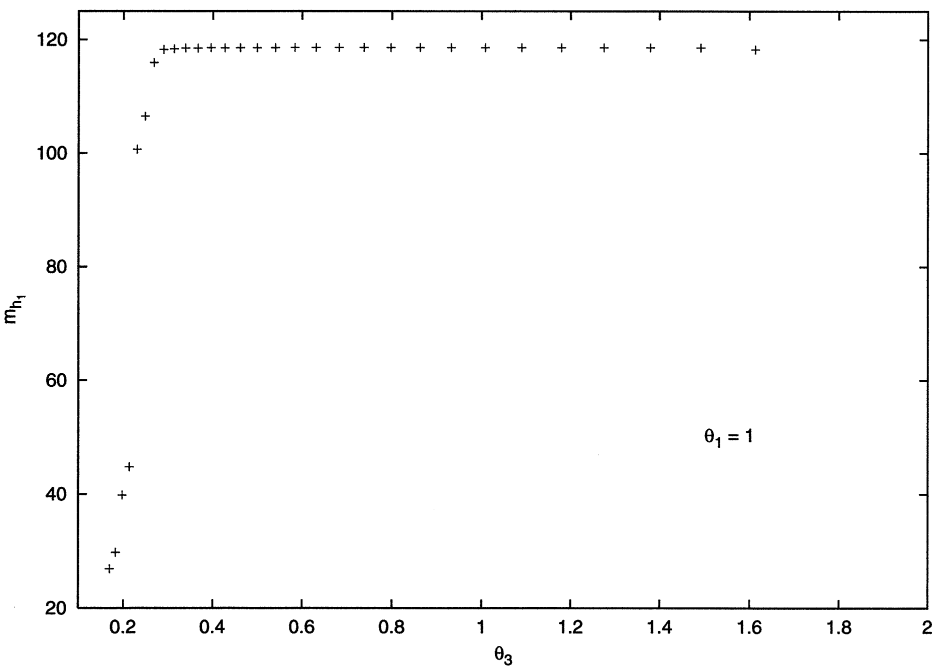

θ_3

Figure 3.14: *Same plot as the one shown in figure 3.11 with* $\theta_1 = 1$.

3.5 Analysis and results: the complete spectrum

Let us now focus our attention on the complete neutral Higgs spectrum. The plots of figure 3.15 and 3.16 show the five eigenvalues[3] $m_{h_1^0}, \ldots, m_{h_5^0}$, as a function of the mass of the charged Higgs particle $m_{H^\pm}$ which is represented by the the dotted line. The CP-violating phases are $\theta_1 = \theta_3 = 10^{-3}\ rad$. The first of the two plots is obtained after maximising numerically the lightest eigenvalue $m_{h_1^0}$ which remains very light as it is $\lesssim 1\ GeV$ even when $m_{H^\pm} \sim 2\ TeV$. The plot of figure 3.16 is obtained after maximising numerically the second lightest eigenvalue $m_{h_2^0}$. The mass $m_{h_2^0}$ reaches its upper limit $\sim 136\ GeV$ already when $m_{H^\pm} \sim 500\ GeV$. Concerning the remaining particles of the neutral Higgs spectrum, we observe $m_{h_3^0}$ ranging from a few hundred GeV in the region of low values of the charged Higgs particle, up to $\sim 1 TeV$ when $m_{H^\pm} \sim 2\ TeV$. The heaviest particles $m_{h_4^0}$ and $m_{h_5^0}$ remain always almost degenerate with[4] $m_{H^\pm}$.

In figures 3.17 and 3.18, the same spectrum is shown in the large CP-violating phases regime: $\theta_1 = \theta_3 = 1\ rad$. The two figures have been obtained after maximising respectively $m_{h_1^0}$ and $m_{h_2^0}$. In the former case, the upper bound on $m_{h_1^0}$ is $\sim 136\ GeV$ as usual. Then the next physical mass eigenvalue $m_{h_2^0}$ is not limited as in the small CP-violating phases case, and increases as the charged Higgs boson mass increases. For a charged Higgs boson mass $m_{H^\pm} \sim 2\ TeV$ then the masses $m_{h_2^0}$ and $m_{h_3^0}$

[3]After diagonalising the 6×6 mass matrix, we have always to keep in mind that one of the eigenvalues is zero corresponding to the Goldstone boson. In the plots this is not reported, but the presence of the massless particle provides a check of the calculations.

[4]Because $m_{h_4^0}$ and $m_{h_5^0}$ are almost degenerate with $m_{H^\pm}$ (see tables 3.2 and 3.3) they are also hardly distinguishable. In these graphs the range of values in which $m_{H^\pm}$ varies goes from $\sim 200\ GeV$ up to $\sim 2\ TeV$.

range between 400 GeV and 700 GeV. As in the small CP-violating limit, the masses of the heaviest neutral Higgs bosons $m_{h_4^0}$ and $m_{h_5^0}$ are almost degenerate with the charged Higgs particle $m_{H^\pm}$. Figure 3.18 shows the neutral Higgs spectrum after maximising $m_{h_2^0}$. The result of this maximisation shows an unexpected quasi-degeneracy between $m_{h_2^0}$ and $m_{h_3^0}$ and for $m_{H^\pm} \sim 2\ TeV$ these masses are $\lesssim 800\ GeV$. For the lightest particle of the spectrum we have a large range of values, $0.1\ GeV \lesssim m_{h_1^0} \lesssim 100\ GeV$, while the remaining particles $m_{h_4^0}$ and $m_{h_5^0}$ show the same pattern as in figure 3.17.

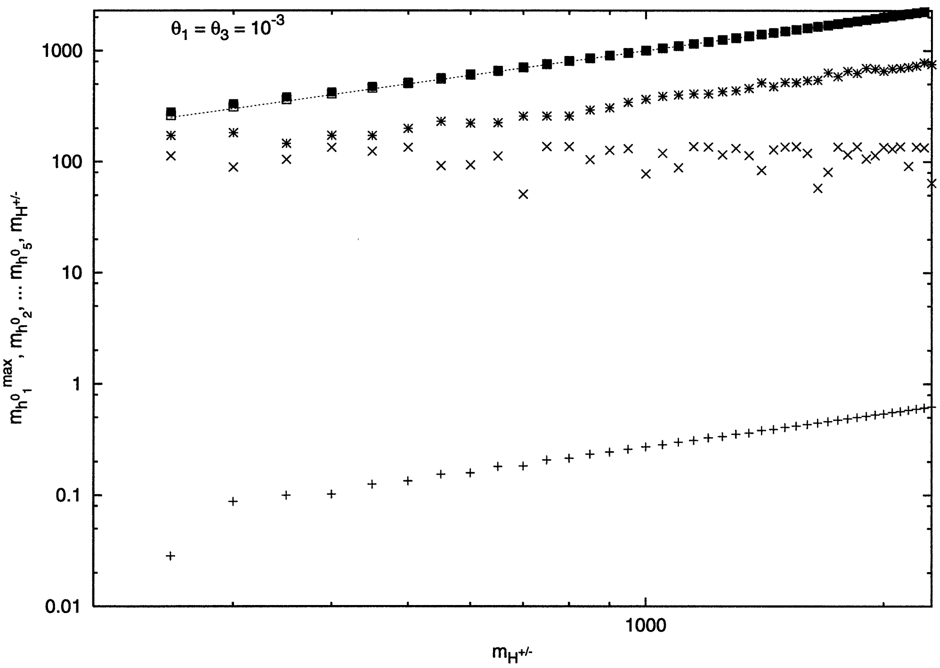

Figure 3.15: *Neutral Higgs spectrum obtained after maximising the lightest mass $m_{h_1^0}$ versus the charged Higgs mass $m_{H^\pm}$. We fixed the CP-violating phases $\theta_1 = \theta_3 = 10^{-3}$ rad and $M_S = 1$ TeV. The dotted line represents $m_{H^\pm}$.*

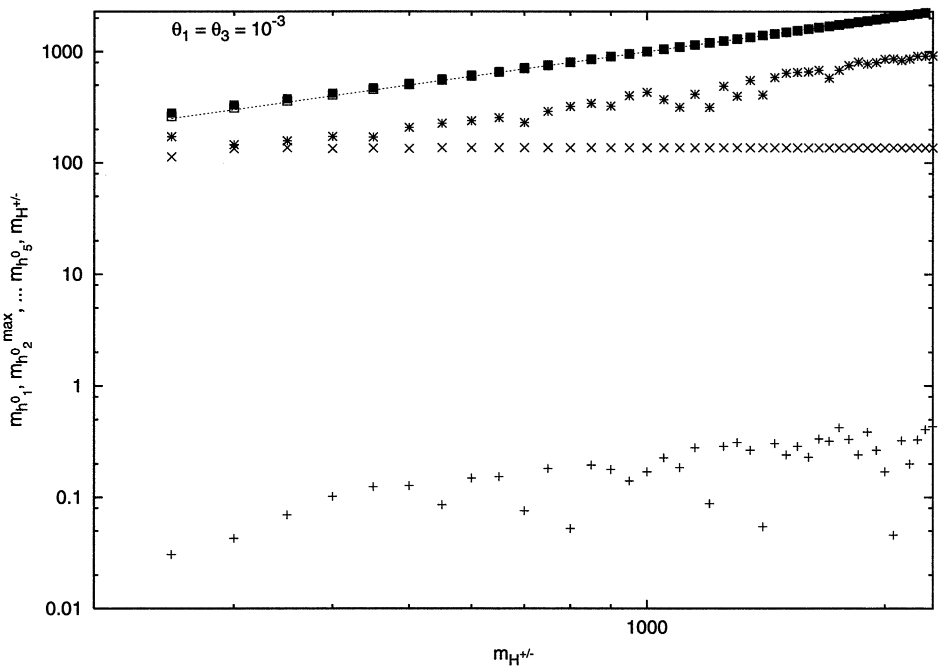

Figure 3.16: *Neutral Higgs spectrum obtained after maximising the second lightest mass $m_{h_1^0}$ versus the charged Higgs mass $m_{H^\pm}$. We fixed the CP-violating phases $\theta_1 = \theta_3 = 10^{-3}$ rad and $M_S = 1$ TeV. The dotted line represents $m_{H^\pm}$.*

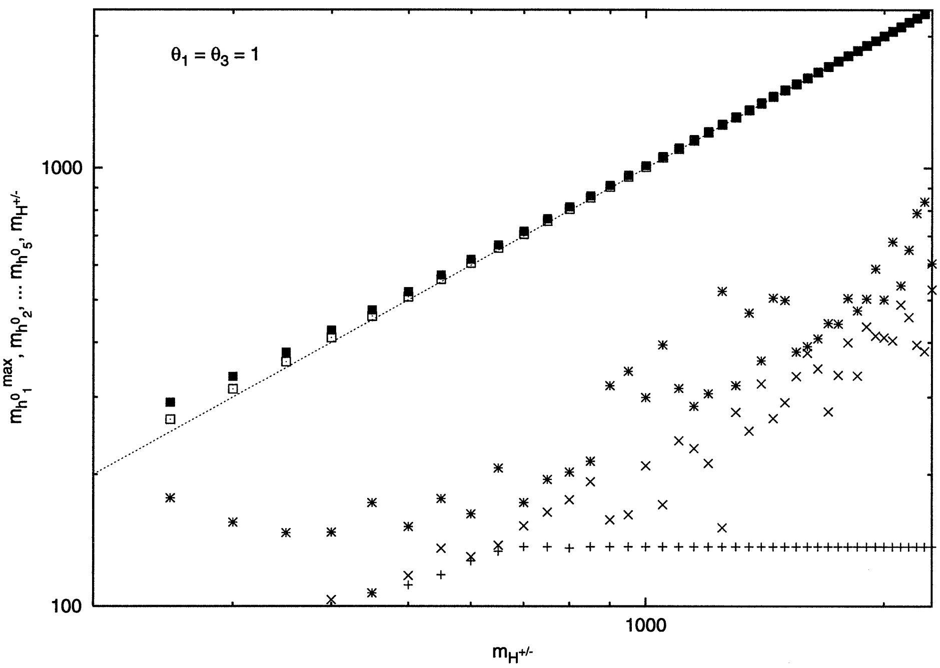

Figure 3.17: *Neutral Higgs spectrum versus $m_{H^\pm}$ and fixed CP-violating phases $\theta_1 = \theta_3 = 1$ rad and $M_S = 1$ TeV. The lightest eigenvalue $m_{h_1^0}$ has been maximised.*

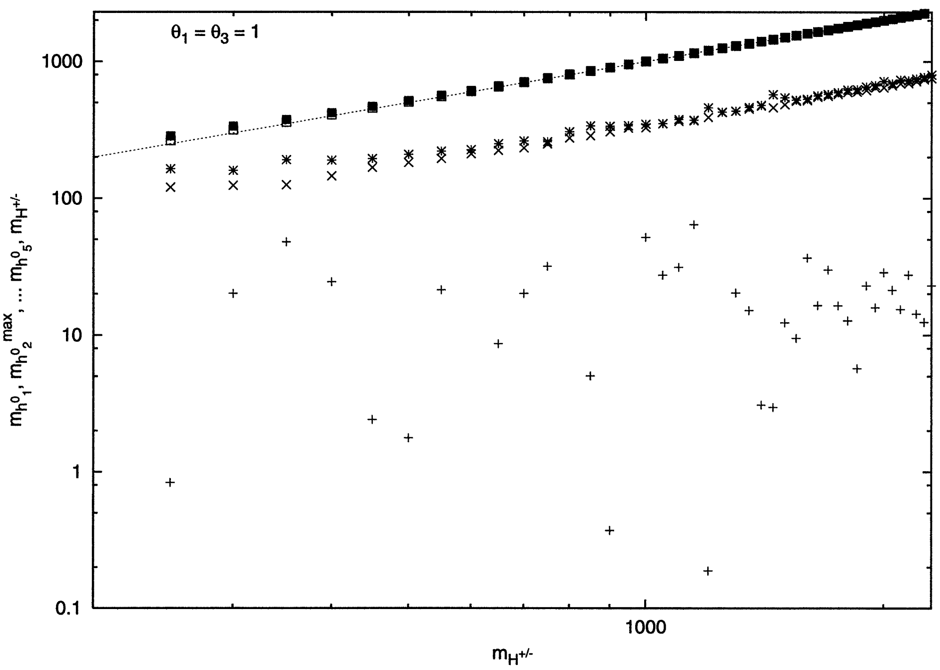

Figure 3.18: *Neutral Higgs spectrum versus $m_{H^\pm}$ and fixed CP-violating phases $\theta_1 = \theta_3 = 1$ rad and $M_S = 1$ TeV. The second lightest eigenvalue $m_{h_2^0}$ has been maximised.*

3.6 The decoupling limit

We conclude the analysis of our results by summarising the nature of the particles that constitute the spectrum in the *decoupling limit*

$$m_{H^\pm}\ ,\ x\ \gg \eta\ , \tag{3.16}$$

where $\eta = 174\ GeV$ is the SM Higgs vev. In this regime, analytic approximation for the eigenvectors provide a useful check for our numerical work.

In table 3.1 we summarise the results in the small CP-violating phase region, with $\theta_1 = \theta_3 = 10^{-3}\ rad$, and the large one with $\theta_1 = \theta_3 = 1\ rad$. In the first limit we see that the lightest Higgs particle is CP-odd, which confirms the theoretical predictions on the eigenvector coming from the approximation (3.9). The dominant part of the eigenvector lies in the direction of the imaginary part of the singlet field. The next to lightest eigenvalue $m_{h_2^0}$ is the closest to the lightest CP-even Higgs boson of the CP-conserving case. The next state h_3^0 is the heavier singlet with the dominant component of the eigenvector in the direction of the real part of the field N. Finally the heaviest particles h_4^0 h_5^0, whose masses are nearly degenerate with the mass of the charged Higgs boson $m_{H^\pm}$, have a strong doublet predominancy, CP-even and CP-odd respectively. In the parenthesis is expressed the particular doublet field with the highest component in the respective eigenvector. For completeness, the Goldstone boson is included.

When we consider the large phase case, $\theta_1 = \theta_3 = 1$, it is not possible to determine the CP-state because these are not eigenstates of CP. From table 3.1 we can see that the singlet-doublet character remains un-

$\theta_1 = \theta_2 = 10^{-3}$

G^0	doublet (H_2)	CP-odd
h_1^0	singlet	CP-odd
h_2^0	doublet (H_2)	CP-even
h_3^0	singlet	CP-even
h_4^0	doublet (H_1)	CP-even
h_5^0	doublet (H_1)	CP-odd

$\theta_1 = \theta_2 = 1$

G^0	doublet (H_2)
h_1^0	doublet (H_2)
h_2^0	singlet
h_3^0	singlet
h_4^0	doublet (H_1)
h_5^0	doublet (H_1)

Table 3.1: *Nature of the neutral Higgs spectrum particles in two CP-violating phases cases: $\theta_1 = \theta_3 = 10^{-3}$ and $\theta_1 = \theta_3 = 1$.*

changed compared to the small phase limit as far as the three heaviest Higgs are concerned, but that of the two lightest particles $m_{h_1^0}$ and $m_{h_2^0}$: is inverted. The dominance of a particular Higgs field in each eigenstate depends on the choice of $\tan\beta$ and the following analysis shows how this is determined.

In the decoupling limit the physical eigenstates can be better understood by making the transformation [39]:

$$\begin{pmatrix} H \\ \tilde{H} \end{pmatrix} = \begin{pmatrix} -\cos\beta & \sin\beta \\ \sin\beta & \cos\beta \end{pmatrix} \begin{pmatrix} e^{i\theta_1} & 0 \\ 0 & 1 \end{pmatrix} \begin{pmatrix} \tilde{H}_1 \\ H_2 \end{pmatrix}, \tag{3.17}$$

where H represents the effective SM Higgs field and $\left(\tilde{H}_1\right)^T = \left(\tilde{H}_1^+, \tilde{H}_1^0\right)$ is defined as $\tilde{H}_1 = \varepsilon(H_1)^*$ with ε the antisymmetric tensor introduced in eq. (1.5). Explicitly we have

$$\begin{pmatrix} \tilde{H}_1^+ \\ \\ \tilde{H}_1^0 \end{pmatrix} = \begin{pmatrix} H_1^{-*} \\ \\ -H_1^{0*} \end{pmatrix} \tag{3.18}$$

Following this definition, which is a generalisation of the eqs. (1.11) and (1.12) to the $SCPV$ case, and concentrating on the neutral fields only, then[5]

$$H^0 = \cos\beta e^{i\theta_1}(H_1^0)^* + \sin\beta H_2^0 \ . \tag{3.19}$$

This includes the Goldstone boson and the SM-like Higgs boson in the decoupling limit, the corresponding eigenvectors of the squared mass matrix in the basis $\{H_1, H_2\}$ in which are given by

$$G^0 = -i \begin{pmatrix} \cos\beta e^{i\theta_1} \\ \\ -\sin\beta \end{pmatrix} \quad ; \quad h^0 = - \begin{pmatrix} \cos\beta e^{i\theta_1} \\ \\ \sin\beta \end{pmatrix} . \tag{3.20}$$

Relative to the states shown in table 3.1 this last eigenstate in the small CP-violating phases regime corresponds to h_2^0, and in the the opposite regime corresponds to h_1^0. Concerning the neutral component of the second Higgs field $\tilde{H}^0$, following the transformation (3.17) we have:

$$\tilde{H}^0 = -\sin\beta e^{i\theta_1}(H_1^0)^* + \cos\beta H_2^0 \ . \tag{3.21}$$

This contains the corresponding eigenvectors for the heaviest particles h_4^0 and h_5^0 which, in the basis $\{H_1, H_2\}$, are

$$h_4^0 = - \begin{pmatrix} \sin\beta e^{i(\theta_1-\alpha)} \\ \\ -\cos\beta e^{i\alpha} \end{pmatrix} \quad ; \quad h_5^0 = -i \begin{pmatrix} \sin\beta e^{i(\theta_1-\alpha)} \\ \\ \cos\beta e^{i\alpha} \end{pmatrix} , \tag{3.22}$$

[5]In this notation the symbol H^0 has not to be confused with the one of eq. (1.13)

where α is an additional phase coming from the orthonormality with eigenvectors (3.20). For the last pair of Higgs particles we kept the notation used throughout the chapter because from table 3.1 the doublet character of these two particles remain unchanged as we change from the small to the large CP-violating regime. The phase factor $e^{i\alpha}$ parametrizes the most general $\tilde{H}^0$ orthonormal to H^0. As has been remarked, the masses $m_{h_4^0}$ and $m_{h_5^0}$ are almost degenerate with $m_{H^\pm}$, this being a consequence of the decoupling limit as

$$m_{h_4^0}, m_{h_5^0} \sim m_{H^\pm} + \mathcal{O}\left(\frac{\eta^2}{m_{H^\pm}}\right) \tag{3.23}$$

Concerning the predominantly singlet particles shown in table 3.1, the condition (3.16) affects the 6×6 tree-level squared mass matrix (see appendix C). The matrix elements representing the mixing between the two doublet Higgs fields H_1 and H_2 and the singlet one N become negligible compared to the remaining matrix elements. This means that the eigenstates for these particles are nearly independent of H_1 and H_2. The decoupling limit (3.16) produces the separation in terms of masses between the heavy Higgs particles and the light ones, which provide the effective SM spectrum, and at the same time decouples the doublet Higgs fields and the singlet one. To illustrate this, we provide a numerical example in the different CP-violating regimes shown in table 3.1. To satisfy (3.16) we fix $m_{H^\pm} = 2\ TeV$ and after fixing $\tan\beta = 2.7$ the maximum on $m_{h_1^0}$ saturates when $x \sim 1\ TeV$. Then we express the normalized eigenvectors for the six particle states in the usual basis $\{H_1, H_2, N\}$. With reference to the notation of table 3.1 with $\theta_1 = \theta_3 = 10^{-3}\ rad$ we get the results shown in table 3.2. According to table 3.1, because of the small CP-violating regime, the mass eigenstates are nearly CP-eigenstates. The

	mass (GeV)	H_1	H_2	N
G^0	0	$0.000 - i\ 0.347$	$0.000 + i\ 0.938$	$0.000 + i\ 0.000$
h_1^0	0.54	$0.000 + i\ 0.059$	$0.000 + i\ 0.022$	$0.000 + i\ 0.998$
h_2^0	136	$-0.348 + i\ 0.000$	$-0.937 + i\ 0.000$	$0.033 + i\ 0.000$
h_3^0	657	$-0.014 + i\ 0.000$	$0.040 + i\ 0.000$	$0.999 + i\ 0.000$
h_4^0	2002	$0.937 + i\ 0.000$	$-0.347 + i\ 0.000$	$0.028 + i\ 0.000$
h_5^0	2005	$0.000 - i\ 0.936$	$0.000 - i\ 0.347$	$0.000 + i\ 0.063$

Table 3.2: *The components of the Higgs fields H_1, H_2 and N entering in the eigenstates of the Higgs spectrum fixing $\theta_1 = \theta_3 = 10^{-3}$ rad, $\tan\beta = 2.7$ and $m_{H^\pm} = 2$ TeV. Maximising $m_{h_1^0}$ we find $x \sim 1$ TeV.*

results shown in the table refering to the doublets are confirmed by the eigenvectors (3.20) and (3.22). In particular (3.20) for G^0 and h_2^0 gives $\tan\beta = \frac{0.938}{0.347} \simeq 2.7$ and $\theta_1 = 10^{-3}\ rad$ as expected. Using the eigenvectors (3.22) since h_4^0 is real and h_5^0 is imaginary, we have $\alpha = 0$.

In table 3.3 are shown the same results as table 3.2, but fixing $\theta_1 = \theta_3 = 1\ rad$. In this case, as expected in the large CP-violating regime, the eigenstates are not exact CP eigenstates. Nonetheless, the singlet/doublet nature of each particle confirms the decoupling of H_1 and H_2 from N. (3.20) applied to G^0 and h_1^0 confirms $\tan\beta \simeq 2.7$ and $\theta_1 = 1\ rad$ and (3.22) leads to $\alpha \simeq 0.316\ rad$.

To complete the picture, we go back to the neutral Higgs spectrum in the CP-conserving case. In figure 3.19 is plotted the neutral Higgs spectrum as a function of the mass of the charged Higgs particle $m_{H^\pm}$. In these plots, the CP-even lightest Higgs boson shows the usual upper bound. The remaining particle masses can be divided in two pairs. The masses

	mass (GeV)	H_1	H_2	N
G^0	0	$0.292 - i\ 0.188$	$0.000 + i\ 0.938$	$0.000 + i\ 0.000$
h_1^0	136	$-0.188 - i\ 0.292$	$-0.938 + i\ 0.000$	$0.001 + i\ 0.003$
h_2^0	410	$-0.023 - i\ 0.017$	$0.009 + i\ 0.004$	$0.816 - i\ 0.577$
h_3^0	501	$-0.039 + i\ 0.052$	$-0.005 + i\ 0.023$	$0.576 + i\ 0.814$
h_4^0	2002	$0.726 + i\ 0.592$	$-0.330 - i\ 0.108$	$0.023 - i\ 0.019$
h_5^0	2006	$0.591 - i\ 0.725$	$0.108 - i\ 0.329$	$0.041 + i\ 0.055$

Table 3.3: *The components of the Higgs fields H_1, H_2 and N entering in the eigenstates of the Higgs spectrum fixing $\theta_1 = \theta_3 = 1\ rad$, $\tan\beta = 2.7$ and $m_{H^\pm} = 2\ TeV$. Maximising $m_{h_1^0}$ we find $x \sim 1\ TeV$.*

$m_{h_2^0}$ and $m_{h_3^0}$, of the first pair, range from around 150 GeV up to 1 TeV showing a rather random pattern; they divide into one CP-even and one CP-odd state and both are singlet dominated. The second pair of neutral particles are, like in the CP-violating regime, nearly degenerate with $m_{H^\pm}$ and the eigenstates are dominantly doublet (H_1). Unsurprisingly, they have opposite CP parity. The physical eigenstates are summarised in the table 3.4; after comparison with table 3.1 we can see that the Higgs field components remain unchanged. Finally in table 3.5 is shown the analysis of the eigenvectors. As expected, every particle corresponds to an exact CP state and as a consequence of the decoupling limit the two lightest eigenvalues provide the effective SM Higgs particles remaining completely uncoupled to the singlet vev x.

G^0	doublet (H_2)	CP-odd
h_1^0	doublet (H_2)	CP-even
h_2^0	singlet	CP-odd
h_3^0	singlet	CP-even
h_4^0	doublet (H_1)	CP-odd
h_5^0	doublet (H_1)	CP-even

Table 3.4: *Nature of the neutral Higgs spectrum particles in the CP-conserving case.*

	mass (GeV)	H_1	H_2	N
G^0	0	$0.000 - i\ 0.347$	$0.000 + i\ 0.938$	$0.000 + i\ 0.000$
h_1^0	136	$0.347 + i\ 0.000$	$0.938 + i\ 0.000$	$0.000 + i\ 0.000$
h_2^0	396	$0.040 + i\ 0.000$	$-0.015 + i\ 0.000$	$0.999 + i\ 0.000$
h_3^0	1168	$0.000 + i\ 0.015$	$0.000 + i\ 0.006$	$0.000 + i\ 0.999$
h_4^0	2001	$0.000 + i\ 0.938$	$0.000 + i\ 0.347$	$0.000 + i\ 0.016$
h_5^0	2003	$0.938 + i\ 0.000$	$0.347 + i\ 0.000$	$0.043 + i\ 0.000$

Table 3.5: *The components of the Higgs fields H_1, H_2 and N entering in the eigenstates of the Higgs spectrum in the CP-conserving case with $\tan\beta = 2.7$ and $m_{H^\pm} = 2\ TeV$. Maximising $m_{h_1^0}$ we find $x \sim 1\ TeV$.*

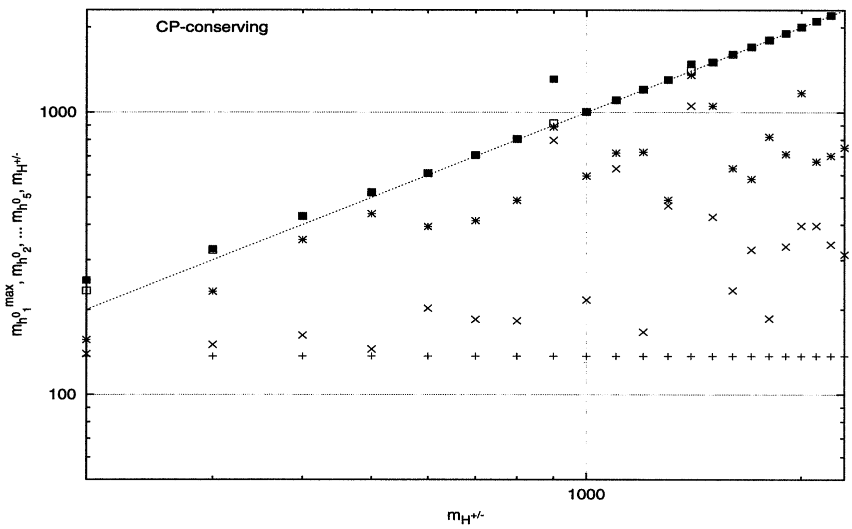

Figure 3.19: *Plots of the Higgs spectrum in the CP-conserving case: $\theta_1 = \theta_3 = 0$. $M_S = 1$ TeV and the maximization has been performed on the lightest mass $m_{h_1^0}$.*

Chapter 4

Renormalization group analysis

4.1 Introduction

In the previous chapters studying the neutral Higgs spectrum, with and without CP conservation, we focused our attention on the upper bound on the lightest Higgs boson mass. Performing this task many parameters entering in the effective potential were selected in such a way as to raise as much as possible the upper bound on m_{h^0}. The only constrained parameters were the dimensionless constants λ_i (with $i = 1, 2, 3$) related to the gauge coupling constants of the groups $U(1)$ and $SU(2)$ through the boundary conditions (1.21). Furthermore using the minimization conditions imposed on the effective potential assuming the *Electroweak Symmetry Breaking (ESB)*, we were able to eliminate some of the parameters, the number of these depending on whether or not CP conservation was imposed.

In this chapter we want to use the RG equations to obtain a relevant set of parameters entering in the neutral Higgs spectrum of the $NMSSM$ at the electroweak scale. The electroweak solutions of this set of differential equations can be calculated once a set of boundary conditions is introduced at a very high scale called M_X. Although the low energy scale solutions of a general set of differential equations depend on such boundary conditions, the RG equations represent a special class of these for which it is possible to have low energy scale solutions concentrated in a narrow space, to a large extent independent of the boundary conditions. These are the so called *InfraRed Quasi Fixed Points (IRQFP)*.

$MSSM$ investigations based on the $IRQFP$ of the RG equations have been made [40]-[41]. The stable RG-equations solutions determining $\tan\beta \simeq 1.8$ correspond to an upper bound on the lightest Higgs boson mass of (94 ± 5) GeV. From the existing $LEPII$ data based on the mass m_t^{pole} (see eq. (2.20)) the mass $m_{h^0} \gtrsim 113$ GeV for low $\tan\beta$ [29]. This rules out the RG-based $MSSM$ in the low $\tan\beta$ limit. In the case of large $\tan\beta$ ($\tan\beta \sim 60$) the RG analysis shows that the $MSSM$ $IRQFP$ is still consistent with the experimental data as $m_{h^0} \leq (125 \pm 5)$ GeV [41]-[42] .

In this chapter we are going to study the properties of the RG equations of the general Z_3-breaking $NMSSM$ in our usual low $\tan\beta$ regime.

4.2 The set of RG equations

The set of RG-equations used in our analysis is given in Appendix A. The methods commonly adopted to determine the RG equations are based on two renormalisation schemes: *dimensional reduction (DRED)* and *dimensional regularization (DREG)*. $DREG$ violates supersymmetry and the RG equations we use are determined using the $DRED$ with modified minimal subtraction ($\overline{DR}$). In Appendix A the set of RG equations used are calculated at one-loop order. For the purposes of this work they are accurate enough and at this level they are scheme independent[1] [5].

The RG-equations of Appendix A consist of 17 differential equations combined, each one integrating the respective β-function from a high scale M_X down to the electroweak scale m_t. The first six equations describe the dimensionless parameters and can be split into two significant groups of three equations each. The first group (see eqs. (A.1)-(A.3)) involves the RG-equations for g_1, g_2 and g_3, respectively the gauge coupling constants of the groups $U(1)_Y$, $SU(2)_L$ and $SU(3)_C$. The second three RG-equations (see eqs. (A.4)-(A.6)) concern respectively the top Yukawa coupling h_t introduced in eq. (2.1), and the two Higgs fields couplings λ and k entering in the superpotential (1.36). As previously mentioned, because we have been interested in the upper bound on the lightest Higgs boson mass and we limited our study to the region where $\tan\beta \lesssim 10$, we can neglect the contribution due to any particle/sparticle except those belonging to the up-type third generation of quark/squark. Because of this, together with the RG-equation of the top Yukawa coupling h_t, we

[1] For a general discussion about the RG equations and the methods to evaluate them see reference [43] and references included therein.

need to solve the RG-equations involving the soft masses entering into the definition of the stop squared mass matrix (2.28). Because all the remaining RG-equations are devoted to the soft $SUSY$ breaking terms, it is useful to write explicitly the soft part of the tree-level potential $V^{(0)}$

$$\begin{aligned} V^{soft} &= m_Q^2|\tilde{Q}|^2 + m_T^2|\tilde{t^c}|^2 \\ &+ m_{H_1}^2|H_1|^2 + m_{H_2}^2|H_2|^2 + m_N^2|N|^2 \\ &+ \frac{1}{2}(M_1\bar{\xi}_1\xi_1 + M_2\bar{\xi}_2\xi_2 + M_3\bar{\xi}_3\xi_3) \\ &- (h_tA_t\tilde{Q}H_2\tilde{t^c} + \lambda A_\lambda NH_1H_2 + \frac{1}{3}kA_kN^3 \\ &\quad -B\mu H_1H_2 + h.c.). \end{aligned} \tag{4.1}$$

In the first and the fourth line of V^{soft} we can see the squared masses m_Q^2, m_T^2 and A_t determining the entries of the mass matrix of the stops (2.28). In the second line we can see the terms containing the scalar masses squared $m_{H_1}^2$, $m_{H_2}^2$ and m_N^2. The remaining trilinear soft terms containing A_λ and A_k enter in the tree-level potential through the soft $SUSY$ breaking masses m_4 and m_5 as follows

$$m_4 = \lambda A_\lambda \ , \tag{4.2}$$

$$m_5 = kA_k \ . \tag{4.3}$$

In the third line of eq. (4.1) ξ_1, ξ_2 and ξ_3 are the gauginos corresponding to the $U(1)_Y$, $SU(2)_L$, $SU(3)_C$ gauge groups respectively. The gaugino masses M_1, M_2 and M_3 enter in most of the β-functions for the soft $SUSY$ breaking terms and the RG-equations for these masses will be discussed later. Finally in the last line of eq. (4.1), the term $-B\mu$ enters in the definition of the soft mass squared m_6^2. In particular from this soft term and from the superpotential (1.36) that defines the tree-level potential

(2.26) we have

$$m_6^2 = -B\mu + \lambda r , \quad (4.4)$$

$$m_7^2 = kr . \quad (4.5)$$

Clearly these two masses depend on r, μ and B which satisfy the *RG*-equations (A.17)-(A.19) and their infrared values will be discussed in section 4.2.4.

4.2.1 Unification of the gauge couplings constants

The idea of a fixed scale M_X, which represents the starting point for the *RG*-equation calculations of the parameters of an effective theory, relies on the well known unification in a *Grand Unified Theory (GUT)* of the gauge coupling constants g_1, g_2 and g_3. At the one-loop level the *RG* equations for these couplings are

$$\frac{d}{dt}g_i = \frac{1}{16\pi^2}c_i g_i^3 , \qquad i = 1, \dots, 3 , \quad (4.6)$$

where we recall the definition (2.17) $t = \log(Q/m_Z)$, and Q is the *RG* scale. Concerning the vector of the coefficients c_i, in the *SM* it is $c_i^{SM} = \left(\frac{41}{10}, -\frac{19}{6}, -7\right)$, while in the *NMSSM* it is $c_i^{NMSSM} = \left(\frac{33}{5}, 1, -3\right)$. The latter coefficient c_1 is expressed in a *GUT* normalisation, which is related with the non-*GUT* normalisation (see eq. (A.1)) by means of the relationship

$$g_1^{GUT} = \sqrt{\frac{5}{3}}g_1 . \quad (4.7)$$

The set of coefficients c_i^{NMSSM} is different from c_i^{SM} because of the extra particles typical of any supersymmetric model[2]. In figure 4.1 we plot

[2]The set of coefficients c_i^{NMSSM} is identical to the set in the *MSSM*.

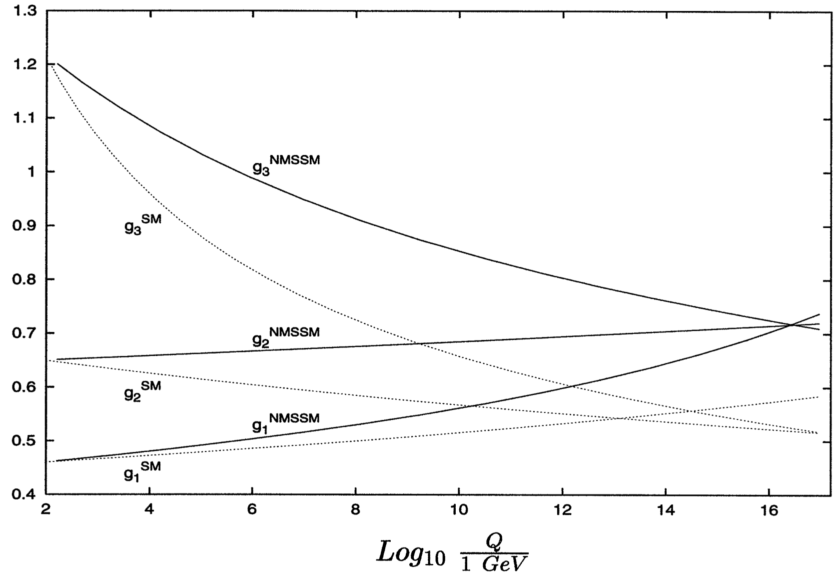

Figure 4.1: *RG evolution of the gauge couplings g_1 ($U(1)_Y$), g_2 ($SU(2)_L$) and g_3 ($SU(3)_C$), in the SM (dotted lines), and in the NMSSM (solid lines).*

the evolution of the coupling constants in the SM and in the $NMSSM$ according to eq. (4.6). In both cases, we can see the gauge coupling constants approaching to closer values as the RG scale increases but the unification occurs only in the latter case. In the supersymmetric case the unification occurs at a scale $M_X \sim 3 \times 10^{16}\ GeV$, and the common value $g_X \simeq 0.71$ is called the universal gauge coupling constant. While such unification of gauge couplings could be an accidental result, it may also be taken as a strong indication in favour of a GUT or of a superstring theory, both of which indeed predict gauge coupling unification below the Plank scale M_{Planck}. Based on this fact we are motivated to use the RG equations as a fundamental tool to determine the couplings and the soft masses of the effective potential at the electroweak scale, from which we determine the mass spectrum of the neutral Higgs bosons in the Z_3-

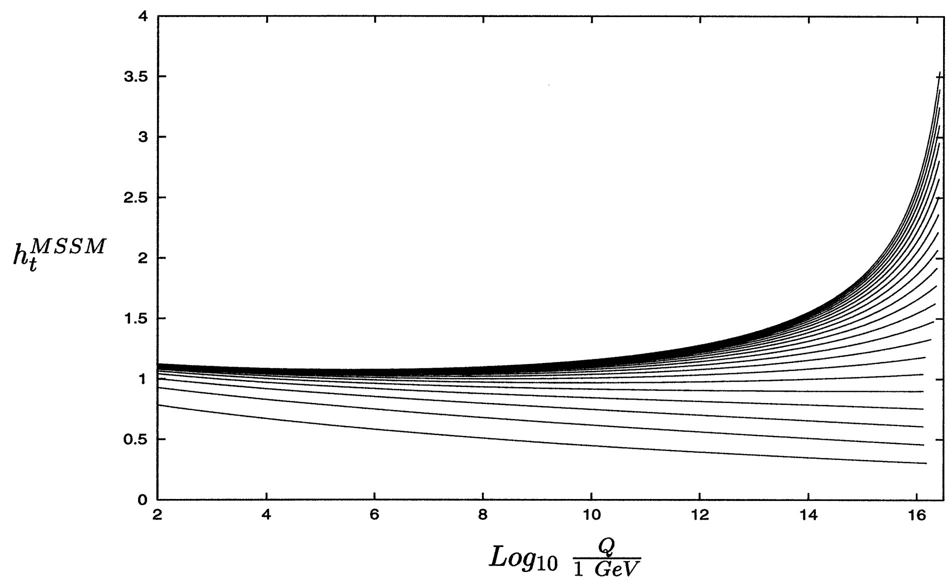

Figure 4.2: *Evolution of h_t versus t after setting $\lambda = k = 0$. In the $MSSM$ the $IRQFP$ limit is defined as the h_t line for which h_t has a Landau pole at the scale M_X.*

breaking $NMSSM$.

After finding the scale M_X it is possible to solve simultaneously all the RG equations of Appendix A governing the gauge coupling constants, the dimensionless Yukawa-type couplings and the soft masses of the model.

4.2.2 Yukawa couplings

Let us now analyse the β functions for the Yukawa couplings h_t, λ and k given in equations (A.4)-(A.6); these are:

$$16\pi^2 \frac{d}{dt} h_t = h_t \left(6h_t^2 + \lambda^2 - \frac{13}{9} g_1^2 - 3g_2^2 - \frac{16}{3} g_3^2 \right) , \tag{4.8}$$

$$16\pi^2 \frac{d}{dt} \lambda = \lambda \left(4\lambda^2 + 2k^2 + 3h_t^2 - g_1^2 - 3g_2^2 \right) , \tag{4.9}$$

$$16\pi^2 \frac{d}{dt} k = 6k \left(\lambda^2 + k^2 \right) . \tag{4.10}$$

The RG equations for λ and k are typical of the $NMSSM$. If we set $\lambda = k = 0$ then the right hand side of eq. (4.8) reduces to the β-function of h_t in the $MSSM$. In this case the study of h_t is easier because there is no dependence on λ and k. The $IRQFP$ for the top Yukawa coupling is defined as the IR value of h_t for which it has a Landau pole at the scale M_X. In other words h_t^{IRQFP} corresponds to the maximum value of $h_t(m_t)$ derived from the equation and allowed by perturbativity up to the scale M_X. Figure 4.2 shows that $h_t^{IRQFP} \simeq 1.12$, the different curves confirming the fact that the solutions in the neighbourhood of the QFP are independent or very weakly dependent on the value of $h_t^2(M_X)$.

More complicated is the situation when λ and k are non-zero in the RG equations. The three equations (4.8)-(4.10) now all depend on each other. We can tackle this more complex problem by fixing in turn λ, k and h_t and then analysing the low energy solutions in the plane of the other two parameters. We start by analysing solutions in the plane (k, h_t) using λ as an input parameter. Setting $\lambda = 0$ then eq. (4.8) does not depend on k and, and because in eq. (4.10) there is not any dependence on the three gauge coupling constants g_1, g_2 and g_3, these equations completely decouple. In figure 4.3 we can see the plots of the so-called Hill line of k versus h_t in four different cases. For each point on this line, the Yukawa coupling constants at the electroweak scale correspond to a Landau pole at the scale M_X [44]. The case $\lambda^2(M_X) = 0$ is shown in plot a, and the cases in which $\lambda^2(M_X) = 2.25, 5, 10$ are shown in plots b, c and d. The points plotted below the Hill line in the four cases indicate solutions for k and h_t at the electroweak scale with starting values such that $2 \leq k^2(M_X), h_t^2(M_X) \leq 10$. The Hill line sets a border line above which no solution without Landau poles can exist. On

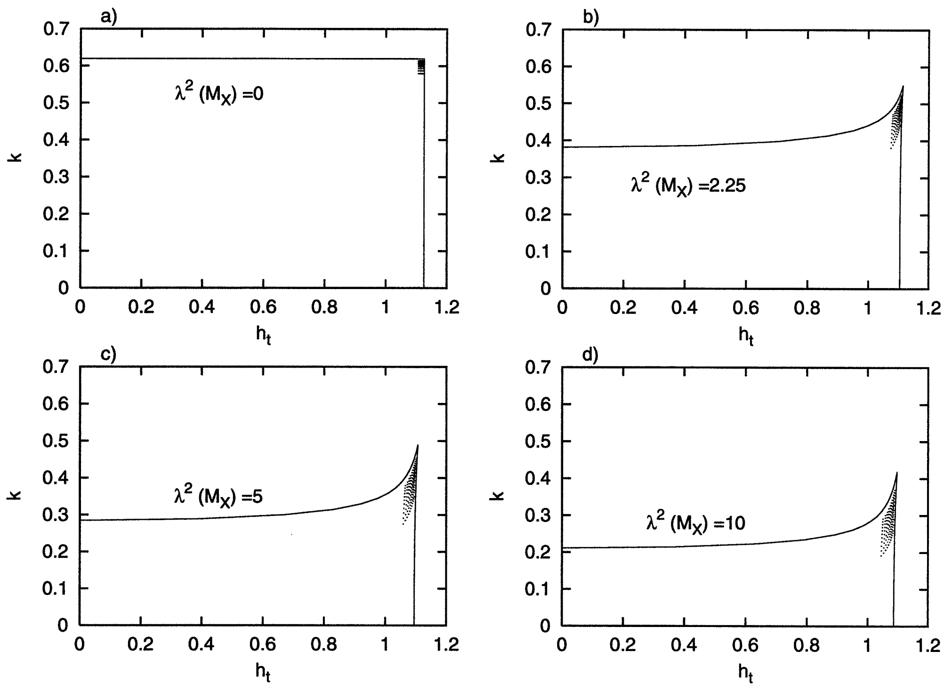

Figure 4.3: *Plot showing the Hill line in the plane (k,h_t) and selecting $\lambda^2(M_X) = 0, 2.25, 5, 10$; respectively shown in figures a, b, c, d. The points below the curve correspond to the solution for k and h_t satisfying the conditions (4.11).*

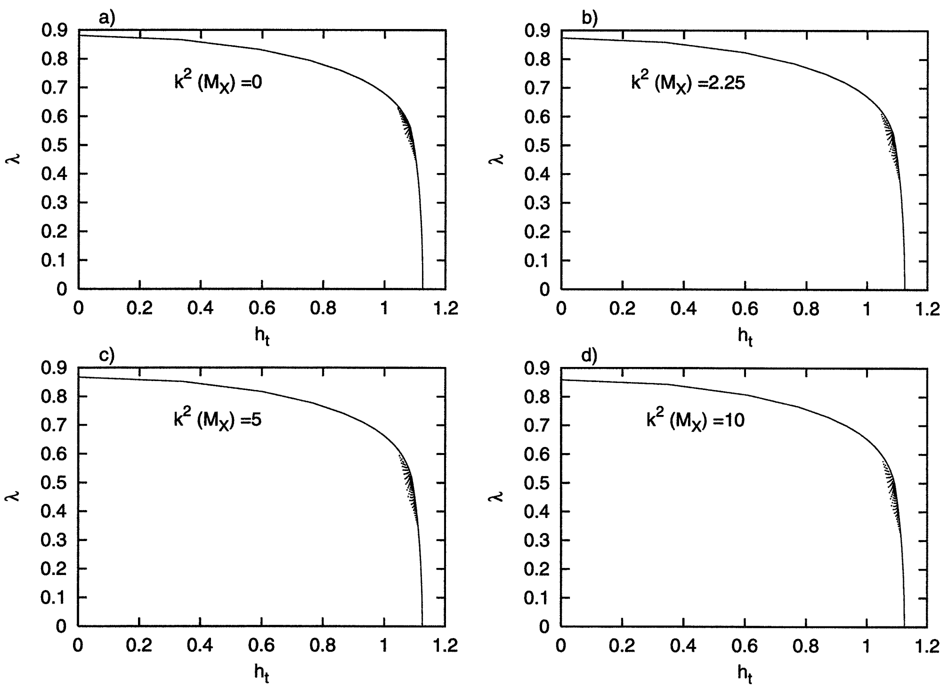

Figure 4.4: *Plot showing the Hill line in the plane (λ,h_t) and selecting $k^2(M_X) = 0, 2.25, 5, 10$; respectively shown in figures a, b, c, d. The points below the curve correspond to the solution for λ and h_t satisfying the conditions (4.11).*

the other hand the majority of the allowed solutions lying below this line are concentrated in the proximity of the highest value of the top Yukawa coupling. From the four cases plotted it is possible to recognize the relationship between λ and k already pictured in section 2.2, according to which increasing $\lambda(M_X)$ reduces $k(m_t)$ (see figures 2.1 and 2.2). This relationship does not appear obvious after looking at figure 4.4, where in analogy with the previous one, the plots show the Hill line in the plane (λ, h_t) after setting $k^2(M_X) = 0, 2.25, 5, 10$, in plots a, b, c and d respectively. The apparent weak dependence of $\lambda(m_t)$ on $k^2(M_X)$ in the four cases is due to the β-function of λ. Contrary to eq. (4.10), eq. (4.9) depends explicitly on h_t, and the further contributions $-g_1^2$ and $-3g_2^2$ keep the dependence on k smooth even in the limit $h_t \simeq 0$ [14]. As in the previous plots, we can see that for the input parameters satisfying the condition $2 \leq \lambda^2(M_X), h_t^2(M_X) \leq 10$, the solutions at the electroweak scale are concentrated below the Hill line where $h_t \lesssim h_t^{max}$. Finally figure 4.5 shows the RG analysis in the plane (λ, k) for the four different cases $h_t^2(M_X) = 0, 2.225, 5, 10$ in the plots a, b, c and d respectively. As usual the points below the plotted lines represent the solution at the electroweak scale of the RG equations corresponding to the starting values $2 \leq \lambda^2(M_X), k^2(M_X) \leq 10$. The distribution of these points is not as sharp as the cases observed in figures 4.3 and 4.4. However based on the latter plots, where the majority of the solutions are concentrated where h_t approaches its maximum, we conclude that the solutions of plot d in figure 4.5 represents the one in which to look for the $IRQFP$ for the three Yukawa couplings.

To help us to understand better the results of our analysis, it is appealing to summarize the results obtained in the plot of figure 4.6. The

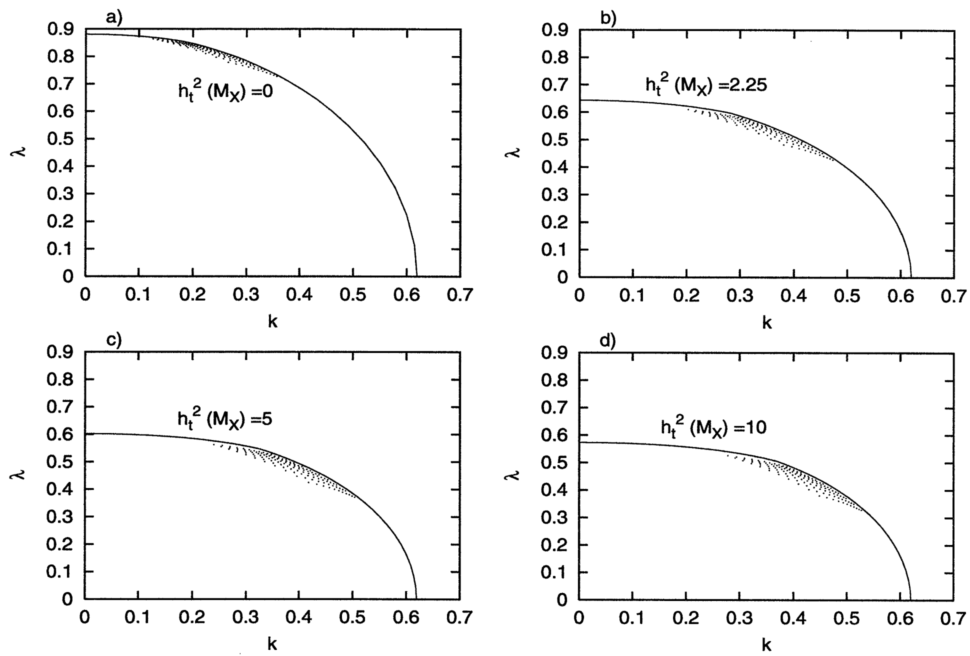

Figure 4.5: *Plot showing the Hill line in the plane (λ,k) and selecting $h_t^2(M_X) = 0, 2.25, 5, 10$; respectively shown in figures a, b, c, d. The points below the curve correspond to the solution for λ and k satisfying the conditions (4.11).*

surface represents the tridimensional generalisation of the Hill lines of figures 4.3-4.5 and the shaded area contains all those infrared solutions corresponding to the initial conditions

$$2 \leq h_t^2(M_X), \lambda^2(M_X), k^2(M_X) \leq 10 \ . \tag{4.11}$$

At the centre of this shaded area are the calculated $IRQFP$ values of the Yukawa coupling obtained by solving numerically the RG equations[3] (4.8)-(4.10):

$$h_t^{QFP} = 1.09 \ , \quad \lambda^{QFP} = 0.49 \quad \text{and} \quad k^{QFP} = 0.38 \ . \tag{4.12}$$

[3]The RG analysis shown is inspired by the analysis reported in reference [45], whose results concerning the $IRQFP$ values are confirmed by eq. (4.12).

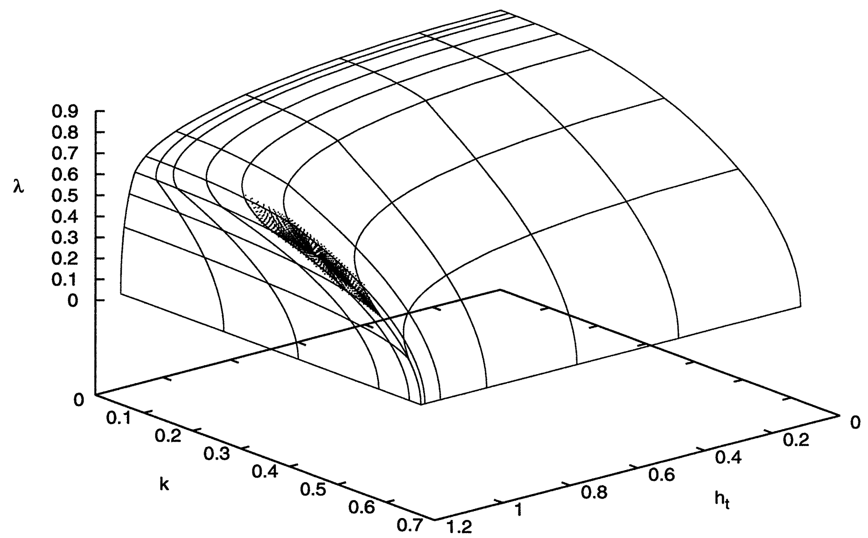

Figure 4.6: *Surface representing the Hill surface for the Yukawa coupling constants h_t, λ and k. The shaded corresponds to all the solutions for the Yukawa couplings at the electroweak scale satisfying the condition (4.11).*

In the following part of this thesis, we perform a RG analysis in the regime characterised by these $IRQFP$ solutions. Because of the choice of the input parameters (see conditions (4.11)) we can see that the Yukawa couplings satisfy the following conditions:

$$\frac{h_t^2(M_X)}{g_X^2} \gg 1 \ , \quad \frac{\lambda^2(M_X)}{g_X^2} \gg 1 \ , \quad \frac{k^2(M_X)}{g_X^2} \gg 1 \ , \tag{4.13}$$

which define the strong Yukawa coupling regime.

A comparison between the $IRQFP$ regime and the regime adopted in the previous chapters leads to some further considerations. In section 2.2 the Yukawa couplings were chosen with the aim of maximising m_{h^0}. Looking at the plots of figure 2.2 we can see that $\lambda_{max} \simeq 0.7$, corresponding to $k = 0$, was directly related to the value of $h_t(m_t) = 1.01 < h_t^{QFP}$. Although the inequality reveals a small relative difference between $h_t(m_t) = 1.01$ and $h_t(m_t) = h_t^{IRQFP}$, it has to be emphasized that a small change in the top Yukawa coupling can cause great differences in the dependent parameters: this is known as the *fine tuning problem* (see reference [46] and references included). The plots shown in figure 4.5 give an idea of the behaviour of λ and k with different values of $h_t^2(M_X)$.

Recalling the definition (1.10) we can recast eq. (2.3) at the electroweak scale as follows:

$$m_t^2 = h_t^2 \eta^2 \sin^2\beta \ . \tag{4.14}$$

From this and using the results found in the $IRQFP$ limit (see eq. (4.12)) we find $\tan\beta \simeq 1.82$. In this limit the maximum allowed value of λ corresponding to $k = 0$ is $\lambda_{max} \simeq 0.57$, which is well below the value $\lambda_{max} \simeq 0.7$ of section 2.2.

4.2.3 Soft $SUSY$ breaking terms

Continuing the description of the set of RG equations from Appendix A, we arrive at the group containing the β-functions describing the soft $SUSY$ breaking terms. Let us start with the equations referring to the soft trilinear terms. These are A_t, the off-diagonal entry of the squared mass matrix of the stops (see equations (2.7) and (2.28)), then A_λ and A_k introduced in eqs. (4.2) and (4.3) respectively. Recalling equations (A.7)-(A.9) we have:

$$\begin{aligned} 16\pi^2 \frac{d}{dt} A_t &= 12 h_t^2 A_t + 2\lambda^2 A_\lambda \\ &- 4\left(\frac{13}{18} g_1^2 M_1 + \frac{3}{2} g_2^2 M_2 + \frac{8}{3} g_3^2 M_3\right) , \end{aligned} \tag{4.15}$$

$$\begin{aligned} 16\pi^2 \frac{d}{dt} A_\lambda &= 8\lambda^2 A_\lambda - 4k^2 A_k + 6h_t^2 A_t \\ &- 2\left(g_1^2 M_1 + 3g_2^2 M_2\right) , \end{aligned} \tag{4.16}$$

$$16\pi^2 \frac{d}{dt} A_k = 12\left(k^2 A_k - \lambda^2 A_\lambda\right) , \tag{4.17}$$

where M_1, M_2 and M_3 are the gaugino masses.

The remaining five RG equations are those describing the evolution of the scalar squared masses:

$$\begin{aligned} 16\pi^2 \frac{d}{dt} m_Q^2 &= 2h_t^2\left(m_Q^2 + m_{H_2}^2 + m_T^2 + A_t^2\right) \\ &- 8\left(\frac{1}{36} g_1^2 M_1^2 + \frac{3}{4} g_2^2 M_2^2 + \frac{4}{3} g_3^2 M_3^2\right) , \end{aligned} \tag{4.18}$$

$$\begin{aligned} 16\pi^2 \frac{d}{dt} m_T^2 &= 4h_t^2\left(m_Q^2 + m_{H_2}^2 + m_T^2 + A_t^2\right) \\ &- 8\left(\frac{4}{9} g_1^2 M_1^2 + \frac{4}{3} g_3^2 M_3^2\right) , \end{aligned} \tag{4.19}$$

$$\begin{aligned} 16\pi^2 \frac{d}{dt} m_{H_1}^2 &= 2\lambda^2\left(m_{H_1}^2 + m_{H_2}^2 + m_N^2 + A_\lambda^2\right) \\ &- 8\left(\frac{1}{4} g_1^2 M_1^2 + \frac{3}{4} g_2^2 M_2^2\right) , \end{aligned} \tag{4.20}$$

$$\begin{aligned} 16\pi^2 \frac{d}{dt} m_{H_2}^2 &= 6h_t^2\left(m_Q^2 + m_{H_2}^2 + m_T^2 + A_t^2\right) + 2\lambda^2\left(m_{H_1}^2 + m_{H_2}^2 + m_N^2 + A_\lambda^2\right) \\ &- 8\left(\frac{1}{4} g_1^2 M_1^2 + \frac{3}{4} g_2^2 M_2^2\right) , \end{aligned} \tag{4.21}$$

$$16\pi^2 \frac{d}{dt} m_N^2 = 4\lambda^2\left(m_{H_1}^2 + m_{H_2}^2 + m_N^2 + A_\lambda^2\right) + 4k^2\left(3m_N^2 + A_k^2\right) . \tag{4.22}$$

The first two β-functions refer to the on-diagonal entries of the squared stop mass matrix of equations (2.7) and (2.28), while the last three involve the β-functions describing the evolution of the squared soft masses $m_{H_1}^2$, $m_{H_2}^2$ and m_N^2 of the Higgs fields H_1, H_2 and N respectively. Like equations (A.7)-(A.9) concerning the soft terms A_i, the last five equations are also related to the gaugino masses M_i (with $i = 1, 2, 3$). Before proceeding to the integration of the β-functions, it is necessary to focus our attention on how these masses evolve with the RG scale. It turns out that the RG equations for the gaugino masses at one-loop level are:

$$16\pi^2 \frac{d}{dt} M_i = 2c_i g_i^2 M_i \ , \qquad i = 1, \ldots, 3 \ . \tag{4.23}$$

The form of these equations makes the evolution of M_i identical to the evolution of g_i^2, which allows us to write the relationship:

$$\frac{M_i(Q)}{M_{\frac{1}{2}}} = \frac{g_i^2(Q)}{g_X^2} \ , \tag{4.24}$$

at any scale Q between m_t and M_X. $M_{\frac{1}{2}}$ is the universal gaugino mass. The last relationship introduces the important issue of the boundary conditions for equations (4.15)-(4.22) at the scale M_X. These are assumed to satisfy *universality*, that translates into:

$$g_1^2(M_X) = g_2^2(M_X) = g_3^2(M_X) = g_X^2 \ , \tag{4.25}$$

$$M_1(M_X) = M_2(M_X) = M_3(M_X) = M_{1/2} \ , \tag{4.26}$$

$$A_t(M_X) = A_\lambda(M_X) = -A_k(M_X) = A_0 \ , \tag{4.27}$$

$$m_i^2(M_X) = m_0^2 \ , \tag{4.28}$$

where in the last line $i = H_1, H_2, N, Q, T$, and the convention used in our work follows the one of reference [22]. The universality gives the advantage of reducing the number of independent parameters by expressing them in terms of only three: $M_{1/2}$, A_0 and m_0^2. Thanks to this hypothesis, the β-functions (4.18)-(4.22) appear in the simplest possible form [22]. Beside this technical issue, the choice of universality makes it possible to avoid unwanted *flavor changing neutral current (FCNC)* in the low energy $SUSY$ phenomenology.

Performing the RG analysis of the A_i and the m_i^2, we study the be-

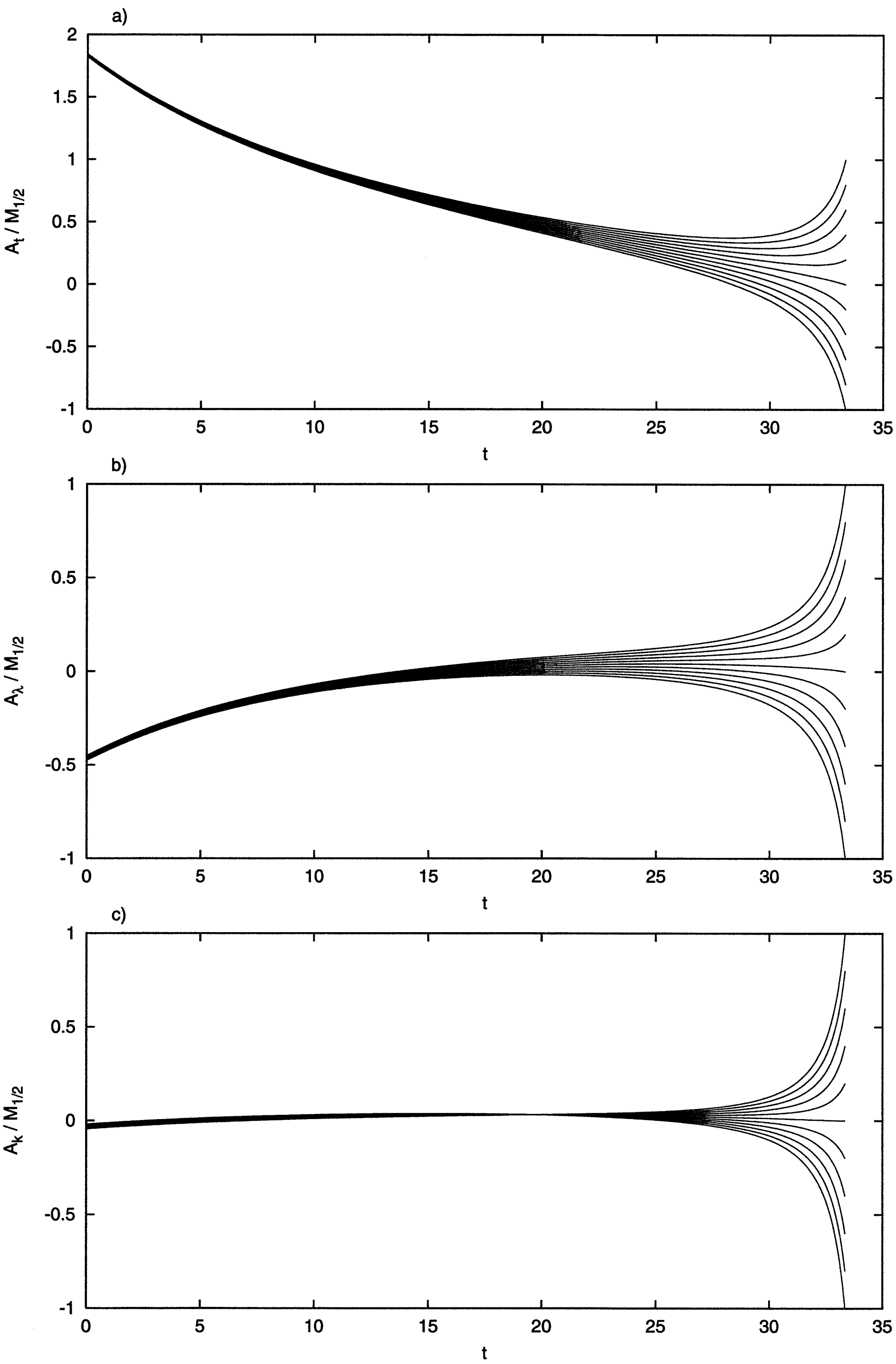

Figure 4.7: *Evolution of $A_t/M_{1/2}$, $A_\lambda/M_{1/2}$ and $A_k/M_{1/2}$ versus t (figures a, b and c respectively) and assuming $h_t^2(M_X) = \lambda^2(M_X) = k^(M_X) = 10$. The parameter A_0 is set to vary in the renge $-M_{1/2} < A_0 < M_{1/2}$.*

haviour focusing on the $IRQFP$ for the Yukawa couplings. The most natural thing to do is to check if these are compatible with QFP solutions for equations (4.15)-(4.22). What turns out is that the strong Yukawa coupling limit, and of course at the $IRQFP$, is the only regime for which the entire set of equations, or some linear combinations of these, have simultaneously $IRQFP$ solutions. Then we fixed $h_t^2(M_X)$, $\lambda^2(M_X)$ and $k^2(M_X)$ in such a way as to obtain the $IRQFP$ values (4.12) after the numerical integrations have been performed.

Let us start with the results concerning the trilinear terms A_i. In figure 4.7 plots a, b and c, referring respectively to A_t, A_λ and A_k expressed in units of the universal gaugino mass $M_{\frac{1}{2}}$, show the evolution of the A_i versus t. At the electroweak scale m_t the three terms show a QFP; these are

$$\left(\frac{A_t}{M_{\frac{1}{2}}}\right)^{QFP} \simeq 1.73 \ , \tag{4.29}$$

$$\left(\frac{A_\lambda}{M_{\frac{1}{2}}}\right)^{QFP} \simeq -0.43 \ , \tag{4.30}$$

$$\left(\frac{A_k}{M_{\frac{1}{2}}}\right)^{QFP} \simeq -0.033 \ . \tag{4.31}$$

The three plots show a weak dependence on the universal trilinear soft term A_0, while their values at the electroweak scale depend entirely on the choice of $M_{1/2}$. This choice will be an important issue in calculating the neutral Higgs spectrum at the electroweak scale.

Analysing the infrared behaviour of the RG-equations involving the β-functions of m_i^2, we observe that they can be expressed in terms of the linear combinations:

$$\mathfrak{M}_t^2 = m_Q^2 + m_T^2 + m_{H_2}^2 \ , \tag{4.32}$$

$$\mathfrak{M}_\lambda^2 = m_{H_1}^2 + m_{H_2}^2 + m_N^2 \ , \tag{4.33}$$

$$\mathfrak{M}_k^2 = 3m_N^2 \ . \tag{4.34}$$

In fact we can recast the RG equations (4.18)-(4.22) in terms of these variables and obtain the three RG equations in the following form:

$$16\pi^2 \frac{d}{dt} \mathfrak{M}_t^2 = 12h_t^2 \left(\mathfrak{M}_t^2 + A_t^2\right) + 2\lambda^2 \left(\mathfrak{M}_\lambda^2 + A_\lambda^2\right) \tag{4.35}$$

$$- 8 \left(\frac{13}{18} g_1^2 M_1^2 + \frac{3}{2} g_2^2 M_2^2 + \frac{8}{3} g_3^2 M_3^2\right) \ , \tag{4.36}$$

$$\begin{aligned} 16\pi^2 \frac{d}{dt} \mathfrak{M}_\lambda^2 &= 6h_t^2 \left(\mathfrak{M}_t^2 + A_t^2\right) + 8\lambda^2 \left(\mathfrak{M}_\lambda^2 + A_\lambda^2\right) \\ &- 8 \left(\frac{1}{2} g_1^2 M_1^2 + \frac{3}{2} g_2^2 M_2^2\right) \ , \end{aligned} \tag{4.37}$$

$$16\pi^2 \frac{d}{dt} \mathfrak{M}_k^2 = 12\lambda^2 \left(\mathfrak{M}_\lambda^2 + A_\lambda^2\right) + 12k^2 \left(\mathfrak{M}_k^2 + A_k^2\right) \ . \tag{4.38}$$

The reason we perform the analysis in terms of $\mathfrak{M}_t^2$, $\mathfrak{M}_\lambda^2$ and $\mathfrak{M}_k^2$ lies in the fact that it is possible to find $IRQFP$ solutions for these combinations of soft masses . As we have seen for the trilinear terms A_i, the strong Yukawa coupling regime is compatible with the following $IRQFP$ values for the masses (4.32)-(4.34):

$$\left(\frac{\mathfrak{M}_t^2}{M_{\frac{1}{2}}^2}\right)^{IRQFP} \simeq 6.5 \ , \tag{4.39}$$

$$\left(\frac{\mathfrak{M}_\lambda^2}{M_{\frac{1}{2}}^2}\right)^{IRQFP} \simeq -2.56 \ , \tag{4.40}$$

$$\left(\frac{\mathfrak{M}_k^2}{M_{\frac{1}{2}}^2}\right)^{IRQFP} \simeq 0.29 \ . \tag{4.41}$$

Figure 4.8 shows the evolution of the soft squared masses $\mathfrak{M}_t^2$, $\mathfrak{M}_\lambda^2$ and $\mathfrak{M}_k^2$, in the plots a, b and c respectively, expressed in units of $M_{1/2}$. The plots are shown versus t and we set $A_0 = 0$. Because these soft masses have $IRQFP$s their values are independent of m_0^2. In figures 4.9 and 4.10 the plots show the evolutions of the $\mathfrak{M}_i^2$ assuming the initial condition $A_0 = -M_{1/2}$ and $A_0 = M_{1/2}$ respectively. The nicest property of the $IRQFP$ scenario is to allow us to greatly reduce the number of independent variables. Another important issue related to the $IRQFP$ solutions of the RG equations is the possibility to obtain the radiative electroweak symmetry breaking when the soft parameter are used to evaluate the effective potential. These two results have significant consequences when one tries to calculate the mass spectrum of the neutral Higgs particles in the $NMSSM$.

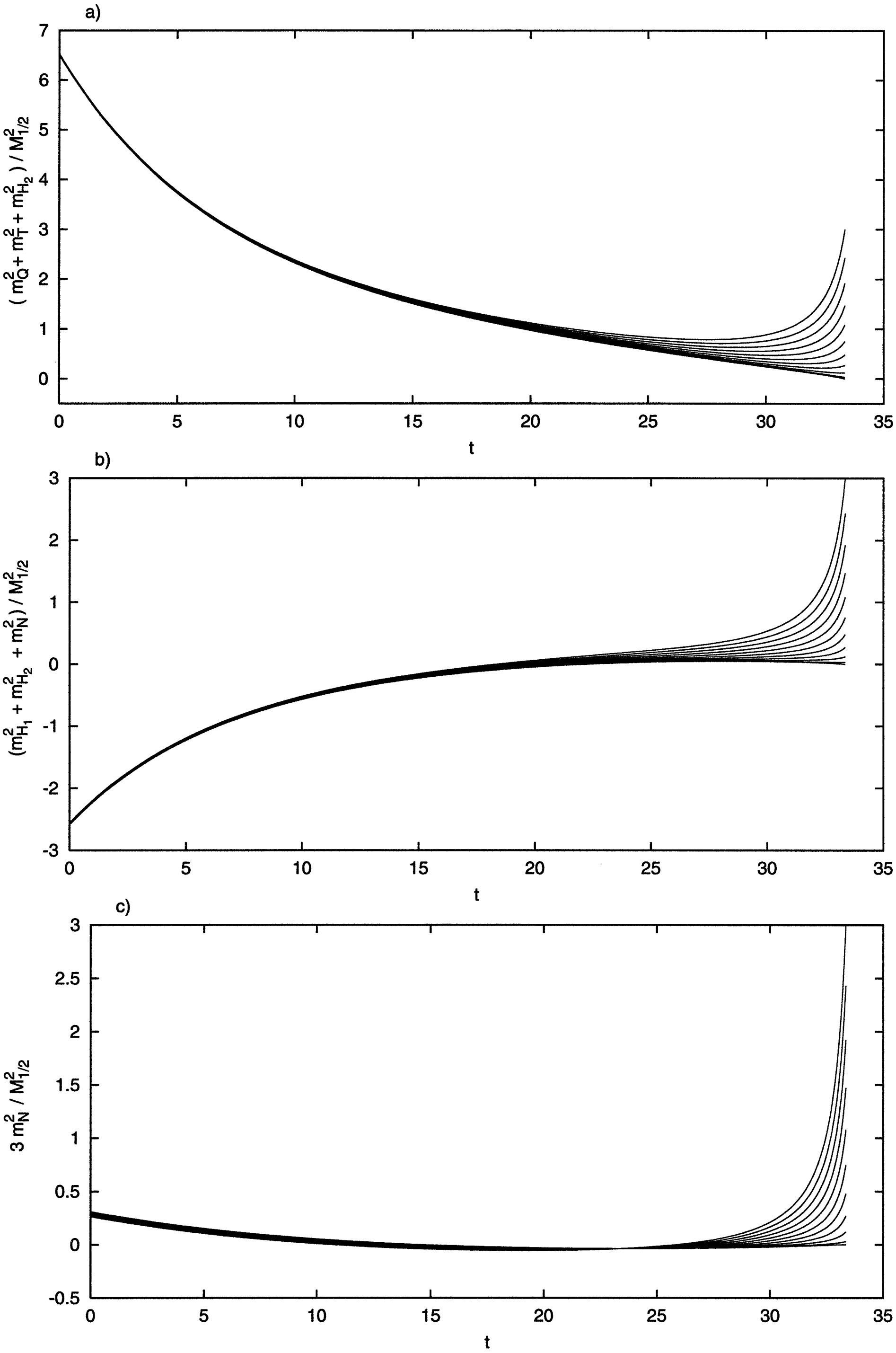

Figure 4.8: *Evolution of $\mathfrak{M}_t^2/M_{1/2}^2$, $\mathfrak{M}_\lambda^2/M_{1/2}^2$ and $\mathfrak{M}_k^2/M_{1/2}^2$ versus t (figures a, b and c respectively) and assuming $h_t^2(M_X) = \lambda^2(M_X) = k^{(}M_X) = 10$. We fix $A_0 = 0$ and m_0^2 is set to vary in the range $0 < m_0^2 < M_{1/2}^2$.*

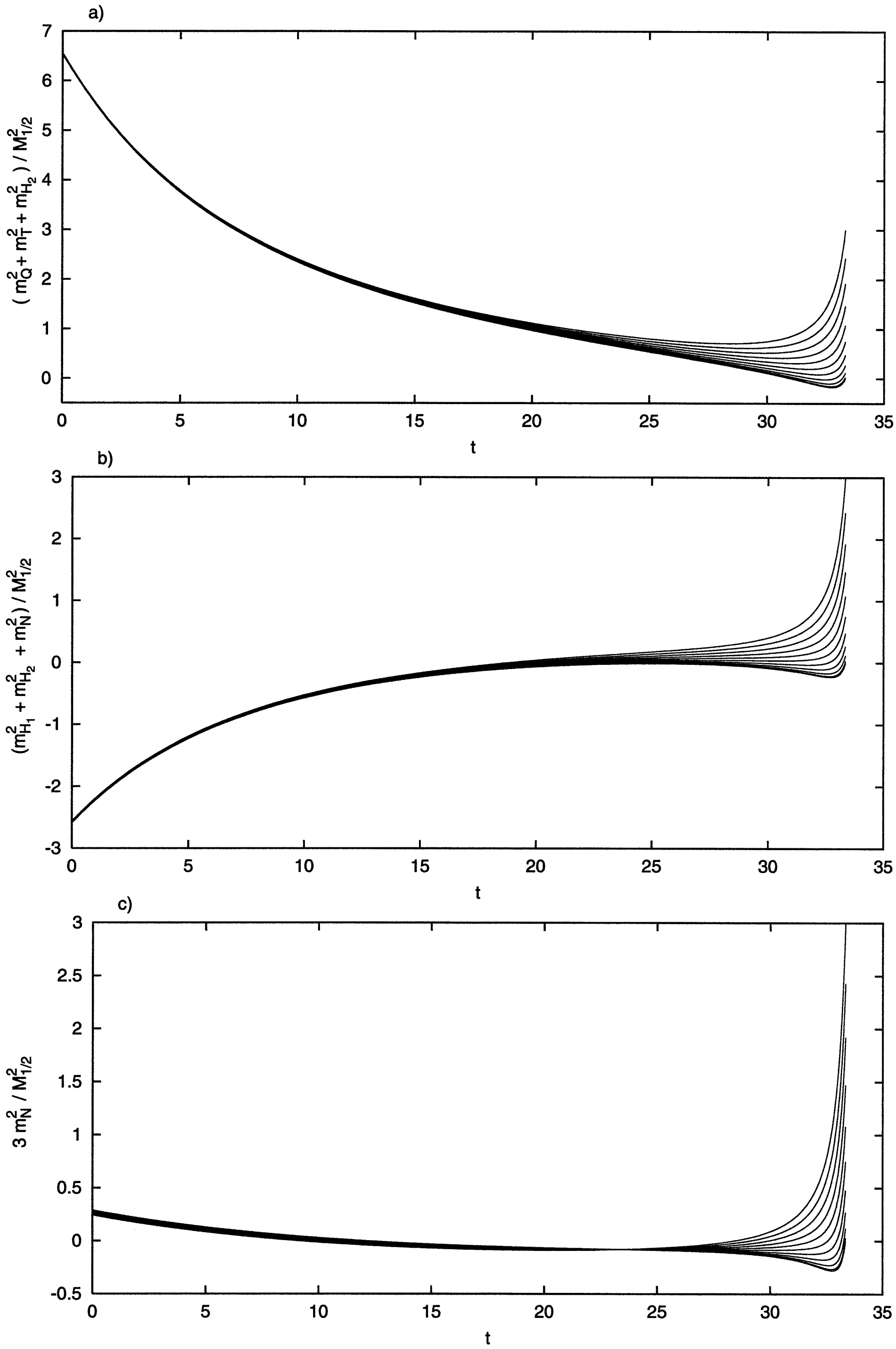

Figure 4.9: *Evolution of $\mathfrak{M}_t^2/M_{1/2}^2$, $\mathfrak{M}_\lambda^2/M_{1/2}^2$ and $\mathfrak{M}_k^2/M_{1/2}^2$ versus t (figures a, b and c respectively) and assuming $h_t^2(M_X) = \lambda^2(M_X) = k^{(}M_X) = 10$. We fix $A_0 = -M_{1/2}$ and m_0^2 is set to vary in the range $0 < m_0^2 < M_{1/2}^2$.*

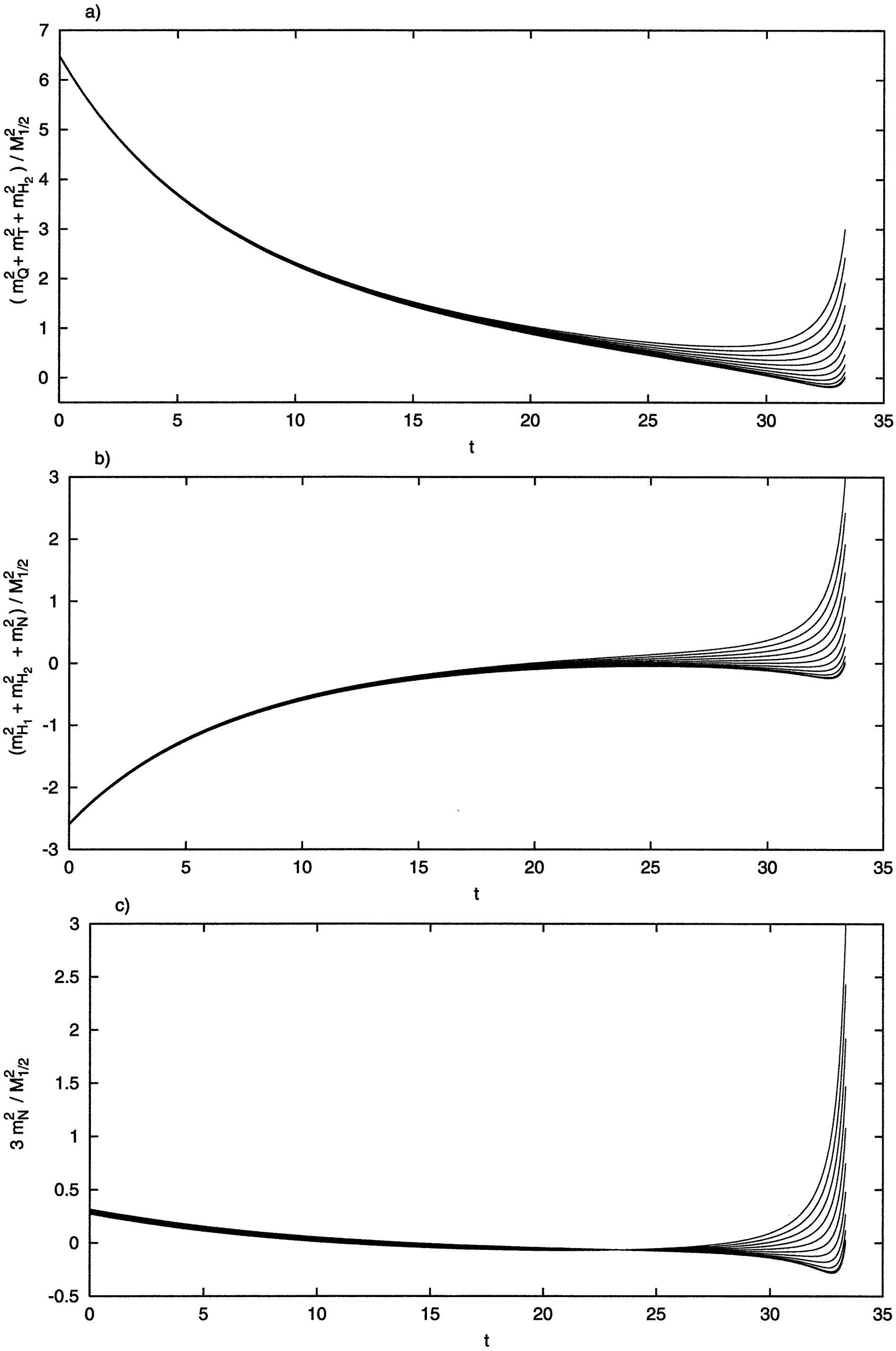

Figure 4.10: *Evolution of $\mathfrak{M}_t^2/M_{1/2}^2$, $\mathfrak{M}_\lambda^2/M_{1/2}^2$ and $\mathfrak{M}_k^2/M_{1/2}^2$ versus t (figures a, b and c respectively) and assuming $h_t^2(M_X) = \lambda^2(M_X) = k^{(}M_X) = 10$. We fix $A_0 = M_{1/2}$ and m_0^2 is set to vary in the range $0 < m_0^2 < M_{1/2}^2$.*

4.2.4 Three more equations: Z_3 breaking terms

In the previous sections we introduced the set of RG-equations for the traditional $NMSSM$. On the other hand equations (4.15)-(4.22) represent also part of the RG equations of the Z_3-breaking $NMSSM$. As we already had the opportunity to notice in the tree-level potential of eq. (1.37), this most general model introduces three new terms:

$$\mu\,, \quad m_6^2 \quad , m_7^2\,, \tag{4.42}$$

where μ is the mass factor that multiplies H_1 and H_2 in the superpotential (1.36) while m_6^2 and m_7^2 are defined in eqs. (4.4) and (4.5) respectively. m_7^2 is proportional to r: the (mass)^2 factor of the linear term in the field N. m_6^2 is the generalisation of the $MSSM$ term m_{12}^2 introduced in the tree-level potential (1.6). Then to complete the set of RG equations for the general $NMSSM$ we have the additional three equations

$$\begin{aligned} 16\pi^2\frac{d}{dt}\mu &= \mu\left(\frac{3}{2}h_t^2+\lambda^2+k^2-\frac{1}{2}g_1^2-\frac{3}{2}g_2^2\right)\,, && (4.43)\\ 16\pi^2\frac{d}{dt}r &= r\left(\lambda^2+k^2\right)\,, && (4.44)\\ 16\pi^2\frac{d}{dt}B &= 2\lambda^2B+3h_t^2A_t+2\lambda^2A_\lambda+g_1^2M_1+3g_2^2M_2\,. && (4.45)\end{aligned}$$

The treatment of these three equations is different compared to the ones of the previous sections. μ and r are soft parameters but they do not break supersymmetry because they appear in the superpotential. B is a soft $SUSY$ breaking parameter, but it is neither a trilinear parameter or a soft squared scalar mass parameter, B is a soft bilinear parameter. At the input scale we have:

$$B(M_X) = B_0 . \tag{4.46}$$

$$\mu(M_X) = \mu_0 . \tag{4.47}$$

$$r(M_X) = r_0 . \tag{4.48}$$

We have analysed the infrared behaviour of the β-functions in (4.43)-(4.45). Our main result is that there is not any QFP: the solutions of the RG equations show a strong dependence on the universal trilinear soft parameter A_0 in any regime of the Yukawa couplings h_t, λ and k. One might think this would cause some difficulties determining the Higgs mass matrix because still some of the parameters remain unknown. However this uncertainty will be eliminated in the next chapter, where the first derivative minimisation conditions on the effective potential are used to fix these three parameters, allowing us at the same time to have a local minimum in the effective potential.

Chapter 5

Higgs spectrum at the $IRQFP$

5.1 Introduction

The RG analysis made in the last chapter led to the interesting results represented by the $IRQFP$ scenario in the general $NMSSM$ after the assumption of universality made in eqs. (4.25)-(4.28). These include stable solutions for the Yukawa couplings λ, k and h_t and the infrared stability of the soft trilinear couplings A_λ, A_k and A_t and of the linear combinations $\mathfrak{M}_t^2$, $\mathfrak{M}_\lambda^2$ and $\mathfrak{M}_k^2$. Until this point the set of β-functions considered coincides with that of the traditional $NMSSM$ [22]. In section 4.2.4 we introduced three extra RG-equations for the parameters originating from the terms $\mu H_1 H_2$ and rN in the superpotential (1.36) and the term $B\mu$ involved in the definition for m_6^2 of eq. (4.4). The behaviour of μ, B and r does not show any infrared stability as they keep a definite dependence on the starting values at the scale M_X. In this chapter we will see how it is possible to determine these parameters using the first derivative minimisation conditions imposed on the effective potential in eq. (2.39) in the CP-conserving case[1].

The advantage in using this *IRQFP* scenario is it provides the *SUSY* phenomenology with a theoretically well motivated set of parameters. This reduces the large number of unknown parameters in any supersymmetric theory, and offers an attractive opportunity of evaluating the particle spectrum. In this chapter we focus on the spectrum of the neutral Higgs bosons and in particular on the lightest CP-even one. We will discuss the possible constraints on the parameters entering in the effective potential and express the results in terms of the remaining free parameters.

5.2 The effective potential

The effective potential we are going to examine in the present chapter is that introduced in section 2.3.1. Assuming CP-invariance, it is convenient to rewrite the tree-level part $V^{(0)}$ in the following manner

$$\begin{aligned} V^{(0)} &= \frac{1}{8}(g_1^2+g_2^2)(v_1^2-v_2^2)^2+\lambda^2 v_1^2 v_2^2+\mu_{eff}^2(v_1^2+v_2^2) \\ &\quad -2\lambda k v_1 v_2 x^2+k^2x^4+m_{H_1}^2 v_1^2+m_{H_2}^2 v_2^2+m_N^2 x^2 \\ &\quad -2m_4 v_1 v_2 x+\frac{2}{3}m_5 x^3+2m_6^2 v_1 v_2+2m_7^2 x^2 \ , \end{aligned} \tag{5.1}$$

where

$$\mu_{eff} = \lambda x + \mu \ . \tag{5.2}$$

The definition of μ_{eff} can be seen as a generalisation of the μ term of the *MSSM*; it affects also the one-loop contribution $V^{(1)}$ (e.g. (2.33))

[1]The analysis of the neutral Higgs spectrum with *SCPV* based on the *RG*-analysis is not treated in this work and is left as a possible future project.

through the mixing parameter of the stops $\tilde{A}_t$. Recalling eq. (2.32), we have

$$\tilde{A}_t = A_t + \mu_{eff} \cot\beta \ . \tag{5.3}$$

An important comment needs to be made here about the supersymmetry breaking scale M_S used in this context. According to the definition (2.30), M_S is defined using the soft squared masses entering in the mass eigenstates of the scalar superpartners of the top quark. In the present calculations we choose to remain consistent with such a definition, making M_S vary depending on $M_{1/2}$ and m_0^2. At the scale m_t then we have

$$M_S^2 \equiv \frac{1}{2}(m_Q^2 + m_T^2) \ . \tag{5.4}$$

From the low energy solutions of the RG equations it is straightforward to deduce $\tan\beta$ from eq. (4.14). So in the $IRQFP$ regime we find $\tan\beta \simeq 1.8$.

The next important feature of the effective potential to be considered is the requirement of electroweak symmetry breaking with a corresponding non-symmetric local minimum. To achieve this we invoke once again the minimisation conditions (2.39). When we calculated the neutral Higgs spectrum in chapters 2 and 3 we were using those conditions to eliminate the soft scalar squared masses $m_{H_1}^2$, $m_{H_2}^2$ and m_N^2 from the tree-level potential. Now, because these are determined by the RG equations we can use the conditions on the first derivatives to eliminate μ_{eff}, m_6^2 and m_7^2 from the effective potential. These three terms are strictly related to μ, B and r through the relationships (5.2), (4.4) and (4.5); then using the RG equations (4.43)-(4.45) (i.e. (A.17)-(A.19)) we can evaluate the three input parameters μ_0, B_0 and r_0 (see respectively (4.47), (4.46) and (4.48)) at the scale M_X if needed. After some algebra we obtain the tree-level relationships:

$$\begin{aligned}
\mu_{eff}^2+\frac{1}{2}m_Z^2 &= \frac{m_{H_1}^2-m_{H_2}^2\tan^2\beta}{\tan^2\beta-1}\,, \qquad (5.5)\\
\lambda k x^2-m_4x+m_6^2 &= -\frac{1}{2}\sin 2\beta\left(m_{H_1}^2+m_{H_2}^2+2\mu_{eff}^2+\lambda^2\eta^2\right)\,,\\
\left(m_N^2+2m_7^2\right)x+\lambda\eta^2\mu_{eff} &= m_5x^2-2k^2x^3+\left(\lambda kx+\frac{1}{2}m_4\right)\eta^2\sin 2\beta\,,
\end{aligned}$$

where the first one leaves the sign of μ_{eff} unknown and it will be considered as a free parameter. We note that in the traditional Z_3-symmetric *NMSSM* the minimisation conditions (2.39) can be used to determine $M_{1/2}$, m_0^2 and A_0. If universality constraints are imposed then the solution can be found but for $\lambda^2(M_X), k^2(M_X)\leq 0.1$. Because of this the *NMSSM* upper bound on the lightest CP-even Higgs boson mass reduces to the *MSSM* one. The Z_3-breaking *NMSSM* allows us to continue to keep universality avoiding the difficulties of the traditional Z_3-symmetric *NMSSM*.

The relationships (5.5) need to be upgraded including the one-loop and two-loop corrections to $V^{(0)}$. Then it is necessary there to make the following replacements

$$\begin{aligned}
m_{H_1}^2 &\longrightarrow m_{H_1}^2+\Delta m_{H_1}^2\,,\\
m_{H_2}^2 &\longrightarrow m_{H_2}^2+\Delta m_{H_2}^2+\delta m_{H_2}^2\,,\\
m_N^2 &\longrightarrow m_N^2+\Delta m_N^2\,,
\end{aligned}$$

where from eq. (2.33) we have

$$\begin{aligned}
\Delta m_{H_1}^2 &= \frac{1}{2v_1}\frac{\partial V^{(1)}}{\partial v_1}\,,\\
\Delta m_{H_2}^2 &= \frac{1}{2v_2}\frac{\partial V^{(1)}}{\partial v_2}\,,\\
\Delta m_N^2 &= \frac{1}{2x}\frac{\partial V^{(1)}}{\partial x}\,,
\end{aligned}$$

and from eq. (2.35) we have

$$\delta m^2_{H_2} \;=\; \frac{1}{2v_2}\frac{\partial V^{(2)}}{\partial v_2} \; .$$

At this point we need to consider the remaining free parameters. We are left with the singlet vev x as the only electroweak scale free parameter and two free parameters defined at the scale M_X; these are the universal gaugino mass $M_{1/2}$ and the soft mass squared m_0^2. Concerning the dependence from the remaining universal trilinear mass A_0, we can see from figures 4.7.a, 4.7.b and 4.7.c that the trilinear soft $SUSY$ breaking masses A_t, A_λ and A_k show $IRQFP$s. This allows us to leave A_0 free to vary as it has no effect on any other soft $SUSY$ breaking parameter at the electroweak scale.

Finally the task to be accomplished now is to perform the numerical calculations for the neutral Higgs spectrum as a function of x, $M_{1/2}$ and m_0^2.

5.3 Results and analysis

We start this section by showing the first result obtained after maximising the mass of the lightest Higgs boson h_0 in the $IRQFP$ regime. There are $IRQFP$ predictions for the linear combinations $\mathfrak{M}_t^2$, $\mathfrak{M}_\lambda^2$ and $\mathfrak{M}_k^2$ but in general the squared masses m_i^2 (where $i = Q, T, H_1, H_2, N$) still have a definite dependence on m_0^2. For this reason in figure 5.1 the plot shows the upper limit on m_{h^0} as a function of $M_{1/2}$ and m_0^2 appropriately scaled. According to the analysis performed in the previous chapter, the universal scalar mass squared m_0^2 has been left to vary in the range $0 < m_0^2 < M_{1/2}^2$ and the universal soft trilinear parameter in the range

$-M_{1/2} < A_0 < M_{1/2}$. The independent universal gaugino mass $M_{1/2}$ ranges between 80 GeV and 1 TeV. Consequently the supersymmetry breaking scale M_S defined by eq. (5.4) changes as follows:

$$M_{1/2} = 80\ GeV \implies M_S \simeq 170\ GeV\ ,$$
$$M_{1/2} = 1\ TeV \implies M_S \simeq 2.2\ TeV\ .$$

Concerning the Yukawa couplings λ, k and h_t, these are calculated from the input values

$$\lambda^2(M_X) = k^2(M_X) = h_t^2(M_X) = 10\ , \tag{5.6}$$

which are close to the $IRQFP$ and therefore in the strong Yukawa coupling regime. Finally the singlet vev has been varied in the interval $100\ GeV < x < 10\ TeV$ and μ_{eff} has been choosen to be positive; this choice of sign has been determined by the fact that it numerically maximizes the lightest CP-even mass. From the plot we can see that when $M_{1/2} = 1\ TeV$ the upper bound for m_{h^0} reaches its maximum at $\simeq 121\ GeV$. From the tridimentional plot of figure 5.1 we see that the dependence of the upper bounds on m_0^2 is rather weak: when $M_{1/2} = 1\ TeV$ we have

$$m_{h^0}|_{m_0^2=M_{1/2}^2} - m_{h^0}|_{m_0^2=0} \sim \mathcal{O}\left(10^{-1}\ GeV\right)\ . \tag{5.7}$$

To better appreciate this difference we can look at figure 5.2, which shows a plot of m_{h^0} versus $M_{1/2}$, the upper and the lower lines represent the upper bound on m_{h^0} assuming $m_0^2 = M_{1/2}^2$ and $m_0^2 = 0$ respectively. The difference between the two curves reflects the difference of eq. (5.7) through all the range of $M_{1/2}$.

The study of the Higgs spectrum in the $NMSSM$ $IRQFP$ regime has

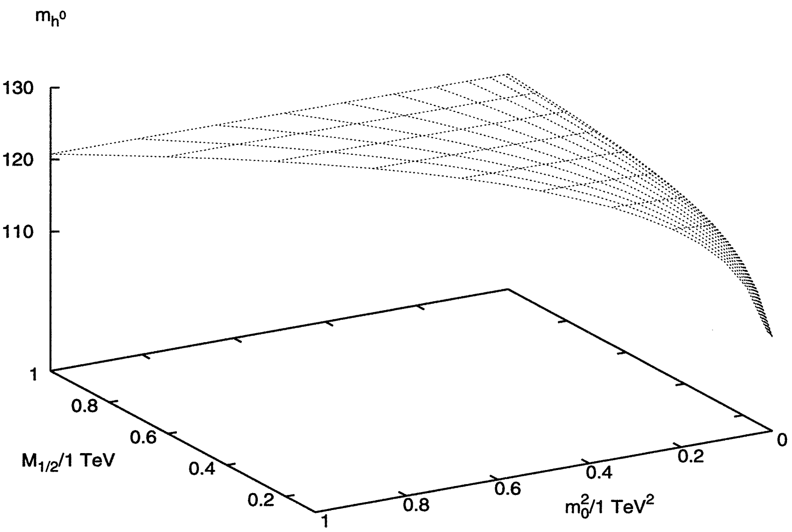

Figure 5.1: *Surface representing the upper bound m_{h^0} as a function of $M_{1/2}/1\,TeV$ and $m_0^2/(1\,TeV)^2$ at the IRQFP with $\tan\beta \simeq 1.8$.*

been performed also in reference [47]. The authors in this paper adopted the following superpotential

$$W_{NMSSM} = \mu H_1 H_2 + \lambda H_1 H_2 N - \frac{k}{3} N^3 - \mu' N^2 + W_{ferm} \ , \qquad (5.8)$$

which is Z_3-breaking and equivalent to the superpotential (1.36). The term rN in the superpotential (1.36) is replaced by the term $\mu' N^2$. In this model $m_7^2 = B'\mu'$ and the extra *RG* equations for μ' and B' replace the one for r. On the other hand it is possible to assume an extra universality condition:

$$B(M_X) = \ B'(M_X) \ = B_0 \ . \qquad (5.9)$$

In reference [47] the *IRQFP* limit is studied assuming $k^2(M_X) = 0$ (see figure 4.4.a). Because of this they obtain an upper bound on m_{h^0}, in-

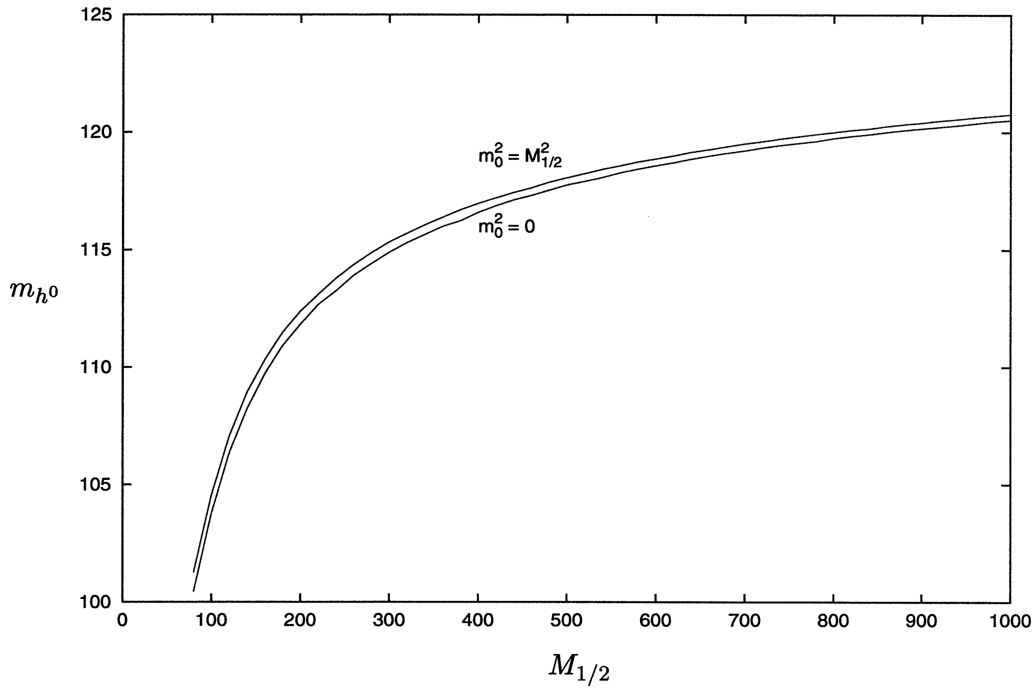

Figure 5.2: *Plots showing the upper bound on m_{h^0} as a function of $M_{1/2}$. The upper (lower) curve refers to the maximal (minimal) choice of the universal mass m_0^2.*

cluding the twoo-loop dominant corrections, at $\sim$ 127 GeV. Another remarkable difference with the results obtained in our calculations concerns the singlet vev. Here the decoupling limit is allowed, and x has been released to range up to 10 TeV, while in the cited reference the singlet vev turns out to be as small as $\sim 10^{-3}$ GeV in magnitude.

An important point to be considered in the $IRQFP$ limit concerns the mixing scenario. It is known that the one-loop contribution to the lightest Higgs boson is maximal when the mixing parameter $\tilde{A}_t = \sqrt{6}M_S$. The first thing to be noticed concerns the definition (2.9) of the masses $m_{\tilde{t}_1}$ and $m_{\tilde{t}_2}$. In the results obtained in chapters 2 and 3 we opted to set $m_Q^2 = m_T^2$. Consequently the splitting between $m_{\tilde{t}_1}$ and $m_{\tilde{t}_2}$ was exclusively determined by the off-diagonal elements of the matrix (2.7). Now, after solving the *RG* equations, the two soft masses m_Q^2 and m_T^2 turn out to be different and our numerical results show that this difference between m_Q^2 and m_T^2 reduces the effect of the mixing between the stops. Furthermore, based on the *RG* analysis, the mixing $\tilde{A}_t = \sqrt{6}M_S$ cannot be achieved. We can see quantitatively this result in figure 5.3, where the solid line represents the ratio $\tilde{A}_t/M_S$ scanned versus the supersymmetry breaking scale M_S. This graph has been obtained using the identical set of parameters used to plot figures 5.1 and 5.2. The dotted line represents the mass of the lightest CP-even boson m_{h^0} expressed in units of 100 GeV. It is easy to see from this plot that the ratio $\tilde{A}_t/M_S$ does not grow to values greater than $\sqrt{2}$, which is far below the $\sqrt{6}$ representing the condition corresponding to the maximum one-loop contribution to the mass of the lightest Higgs neutral particle.

Let us now extend out attention to the remaining particles of the neutral Higgs spectrum. Figure 5.4 shows the masses of the five neutral Higgs bosons as a function of the mass of the charged Higgs $m_{H^\pm}$. The masses are now expressed in the notation in which S_1, S_2 and S_3 refer to the scalar particles and A_1, A_2 to the pseudoscalar particles; the increasing index number indicates the increasing order in the masses. The first thing to be highlighted from these plots is the completely different behaviour of m_{S_1} and the remaining four masses. As we already discussed in chapter 3, this difference is due to the decoupling limit. The behaviour of m_{S_1} is indeed better shown in figures 5.1-5.3. The group of heavier neutral particles shows an increase following the growth of the charged Higgs boson denoted by the dotted line. The reason that $m_{H^\pm}$ reaches very high values lies in the fact that the vev of the singlet x is allowed to

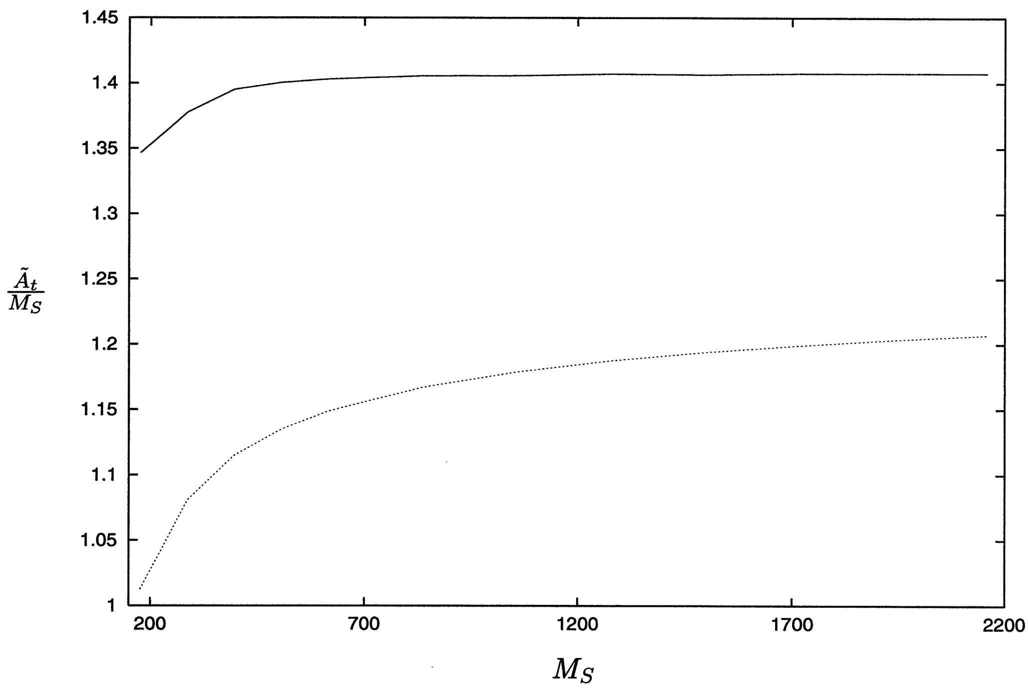

Figure 5.3: *The mixing (solid line) plotted versus M_S. The dotted line expresses the ratio $m_{h^0}/100\ GeV$.*

reach values of the order of $10\ TeV$ and, concerning the extremes of the interval in which it varies, we have:

$$M_{1/2} = 80\ GeV \implies M_S \simeq 300\ GeV\ ,$$
$$M_{1/2} = 1\ TeV \implies M_S \simeq 4\ TeV\ .$$

It turns out to be interesting to compare these results with those obtained in the previous chapters concerning the CP-conserving case. An attempt to compare the results based on RG analysis with those in figure 3.19 is the plot presented in figure 5.5. The graphs are obtained after setting the Yukawa-like constants at the scale M_X as follows:

$$k^2(M_X) = h_t^2(M_X) = 1\ , \tag{5.10}$$
$$\lambda^2(M_X) = 3\ . \tag{5.11}$$

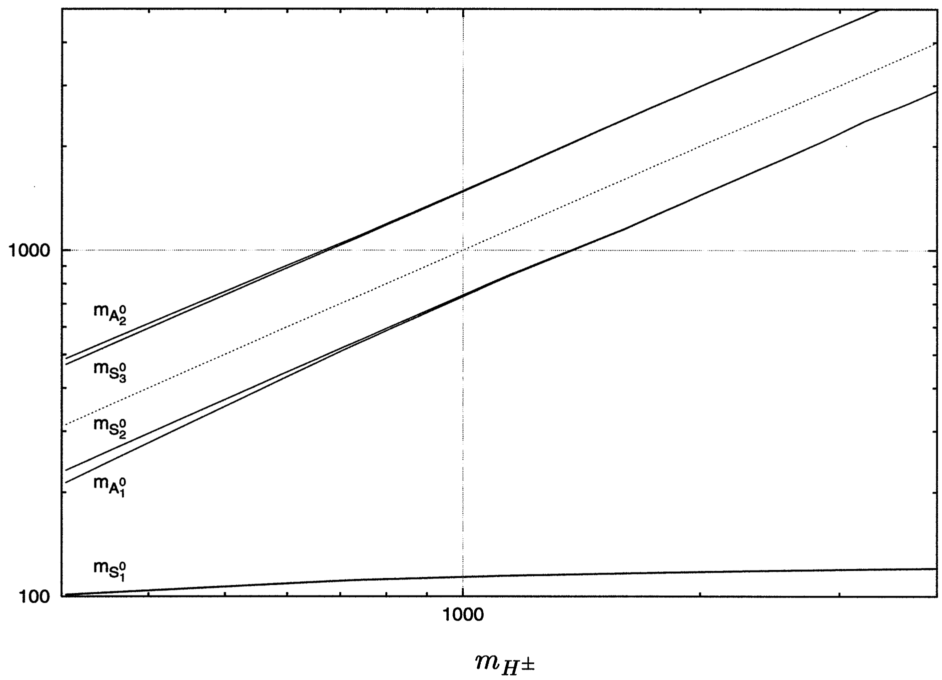

Figure 5.4: *The complete neutral Higgs spectrum versus $m_{H^\pm}$. m_{S_i} (with $i = 1, 2, 3$) and m_{A_j} (with $j = 1, 2$) are the CP-even and CP-odd particles respectively.*

This choice ensures that we obtain $\tan\beta \simeq 2.7$ at the electroweak scale. The solutions of the RG-equations are now far from the $IRQFP$; recalling the conditions (4.13) we see that we are also away from the strong Yukawa coupling regime. On the other hand the values of the Yukawa couplings (5.10) and (5.11) still satisfy the conditions (4.13) in the following weaker form

$$\frac{h_t^2(M_X)}{g_X^2} > 1 \ , \quad \frac{\lambda^2(M_X)}{g_X^2} > 1 \ , \quad \frac{k^2(M_X)}{g_X^2} > 1 \ . \tag{5.12}$$

The real goal of changing the values of the Yukawa couplings lies in the necessity to obtain $\tan\beta$ in the region where m_{h^0} reaches its maximum value. The range of the charged Higgs boson masses in figure 5.5 has been limited to $\lesssim 2\ TeV$, in order to render easier a comparison with figure

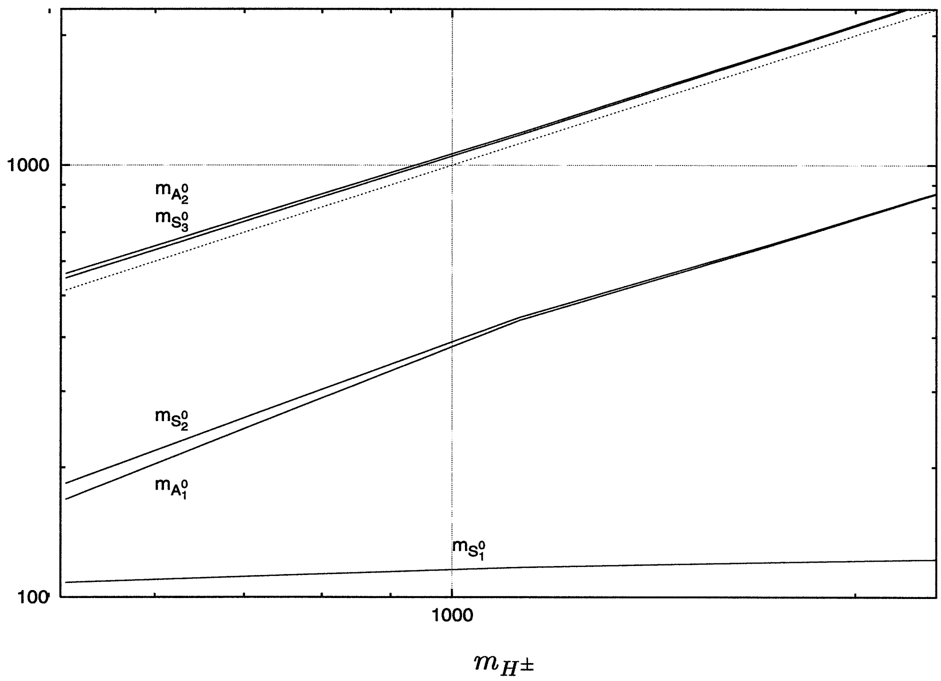

Figure 5.5: *The complete neutral Higgs spectrum versus* $m_{H^\pm}$ *in the same notation as figure 5.4 and* $\tan\beta = 2.7$.

3.19. On the other hand from the RG-analysis the minimum value of $m_{H^\pm}$ is $\simeq 500\ GeV$ and it is determined in correspondence with $M_{1/2} = 80\ GeV$. At this point an important remark should be made concerning the definition of the supersymmetry breaking scale M_S (see (2.30) or (5.4)). In the results of this chapter M_S varies as the universal gaugino mass $M_{1/2}$ does, while in chapters 2 and 3 it was simply fixed to 1 TeV. Aware of this we want to compare the two results with $\tan\beta = 2.7$. The general behaviour of the neutral Higgs spectrum in the two different scenarios seems to agree, with the two heaviest masses (m_{S_3} and m_{A_2}) following closely $m_{H^\pm}$ represented by the dotted line. The intermediate masses, namely m_{A_1} and m_{S_2}, show a smoother behaviour than the one of figure 3.19. The reason for the smoother plots here lies in the fact

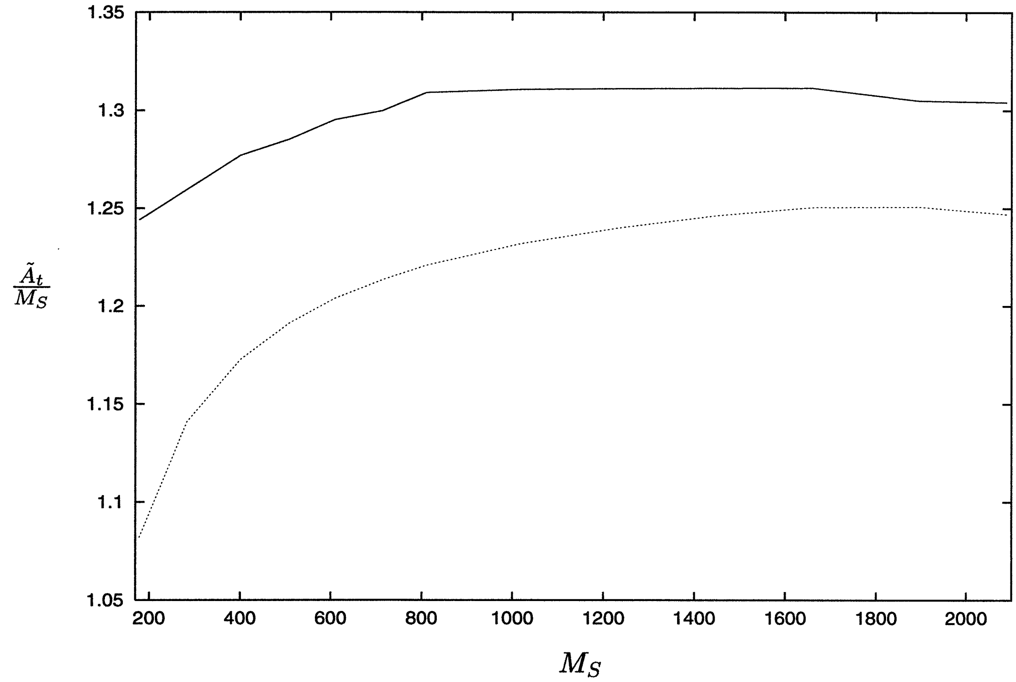

Figure 5.6: *In analogy with figure 5.3 the mixing (solid line) plotted versus M_S. The dotted line expresses the ratio $m_{h^0}/100$ GeV and $\tan\beta = 2.7$.*

that the input parameters at the electroweak scale are driven by the *RG*-analysis. Although the condition (5.12) does not ensure we are in the strong Yukawa coupling limit, it gives enough stability to the solutions of the *RG* equations at the electroweak scale. On the other hand, it is also worthy of note to recall that the results shown in figure 3.19 were obtained after maximising the lightest Higgs mass as a function of a larger number of independent parameters. Finally the lightest Higgs boson mass m_{S_1} in figure 5.5 shows an upper bound of around 125 GeV. It is easier to figure out the behaviour of the lightest CP-even Higgs boson by looking at figure 5.6. In this graph the curves are plotted versus M_S and, in analogy with figure 5.3, the solid line corresponds to the ratio between the mixing parameter $\tilde{A}_t$ and the $SUSY$ breaking scale M_S, while the dotted line expresses the lightest CP-even boson mass divided by the mass factor 100 GeV. In the region where $M_S \sim 1.6\ TeV$, the upper limit on m_{S_1} approaches to 125 GeV, and $\frac{\tilde{A}_t}{M_S} \lesssim 1.31$, which is even smaller than the value obtained in the $IRQFP$. Selecting $M_S = 1\ TeV$ we obtain $m_{S_1} \simeq 123\ GeV$. Because of the RG-based non-maximal mixing scenario this value is lower than the one illustrated in figure 2.7, 2.8 and 3.19.

Finally we conclude this chapter by remarking the fact that the $IRQFP$ scenario introduced in the previous chapter is consistent with experiment in the regime with $\tan\beta \simeq 1.8$ giving an upper bound of $\sim 121\ GeV$ on the lightest Higgs boson mass. In this low $\tan\beta$ regime, in the $MSSM$ we know there is no possibility of agreement with the experimental results as the upper bound on m_{S_1} is $(94 \pm 5)\ GeV$. In the Z_3-breaking $NMSSM$, as well as the the traditional $NMSSM$, the tree-level extra contribution can raise the upper bound on it at $\sim 136\ GeV$. As described above, the RG analysis reduces the bound to $(121 \pm 3)\ GeV$, where the error reflects the experimental error on m_t^{pole}. This upper bound at the present is still compatible with experiment. This contrasts with the Z_3-conserving $NMSSM$ in which universality lowers the bound below the experimental limit [47].

Chapter 6

Conclusions

In this thesis we have studied the neutral Higgs spectrum of the Z_3-breaking $NMSSM$ in three different contexts. In each of these we have seen a spectrum in which the lightest Higgs boson m_{h^0} has an upper bound.

Chapter 2 is entirely devoted to the study of this upper bound for the mass of this particle assuming CP-invariance. This upper limit is evaluated including the two-loop dominant radiative corrections to the effective potential and the corresponding complete spectrum deriving from this limit on m_{h^0} is shown in figure 3.19. The result for the absolute upper bound on the lightest Higgs boson is $m_{h^0} \lesssim 136\ GeV$ in agreement with the results of reference [30]. This agreement confirms the fact that the upper limit on m_{h^0} in the $NMSSM$ does not depend on any additional terms to the superpotential (1.19), which violate the original Z_3-symmetry with which the $NMSSM$ was born [13].

The $SCPV$ permitted by our model provides a new direction in which to extend our study of the Higgs spectrum. Chapter 3 is completely devoted to this topic and interesting results emerge in both limits of small and large CP-violating phases, although the latter is incompatible with experimental measures of the EDMs. In the small CP-violating case, say $\theta_i \lesssim 10^{-2}\ rad$, the spectrum is characterised by two upper bounds for the two lightest masses $m_{h_1^0}$ and $m_{h_2^0}$. The lightest Higgs particle h_1^0 is a singlet quasi-CP-odd state with a mass not exceeding $\mathcal{O}(10\ GeV)$. This is consistent with the $LEPII$ data as this particle could have not been revealed due to the singlet reluctance to interact with the gauge and matter fields. The second mass upper bound is $\sim 136\ GeV$ and corresponds to a doublet dominated boson h_2^0 almost purely CP-even. In the scenario with large CP-violation the lightest Higgs particle has the usual upper bound at $\sim 136\ GeV$ and is not even approximately a CP eigenstate.

The mass spectra of the neutral Higgs bosons obtained in chapters 2 and 3 depend on many soft $SUSY$ breaking parameters, which are freely chosen to maximise the lightest mass. The third topic is a study of the spectrum with some parameters restricted by RG-analysis assuming CP-invariance and universality at the unification scale M_X. In chapter 4 the RG equations lead the dimensionless couplings and soft $SUSY$ breaking parameters down from the unification scale M_X to the electroweak scale m_t revealing the existence of several quasi-fixed points for the Yukawa couplings h_t, λ and k, the trilinear terms A_t, A_λ and A_k and the linear combinations for the scalar masses squared $\mathfrak{M}_t^2$, $\mathfrak{M}_\lambda^2$ and $\mathfrak{M}_k^2$. After obtaining infrared solutions, these are used in chapter 5 to evaluate the Higgs spectrum.

The first consequence of the $IRQFP$ solutions is the strong Yukawa coupling regime, which implies the significant constraint $\tan\beta \simeq 1.82$.

Because in the $NMSSM$ the absolute upper limit of $\sim 136\ GeV$ for m_{h^0} occurs when $\tan\beta \simeq 2.7$, the upper bound in the $IRQFP$ regime is lowered. Two other factors lower the bound. From the analytical approximation of eq. (2.14) and the numerical results in figure 2.1 the upper bound reaches its maximum when $\lambda = \lambda_{max} \simeq 0.7$, whereas the $IRQFP$ value of eq. (4.12) is $\lambda \simeq 0.49$. The other consideration concerns the mixing between the stops involved in the one-loop contribution to the effective potential. As shown in figure 5.3, the $IRQFP$ determines a mixing parameter $\tilde{A}_t \lesssim \sqrt{2}M_S$ which is considerably below the maximum mixing scenario in which $\tilde{A}_t \lesssim \sqrt{6}M_S$. The numerical result we find for the upper bound on m_{h^0} at the $IRQFP$ is $\sim 121\ GeV$. Although this limit is lower than the one found before, this result is still in agreement with the $LEPII$ lower bound for m_{h^0} at $\sim 113\ GeV$. Unlike the $MSSM$ and the Z_3-conserving $NMSSM$ there is no conflict between experiment and universality for low $\tan\beta$. Because the theoretical and experimental bounds are so close, the result found in chapter 5 might be one of the first predictions to be tested at the coming generation of hadron colliders.

Appendix A

Renormalization Group Equations

Here are listed the set of one-loop *RG* equations in the Z_3-symmetric *NMSSM*. The general set of one-loop equations can be found in [48], and the derivation of the two-loop extension can be found in [43].

Retaining only the top quark Yukawa coupling h_t, we have the *RG* equations for the NMSSM.

$$16\pi^2 \frac{d}{dt} g_1 = 11 g_1^3 \tag{A.1}$$

$$16\pi^2 \frac{d}{dt} g_2 = g_2^3 \tag{A.2}$$

$$16\pi^2 \frac{d}{dt} g_3 = -3 g_3^3 \tag{A.3}$$

$$16\pi^2 \frac{d}{dt} h_t = h_t \left(6h_t^2 + \lambda^2 - \frac{13}{9} g_1^2 - 3g_2^2 - \frac{16}{3} g_3^2 \right) \quad (A.4)$$

$$16\pi^2 \frac{d}{dt} \lambda = \lambda \left(4\lambda^2 + 2k^2 + 3h_t^2 - g_1^2 - 3g_2^2 \right) \quad (A.5)$$

$$16\pi^2 \frac{d}{dt} k = 6k \left(\lambda^2 + k^2 \right) \quad (A.6)$$

$$\begin{aligned} 16\pi^2 \frac{d}{dt} A_t &= 12h_t^2 A_t + 2\lambda^2 A_\lambda \\ &- 4\left(\frac{13}{18} g_1^2 M_1 + \frac{3}{2} g_2^2 M_2 + \frac{8}{3} g_3^2 M_3 \right) \end{aligned} \quad (A.7)$$

$$\begin{aligned} 16\pi^2 \frac{d}{dt} A_\lambda &= 8\lambda^2 A_\lambda - 4k^2 A_k + 6h_t^2 A_t \\ &- 2\left(g_1^2 M_1 + 3g_2^2 M_2 \right) \end{aligned} \quad (A.8)$$

$$16\pi^2 \frac{d}{dt} A_k = 12\left(k^2 A_k - \lambda^2 A_\lambda \right) \quad (A.9)$$

$$\begin{aligned} 16\pi^2 \frac{d}{dt} m_Q^2 &= 2h_t^2 \left(m_Q^2 + m_{H_2}^2 + m_T^2 + A_t^2 \right) \\ &- 8\left(\frac{1}{36} g_1^2 M_1^2 + \frac{3}{4} g_2^2 M_2^2 + \frac{4}{3} g_3^2 M_3^2 \right) \end{aligned} \quad (A.10)$$

$$\begin{aligned} 16\pi^2 \frac{d}{dt} m_T^2 &= 4h_t^2 \left(m_Q^2 + m_{H_2}^2 + m_T^2 + A_t^2 \right) \\ &- 8\left(\frac{4}{9} g_1^2 M_1^2 + \frac{4}{3} g_3^2 M_3^2 \right) \end{aligned} \quad (A.11)$$

$$\begin{aligned} 16\pi^2 \frac{d}{dt} m_{H_1}^2 &= 2\lambda^2 \left(m_{H_1}^2 + m_{H_2}^2 + m_N^2 + A_\lambda^2 \right) \\ &- 8\left(\frac{1}{4} g_1^2 M_1^2 + \frac{3}{4} g_2^2 M_2^2 \right) \end{aligned} \quad (A.12)$$

$$\begin{aligned} 16\pi^2 \frac{d}{dt} m_{H_2}^2 &= 6h_t^2 \left(m_Q^2 + m_{H_2}^2 + m_T^2 + A_t^2 \right) + 2\lambda^2 \left(m_{H_1}^2 + m_{H_2}^2 + m_N^2 + A_\lambda^2 \right) \\ &- 8\left(\frac{1}{4} g_1^2 M_1^2 + \frac{3}{4} g_2^2 M_2^2 \right) \end{aligned} \quad (A.13)$$

$$16\pi^2 \frac{d}{dt} m_N^2 = 4\lambda^2 \left(m_{H_1}^2 + m_{H_2}^2 + m_N^2 + A_\lambda^2 \right) + 4k^2 \left(3m_N^2 + A_k^2 \right) \quad (A.14)$$

where

$$t = \frac{1}{2} \log \frac{Q^2}{m_Z^2} , \quad (A.15)$$

and the universality conditions are assumed. At one-loop level, the gaugino masses M_i evolve identically to α_i, then we have

$$\frac{M_i(Q)}{M_{\frac{1}{2}}} = \frac{g_i^2(Q)}{g_X^2} \ , \tag{A.16}$$

where $M_{\frac{1}{2}}$ is the universal gaugino mass and g_X is the unified coupling at the scale M_X.

When we consider the Z_3-breaking $NMSSM$ we have to add to the existing set of RG equations another three equations:

$$16\pi^2 \frac{d}{dt}\mu = \mu\left(\frac{3}{2}h_t^2 + \lambda^2 + k^2 - \frac{1}{2}g_1^2 - \frac{3}{2}g_2^2\right) \tag{A.17}$$

$$16\pi^2 \frac{d}{dt}r = r\left(\lambda^2 + k^2\right) \tag{A.18}$$

$$16\pi^2 \frac{d}{dt}B = 2\lambda^2 B + 3h_t^2 A_t + 2\lambda^2 A_\lambda + g_1^2 M_1 + 3g_2^2 M_2 \tag{A.19}$$

Appendix B

Higgs mass matrices in the *NMSSM*

The neutral Higgs mass matrix splits in two 3×3 blocks: one CP-even and another one CP-odd.

The tree-level CP-even block in the basis of the real part of the fields $\{H_1, H_2, N\}$ is:

$$M^2_{(0)} \;=\; \begin{pmatrix} 2\lambda_1\nu_1^2 & 2(\lambda_3+\lambda_4)\nu_1\nu_2 & 2\lambda_5 x\nu_1 \\ 2(\lambda_3+\lambda_4)\nu_1\nu_2 & 2\lambda_2\nu_2^2 & 2\lambda_6 x\nu_2 \\ 2\lambda_5 x\nu_1 & 2\lambda_6 x\nu_2 & 4\lambda_8 x^2 - m_5 x \end{pmatrix} +$$

$$+\begin{pmatrix} \tan\beta[m_4x-\lambda_7x^2] & -[m_4x-\lambda_7x^2] & -\frac{\nu_2}{x}[m_4x-2\lambda_7x^2] \\ -[m_4x-\lambda_7x^2] & \cot\beta[m_4x-\lambda_7x^2] & -\frac{\nu_1}{x}[m_4x-2\lambda_7x^2] \\ -\frac{\nu_2}{x}[m_4x-2\lambda_7x^2] & -\frac{\nu_1}{x}[m_4x-2\lambda_7x^2] & \frac{\nu_1\nu_2}{x^2}[m_4x] \end{pmatrix}.$$

From the one-loop correction to the effective potential (2.33), we have the one-loop correction to $M^2_{(0)}$:

$$M^2_{(1)} = \begin{pmatrix} \Delta^2_{11} & \Delta^2_{12} & \Delta^2_{13} \\ \Delta^2_{12} & \Delta^2_{22} & \Delta^2_{23} \\ \Delta^2_{13} & \Delta^2_{23} & \Delta^2_{33} \end{pmatrix} + \begin{pmatrix} \tan\beta & -1 & -\frac{\nu_2}{x} \\ -1 & \cot\beta & -\frac{\nu_1}{x} \\ -\frac{\nu_2}{x} & -\frac{\nu_1}{x} & \frac{\nu_1\nu_2}{x^2} \end{pmatrix}\Delta^2.$$

where

$$\Delta^2 = \frac{3}{16\pi^2}(\lambda x)h_t^2 A_t f(m^2_{\tilde{t}_1}, m^2_{\tilde{t}_2}) \tag{B.2}$$

and the elements of the matrix Δ^2_{ij} are

$$\Delta^2_{11} = \frac{3}{8\pi^2}h_t^4\nu_2^2(\lambda x)^2\left(\frac{A_t+\lambda x\cot\beta}{m^2_{\tilde{t}_2}-m^2_{\tilde{t}_1}}\right)^2 g(m^2_{\tilde{t}_1}, m^2_{\tilde{t}_2})$$

$$\Delta^2_{12} = \frac{3}{8\pi^2}h_t^4\nu_2^2(\lambda x)\left(\frac{A_t+\lambda x\cot\beta}{m^2_{\tilde{t}_2}-m^2_{\tilde{t}_1}}\right) \times\left(\log\frac{m^2_{\tilde{t}_2}}{m^2_{\tilde{t}_1}} + \frac{A_t(A_t+\lambda x\cot\beta)}{m^2_{\tilde{t}_2}-m^2_{\tilde{t}_1}}g(m^2_{\tilde{t}_1}, m^2_{\tilde{t}_2})\right)$$

$$\Delta^2_{13} = \frac{3}{8\pi^2}h_t^4\nu_2^2(\lambda x)(\lambda\nu_1)\left(\frac{A_t\lambda x\cot\beta}{m^2_{\tilde{t}_2}-m^2_{\tilde{t}_1}}\right)^2 g(m^2_{\tilde{t}_1}, m^2_{\tilde{t}_2}) + \frac{3}{8\pi^2}h_t^2(\lambda x)(\lambda\nu_1)f(m^2_{\tilde{t}_1}, m^2_{\tilde{t}_2})$$

$$
\begin{aligned}
\Delta^2_{22} &= \frac{3}{8\pi^2} h_t^4 \nu_2^2 \log \frac{m^2_{\tilde{t}_1} m^2_{\tilde{t}_2}}{m_t^4} \\
&- \frac{3}{8\pi^2} h_t^4 \nu_2^2 \frac{A_t(A_t + \lambda x \cot\beta)}{m^2_{\tilde{t}_2} - m^2_{\tilde{t}_1}} \\
&\times \left(2 \log \frac{m^2_{\tilde{t}_2}}{m^2_{\tilde{t}_1}} + \frac{A_t(A_t + \lambda x \cot\beta)}{m^2_{\tilde{t}_2} - m^2_{\tilde{t}_1}} g(m^2_{\tilde{t}_1}, m^2_{\tilde{t}_2}) \right) \\
\Delta^2_{23} &= \frac{3}{8\pi^2} h_t^4 \nu_2^2 (\lambda \nu_1) \left(\frac{A_t + \lambda x \cot\beta}{m^2_{\tilde{t}_2} - m^2_{\tilde{t}_1}} \right) \\
&\times \left(\log \frac{m^2_{\tilde{t}_2}}{m^2_{\tilde{t}_1}} + \frac{A_t(A_t + \lambda x \cot\beta)}{m^2_{\tilde{t}_2} - m^2_{\tilde{t}_1}} g(m^2_{\tilde{t}_1}, m^2_{\tilde{t}_2}) \right) \\
\Delta^2_{33} &= \frac{3}{8\pi^2} h_t^4 \nu_2^2 (\lambda \nu_1)^2 \left(\frac{A_t + \lambda x \cot\beta}{m^2_{\tilde{t}_2} - m^2_{\tilde{t}_1}} \right)^2 g(m^2_{\tilde{t}_1}, m^2_{\tilde{t}_2})
\end{aligned}
$$

and the functions f and g are defined by

$$
f(m^2_{t_1}, m^2_{t_2}) = \frac{1}{m^2_{t_1} - m^2_{t_2}} \left(m^2_{t_1} \log \frac{m^2_{t_1}}{Q^2} - m^2_{t_2} \log \frac{m^2_{t_2}}{Q^2} - m^2_{t_1} + m^2_{t_2} \right)
$$

$$
g(m^2_{t_1}, m^2_{t_2}) = \frac{1}{m^2_{t_1} - m^2_{t_2}} \left((m^2_{t_1} + m^2_{t_2}) \log \frac{m^2_{t_2}}{m^2_{t_1}} + 2(m^2_{t_1} - m^2_{t_2}) \right) .
$$

The two-loop contribution $M^2_{(2)}$ is

$$
M^2_{(2)} = \begin{pmatrix} \delta M^2_{11} & \delta M^2_{12} & \delta M^2_{13} \\ \delta M^2_{12} & \delta M^2_{22} & \delta M^2_{23} \\ \delta M^2_{13} & \delta M^2_{23} & \delta M^2_{33} \end{pmatrix} 12 \left(\frac{h_t^2}{16\pi^2} \right)^2 \left(32\pi\alpha_s - \frac{3}{2} h_t^2 \right) \quad \text{(B.3)}
$$

where

$$
\delta M^2_{ij} = 0 \quad i,\ j \neq 2 ,
$$

and the only contribution comes from

$$\delta M_{22}^2 = v_2^2 \left[t^2 - t\frac{M_S^2}{M_S^2+m_t^2}\left(3+\frac{m_t^2}{M_S^2+m_t^2}\right)+\left(\frac{M_S^2}{M_S^2+m_t^2}\right)^2\right]$$

The second block of the neutral Higgs mass matrix is the CP-odd one. In the basis of the imaginary perts of the fields $\{H_1, H_2, N\}$ this is given by:

$$\tilde{M}_{(0)}^2 = \begin{pmatrix} \tan\beta[m_4x-\lambda_7x^2] & [m_4x-\lambda_7x^2] & \frac{\nu_2}{x}[m_4x+2\lambda_7x^2] \\ [m_4x-\lambda_7x^2] & \cot\beta[m_4x-\lambda_7x^2] & \frac{\nu_1}{x}[m_4x+2\lambda_7x^2] \\ \frac{\nu_2}{x}[m_4x+2\lambda_7x^2] & \frac{\nu_1}{x}[m_4x+2\lambda_7x^2] & 3m_5x+\frac{\nu_1\nu_2}{x^2}[m_4x-4\lambda_7x^2] \end{pmatrix} \tag{B.4}$$

In the same way as we did for the CP-even mass matrix, we have the one-loop corrections to $\tilde{M}_{(0)}^2$:

$$\tilde{M}_{(1)}^2 = \begin{pmatrix} \tan\beta & 1 & \frac{\nu_2}{x} \\ 1 & \cot\beta & \frac{\nu_1}{x} \\ \frac{\nu_2}{x} & \frac{\nu_1}{x} & \frac{\nu_1\nu_2}{x^2} \end{pmatrix} \Delta^2 \tag{B.5}$$

where Δ^2 has been defined in eq (B.2). Finally we have the two-loop contribution:

$$\tilde{M}_{(2)}^2 = \begin{pmatrix} \delta\tilde{M}_{11}^2 & \delta\tilde{M}_{12}^2 & \delta\tilde{M}_{13}^2 \\ \delta\tilde{M}_{12}^2 & \delta\tilde{M}_{22}^2 & \delta\tilde{M}_{23}^2 \\ \delta\tilde{M}_{13}^2 & \delta\tilde{M}_{23}^2 & \delta\tilde{M}_{33}^2 \end{pmatrix} 12\left(\frac{h_t^2}{16\pi^2}\right)^2\left(32\pi\alpha_s-\frac{3}{2}h_t^2\right) \tag{B.6}$$

where

$$\delta \tilde{M}_{ij}^2 = 0 \quad i,\ j \neq 2\ ,$$

and the only contribution comes from

$$\delta \tilde{M}_{22}^2 \ = \ v_2^2 t^2$$

Finally, to complete the Higgs spectrum we report the mass matrix of the charged Higgs in the basis $\{H_1^-, H_2^+\}$

$$M_c^2 = \begin{pmatrix} \tan\beta & 1 \\ 1 & \cot\beta \end{pmatrix} (m_4 x - \lambda_7 x^2 - \lambda_4 \nu_1 \nu_2). \qquad \text{(B.7)}$$

The one-loop radiative corrections to the charged Higgs matrix are

$$\Delta M_c^2 = \begin{pmatrix} \tan\beta & 1 \\ 1 & \cot\beta \end{pmatrix} \Delta_c^2 \qquad \text{(B.8)}$$

where

$$\Delta_c^2 = \frac{3}{16\pi^2} \sum_{m_a \in \{m_{\tilde{t}_1}, m_{\tilde{t}_2}\}} m_a^2 \left(\ln \frac{m_a^2}{M_{SUSY}^2} - 1 \right) \frac{\partial^2 m_a^2}{\partial H_1^- \partial H_2^+} |_{vevs} \ .$$

Appendix C

Higgs mass matrix in the Z_3-breaking $NMSSM$

In this appendix we give the details of the 6×6 symmetric Higgs mass matrix $\mathcal{M}^2$ in the most general $NMSSM$ with spontaneous CP-violation. Here we will express the two-loop corrected mass matrix in the basis $\{ReH_1, ReH_2, ReN, ImH_1, ImH_2, ImN\}$:

$$\mathcal{M}^2 = M^2 + \Delta M^2 + \delta M^2 \ . \tag{C.1}$$

Let us start with the tree-level part. Let us calculate the matrix of the second derivatives of the tree-level potential $V^{(0)}$.

$$\begin{aligned} \partial_{11} V^{(0)} &= 2\lambda_1 v_1^2 \cos^2\theta_1 \\ &\quad + \tan\beta \left\{ m_4 x \left[\cos\theta_P - \sin\theta_P \cot\theta_{12}\right] \right. \\ &\qquad\qquad \left. - \lambda_7 x^2 \left[\cos\theta_M - \sin\theta_M \cot\theta_{12}\right] \right\} \ , \end{aligned}$$

$$\begin{aligned}
\partial_{12}V^{(0)} &= 2(\lambda_3+\lambda_4)v_1v_2\cos\theta_1\cos\theta_2 \\
&\quad +\lambda_7x^2\left[\cos(2\theta_3)-\frac{\sin\theta_M}{\sin\theta_{12}}\right]-m_4x\left[\cos(2\theta_3)-\frac{\sin\theta_P}{\sin\theta_{12}}\right] \ ,
\end{aligned}$$

$$\begin{aligned}
\partial_{13}V^{(0)} &= 2\lambda_5xv_1\cos\theta_1\cos\theta_3 \\
&\quad +2\lambda_7xv_2(\cos\theta_2\cos\theta_3+\sin\theta_2\sin\theta_3)-m_4v_2\cos\theta_2+2\lambda\mu v_1\cos\theta_1 \\
\partial_{14}V^{(0)} &= \lambda_1v_1^2\sin(2\theta_1)
\end{aligned}$$

$$\partial_{15}V^{(0)} = 2(\lambda_3+\lambda_4)v_1v_2\cos\theta_1\sin\theta_2+\lambda_7x^2\sin(2\theta_3)+m_4x\sin\theta_3 \ ,$$

$$\begin{aligned}
\partial_{16}V^{(0)} &= 2\lambda_5xv_1\cos\theta_1\sin\theta_3 \\
&\quad -2\lambda_7xv_2(\sin\theta_2\cos\theta_3-\cos\theta_2\sin\theta_3)+m_4v_2\sin\theta_2
\end{aligned}$$

$$\begin{aligned}
\partial_{22}V^{(0)} &= 2\lambda_2v_2^2\cos^2\theta_2 \\
&\quad +\cot\beta\left\{m_4x\left[\cos\theta_P-\sin\theta_P\cot\theta_{12}\right]\right. \\
&\qquad\qquad \left.-\lambda_7x^2\left[\cos\theta_M-\sin\theta_M\cot\theta_{12}\right]\right\} \ ,
\end{aligned}$$

$$\begin{aligned}
\partial_{23}V^{(0)} &= 2\lambda_6xv_2\cos\theta_2\cos\theta_3 \\
&\quad +2\lambda_7xv_1(\cos\theta_1\cos\theta_3+\sin\theta_1\sin\theta_3)-m_4v_1\cos\theta_1+2\lambda\mu v_2\cos\theta_2
\end{aligned}$$

$$\begin{aligned}
\partial_{24}V^{(0)} &= 2(\lambda_3+\lambda_4)v_1v_2\sin\theta_1\cos\theta_2 \\
&\quad +\lambda_7x^2\sin(2\theta_3)+m_4x\sin\theta_3 \ ,
\end{aligned}$$

$$\partial_{25}V^{(0)} = \lambda_2v_2^2\sin(2\theta_2)$$

$$
\begin{aligned}
\partial_{26} V^{(0)} &= 2\lambda_6 x v_2 \cos\theta_2 \sin\theta_3 \\
&\quad +2\lambda_7 x v_1 (\sin\theta_1 \cos\theta_3 - \cos\theta_1 \sin\theta_3) + m_4 v_1 \sin\theta_1
\end{aligned}
$$

$$
\begin{aligned}
\partial_{33} V^{(0)} &= 4\lambda_8 x^2 \cos^2\theta_3 + m_5 x \left\{\cos(3\theta_3) - 2\cos\theta_3 + \sin\theta_3 \left[\mathrm{cosec}(2\theta_3) - \cot(2\theta_3)\right]\right\} \\
&\quad + m_4 \frac{v_1 v_2}{x} \left\{\cos\theta_P + \sin\theta_P \left[\mathrm{cosec}(2\theta_3) - \cot(2\theta_3)\right]\right\} \\
&\quad + 2\lambda_7 v_1 v_2 \left\{\cos\theta_M + \sin\theta_M \left[\mathrm{cosec}(2\theta_3) - \cot(2\theta_3)\right]\right\} \\
&\quad - \lambda\mu \frac{\eta^2}{x} \left\{\cos\theta_3 + \sin\theta_3 \left[\mathrm{cosec}(2\theta_3) - \cot(2\theta_3)\right]\right\}
\end{aligned}
$$

$$
\begin{aligned}
\partial_{34} V^{(0)} &= 2\lambda_5 x v_1 \sin\theta_1 \cos\theta_3 \\
&\quad +\lambda_7 x v_2 (\cos\theta_2 \sin\theta_3 - \sin\theta_2 \cos\theta_3) + m_4 v_2 \sin\theta_2 + 2\lambda\mu v_1 \sin\theta_1 \ , \\
\partial_{35} V^{(0)} &= 2\lambda_6 x v_2 \sin\theta_2 \cos\theta_3 \\
&\quad +\lambda_7 x v_1 (\cos\theta_1 \sin\theta_3 - \sin\theta_1 \cos\theta_3) + m_4 v_1 \sin\theta_1 + 2\lambda\mu v_2 \sin\theta_2 \\
\partial_{36} V^{(0)} &= 2\lambda_7 v_1 v_2 \cos\theta_{12} + 2\lambda_8 x^2 \sin(2\theta_3) + m_5 x \sin\theta_3 \\
\partial_{44} V^{(0)} &= 2\lambda_1 v_1^2 \sin^2\theta_1 \\
&\quad + \tan\beta \left\{ m_4 x \left[\cos\theta_P - \sin\theta_P \cot\theta_{12}\right] \right. \\
&\qquad\quad \left. - \lambda_7 x^2 \left[\cos\theta_M - \sin\theta_M \cot\theta_{12}\right] \right\} \ ,
\end{aligned}
$$

$$
\begin{aligned}
\partial_{45} V^{(0)} &= 2(\lambda_3 + \lambda_4) v_1 v_2 \sin\theta_1 \sin\theta_2 \\
&\quad -\lambda_7 x^2 \left[\cos(2\theta_3) - \frac{\sin\theta_M}{\sin\theta_{12}}\right] + m_4 x \left[\cos\theta_3 - \frac{\sin\theta_P}{\sin\theta_{12}}\right] \ ,
\end{aligned}
$$

$$
\begin{aligned}
\partial_{46} V^{(0)} &= 2\lambda_5 x v_1 \sin\theta_1 \sin\theta_3 \\
&\quad +2\lambda_7 x v_2 (\cos\theta_2 \cos\theta_3 + \sin\theta_2 \sin\theta_3) + m_4 v_2 \cos\theta_2
\end{aligned}
$$

$$\begin{aligned}
\partial_{55}V^{(0)} &= 2\lambda_2 v_2^2 \sin^2\theta_2 \\
&\quad +\cot\beta\left\{m_4 x\left[\cos\theta_P - \sin\theta_P\cot\theta_{12}\right]\right. \\
&\qquad\qquad \left. -\lambda_7 x^2\left[\cos\theta_M - \sin\theta_M\cot\theta_{12}\right]\right\}\ ,
\end{aligned}$$

$$\begin{aligned}
\partial_{56}V^{(0)} &= 2\lambda_6 x v_2 \sin\theta_2\sin\theta_3 \\
&\quad +2\lambda_7 x v_1(\cos\theta_1\cos\theta_3+\sin\theta_1\sin\theta_3)+m_4 v_1\cos\theta_1
\end{aligned}$$

$$\begin{aligned}
\partial_{66}V^{(0)} &= 4\lambda_8 x^2\sin^2\theta_3 + m_5 x\left[\cos(3\theta_3)-\sin\theta_3\cot(2\theta_3)\right] \\
&\quad +m_4\frac{v_1 v_2}{x}\left[\cos\theta_P-\sin\theta_P\cot(2\theta_3)\right] \\
&\quad +2\lambda_7 v_1 v_2\left[\cos\theta_{12}+2\sin\theta_M+\cos\theta_M\cot(2\theta_3)\right] \\
&\quad -\lambda\mu\frac{\eta^2}{x}\left[\cos\theta_3-\sin\theta_3\cot(2\theta_3)\right]
\end{aligned}$$

where θ_M, θ_P and θ_{12} are correspond to the linear combinations of the phases θ_1, θ_2 and θ_3 as defined in eq. (3.3).

The one-loop dominant correction to M^2 in the limit where $\tan\beta \lesssim 10$ comes from the top/stop contribution. The one-loop contribution ΔM^2 is calculated from the field-dependant one-loop effective potential given in eq. (2.33). Then applying the formula (1.27) to $V^{(1)}$ we calculate the matrix of the second derivatives of $V^{(1)}$ respect to the fields $\phi_1,\ldots,\phi_6$:

$$\begin{aligned}
\left.\frac{\partial^2 V^{(1)}}{\partial\phi_i\phi_j}\right|_{\langle\phi\rangle} &= \frac{3}{16\pi^2}\left\{m_{\tilde{t}_1}^2\frac{\partial^2 m_{\tilde{t}_1}^2}{\partial\phi_i\phi_j}\left(\log\frac{m_{\tilde{t}_1}^2}{Q^2}-1\right)+\frac{\partial m_{\tilde{t}_1}^2}{\partial\phi_i}\frac{\partial m_{\tilde{t}_1}^2}{\partial\phi_j}\right. \\
&\quad + m_{\tilde{t}_2}^2\frac{\partial^2 m_{\tilde{t}_2}^2}{\partial\phi_i\phi_j}\left(\log\frac{m_{\tilde{t}_2}^2}{Q^2}-1\right)+\frac{\partial m_{\tilde{t}_2}^2}{\partial\phi_i}\frac{\partial m_{\tilde{t}_2}^2}{\partial\phi_j} \qquad \text{(C.2)} \\
&\quad \left.\left. -2\left[m_t^2\frac{\partial^2 m_t^2}{\partial\phi_i\phi_j}\left(\log\frac{m_t^2}{Q^2}-1\right)+\frac{\partial m_t^2}{\partial\phi_i}\frac{\partial m_t^2}{\partial\phi_j}\right]\right\}\right|_{\langle\phi\rangle}\ ,
\end{aligned}$$

where $i, j = 1, \ldots, 6$ and the vevs of the fields are assumed to be $\langle\phi_i\rangle \neq 0$ realising the $SCPV$. In eq. (C.2) the first derivatives of the field-dependant top/stop masses squared are:

$$\frac{\partial m_t^2}{\partial \phi_i} = \begin{cases} h_t^2 \phi_i & i = 2, 5 \\ \\ 0 & i = 1, 3, 4, 6 \end{cases} \tag{C.3}$$

for the top. Concerning the masses squared of the supersymmetric partners we have:

$$\frac{\partial m^2_{\tilde{t}_1, \tilde{t}_2}}{\partial \phi_i} = \frac{\partial m_t^2}{\partial \phi_i} \pm \frac{h_t^2}{m_{\tilde{t}_1} - m_{\tilde{t}_2}} \Delta_i^t ,$$

where

$$\begin{aligned}
\Delta_1^t &= \frac{1}{2}\lambda^2 \phi_1 (\phi_3^2 + \phi_6^2) + \mu^2 \phi_1 + \frac{1}{\sqrt{2}} \lambda A_t (\phi_2 \phi_3 - \phi_5 \phi_6) \\
&\quad + \mu A_t \phi_2 + \sqrt{2} \lambda \mu \phi_1 \phi_3 , \\
\Delta_2^t &= A_t^2 \phi_2 + \frac{1}{\sqrt{2}} \lambda A_t (\phi_1 \phi_3 - \phi_4 \phi_6) + \mu A_t \phi_1 , \\
\Delta_3^t &= \frac{1}{2}\lambda^2 \phi_3 (\phi_1^2 + \phi_4^2) + \frac{1}{\sqrt{2}} \lambda A_t (\phi_1 \phi_2 - \phi_4 \phi_5) + \frac{1}{\sqrt{2}} \lambda \mu (\phi_1^2 + \phi_4^2) , \\
\Delta_4^t &= \frac{1}{2}\lambda^2 \phi_4 (\phi_3^2 + \phi_6^2) + \mu^2 \phi_4 - \frac{1}{\sqrt{2}} \lambda A_t (\phi_2 \phi_6 + \phi_3 \phi_5) \\
&\quad - \mu A_t \phi_5 + \sqrt{2} \lambda \mu \phi_3 \phi_4 , \\
\Delta_5^t &= A_t^2 \phi_5 - \frac{1}{\sqrt{2}} \lambda A_t (\phi_1 \phi_6 + \phi_3 \phi_4) - \mu A_t \phi_4 , \\
\Delta_6^t &= \frac{1}{2}\lambda^2 \phi_6 (\phi_1^2 + \phi_4^2) - \frac{1}{\sqrt{2}} \lambda A_t (\phi_1 \phi_5 + \phi_2 \phi_4) .
\end{aligned}$$

The second derivatives are for the top

$$\frac{\partial^2 m_t^2}{\partial \phi_i \partial \phi_j} = \begin{cases} h_t^2 & i = j = 2, 5 \\ \\ 0 & \text{otherwise} \end{cases} \tag{C.4}$$

and for the stops

$$\frac{\partial^2 m^2_{\tilde{t}_1,\tilde{t}_2}}{\partial\phi_i\partial\phi_j} = \frac{\partial^2 m^2_t}{\partial\phi_i\partial\phi_j} \pm \frac{h_t^2}{m_{\tilde{t}_1} - m_{\tilde{t}_2}}\Delta^t_{ij} \mp \frac{h_t^4}{(m_{\tilde{t}_1} - m_{\tilde{t}_2})^2}\Delta^t_i\Delta^t_j \ ,$$

where

$$\begin{aligned}
\Delta^t_{11} &= \tfrac{1}{\sqrt{2}}\lambda^2(\phi_3^2+\phi_6^2) + \mu^2 + \sqrt{2}\lambda\mu\phi_3 \ , & \Delta^t_{12} &= \tfrac{1}{\sqrt{2}}\lambda A_t\phi_3 + \mu A_t \ , \\
\Delta^t_{13} &= \lambda^2\phi_1\phi_3 + \tfrac{1}{\sqrt{2}}\lambda A_t\phi_2 + \sqrt{2}\lambda\mu\phi_1 \ , & \Delta^t_{14} &= 0 \ , \\
\Delta^t_{15} &= -\tfrac{1}{\sqrt{2}}\lambda A_t\phi_6 \ , & \Delta^t_{16} &= \lambda^2\phi_1\phi_6 - \tfrac{1}{\sqrt{2}}\lambda A_t\phi_5 \ , \\
\Delta^t_{22} &= A_t^2 \ , & \Delta^t_{23} &= \tfrac{1}{\sqrt{2}}\lambda A_t\phi_1 \ , \\
\Delta^t_{24} &= -\tfrac{1}{\sqrt{2}}\lambda A_t\phi_6 \ , & \Delta^t_{25} &= 0 \ , \\
\Delta^t_{26} &= -\tfrac{1}{\sqrt{2}}\lambda A_t\phi_4 \ , & \Delta^t_{33} &= \tfrac{1}{2}\lambda^2(\phi_1^2+\phi_4^2) \ , \\
\Delta^t_{34} &= \lambda^2\phi_3\phi_4 - \tfrac{1}{\sqrt{2}}\lambda A_t\phi_5 + \sqrt{2}\lambda\mu\phi_4 \ , & \Delta^t_{35} &= -\tfrac{1}{\sqrt{2}}\lambda A_t\phi_4 \ , \\
\Delta^t_{36} &= 0 \ , & \Delta^t_{44} &= \tfrac{1}{\sqrt{2}}\lambda^2(\phi_3^2+\phi_6^2) + \mu^2 + \sqrt{2}\lambda\mu\phi_3 \\
\Delta^t_{45} &= \tfrac{1}{\sqrt{2}}\lambda A_t\phi_3 - \mu A_t \ , & \Delta^t_{46} &= \lambda^2\phi_4\phi_6 - \tfrac{1}{\sqrt{2}}\lambda A_t\phi_2 \ , \\
\Delta^t_{55} &= A_t^2 \ , & \Delta^t_{56} &= -\tfrac{1}{\sqrt{2}}\lambda A_t\phi_1 \ , \\
\Delta^t_{66} &= -\tfrac{1}{2}\lambda^2(\phi_1^2+\phi_4^2) \ .
\end{aligned}$$

Finally the two-loop correction. The matrix of the second derivatives is a generalisation of the matrices (B.3) and (B.6). This is given by

$$
\begin{aligned}
\frac{\partial^2 V_{LL}^{(2)}}{\partial \phi_2^2} &= \left(\frac{h_t^2}{16\pi^2}\right)^2 \left(32\pi\alpha_s - \frac{3}{2}h_t^2\right) \\
&\left\{(3\phi_2^2+\phi_5^2)t^2 + 4\phi_2(\phi_2^2+\phi_5^2)t\frac{\partial t}{\partial \phi_2}\right. \\
&\left. + \frac{1}{2}(\phi_2^2+\phi_5^2)^2\left(\frac{\partial t}{\partial \phi_2}\right)^2 + \frac{1}{2}(\phi_2^2+\phi_5^2)^2 t\frac{\partial^2 t}{\partial \phi_2^2}\right\}
\end{aligned}
$$

$$
\begin{aligned}
\frac{\partial^2 V_{LL}^{(2)}}{\partial \phi_5^2} &= \left(\frac{h_t^2}{16\pi^2}\right)^2 \left(32\pi\alpha_s - \frac{3}{2}h_t^2\right) \\
&\left\{(\phi_2^2+3\phi_5^2)t^2 + 4\phi_5(\phi_2^2+\phi_5^2)t\frac{\partial t}{\partial \phi_5}\right. \\
&\left. + \frac{1}{2}(\phi_2^2+\phi_5^2)^2\left(\frac{\partial t}{\partial \phi_5}\right)^2 + \frac{1}{2}(\phi_2^2+\phi_5^2)^2 t\frac{\partial^2 t}{\partial \phi_5^2}\right\}
\end{aligned}
$$

$$
\begin{aligned}
\frac{\partial^2 V_{LL}^{(2)}}{\partial \phi_2 \phi_5} &= \left(\frac{h_t^2}{16\pi^2}\right)^2 \left(32\pi\alpha_s - \frac{3}{2}h_t^2\right) \\
&\left\{2\phi_2\phi_5 t^2 + 2\phi_2(\phi_2^2+\phi_5^2)t\frac{\partial t}{\partial \phi_5} + 2\phi_5(\phi_2^2+\phi_5^2)t\frac{\partial t}{\partial \phi_2}\right. \\
&\left. + \frac{1}{2}(\phi_2^2+\phi_5^2)^2\frac{\partial t}{\partial \phi_2}\frac{\partial t}{\partial \phi_5} + \frac{1}{2}(\phi_2^2+\phi_5^2)^2 t\frac{\partial^2 t}{\partial \phi_2 \partial \phi_5}\right\}
\end{aligned}
$$

$$
\frac{\partial^2 V_{LL}^{(2)}}{\partial \phi_i \phi_j} = 0 \quad i,j = 1,3,4,6
$$

In these derivatives t is defined as

$$
t \equiv \ln\left(\frac{M_S^2+m_t^2}{m_t^2}\right), \tag{C.5}
$$

and its first and second derivatives are

$$
\frac{\partial t}{\partial \phi_i} = \begin{cases} -\frac{Q^2}{m_t^2(Q^2+m_t^2)}\frac{\partial m_t^2}{\partial \phi_i} & i = 2,5 \\ 0 & i = 1,3,4,6 \end{cases} \tag{C.6}
$$

$$
\begin{aligned}
\frac{\partial^2 t}{\partial\phi_i\phi_j} &= -\frac{Q^2}{m_t^2(Q^2+m_t^2)}\left\{\frac{\partial^2 m_t^2}{\partial\phi_i\phi_j}\right. \\
&\quad \left. -\left[\frac{1}{m_t^2}+\frac{1}{Q^2+m_t^2}\right]\frac{\partial m_t^2}{\partial\phi_i}\frac{\partial m_t^2}{\partial\phi_j}\right\}
\end{aligned}
$$

At this point we can obtain the the correct Higgs mass squared matrix $\mathcal{M}^2$ after dividing by $Z_{H_2}^{1/2}$ every element which is obtained by differentiating V_{eff} by one of the components of H_2; that is to say that matrix elements like $\partial_{14}V_{eff}$ simply remain unchanged, and matrix elements like $\partial_{15}V_{eff}$ and $\partial_{55}V_{eff}$ have to be divided by a factor $Z_{H_2}^{1/2}$ and Z_{H_2} respectively. The neutral Higgs mass matrix obtained has been expressed after eliminating $m_{H_1}^2$, $m_{H_2}^2$, m_N^2, m_6^2, m_7^2 by means of the minimisation conditions on V_{eff} given in eqs. (3.5) and (3.5). From those conditions we have the explicit expressions for these five soft masses corrected at the two-loop-leading-order:

$$
\begin{aligned}
m_{H_1}^2 &= \left[m_4 x\left(\cos\theta_P - \sin\theta_P\cot\theta_{12}\right)\right. \\
&\quad \left. -\lambda_7 x^2\left(\cos\theta_M - \sin\theta_M\cot\theta_{12}\right)\right]\tan\beta \\
&\quad -\lambda_1 v_1^2 - (\lambda_3+\lambda_4)v_2^2 - \lambda_5 x^2 - \left(\mu^2 + 2\lambda\mu x\cos\theta_3\right) \\
&\quad -\frac{\tan\beta}{2v_1v_2}\cot\theta_{12}\frac{\partial V^{(1)}}{\partial\theta_1}
\end{aligned}
\tag{C.7}
$$

$$
\begin{aligned}
m_{H_2}^2 &= \left[m_4 x\left(\cos\theta_P - \sin\theta_P\cot\theta_{12}\right)\right. \\
&\quad \left. -\lambda_7 x^2\left(\cos\theta_M - \sin\theta_M\cot\theta_{12}\right)\right]\cot\beta \\
&\quad -\lambda_2 v_2^2 - (\lambda_3+\lambda_4)v_1^2 - \lambda_6 x^2 - \left(\mu^2 + 2\lambda\mu x\cos\theta_3\right) \\
&\quad -\frac{1}{2v_1v_2}\left(v_1\frac{\partial V^{(1)}}{\partial v_2} + \cot\beta\ \cot\theta_{12}\ \frac{\partial V^{(1)}}{\partial\theta_1}\right) \\
&\quad -\frac{1}{2v_2}\frac{\partial V^{(2)}}{\partial v_2}
\end{aligned}
\tag{C.8}
$$

$$\begin{aligned} m_N^2 &= m_4\frac{v_1v_2}{x}\left\{\cos\theta_P+\sin\theta_P\cot(2\theta_3)\right\} \\ &\quad +m_5x\left\{\cos(3\theta_3)-\sin(3\theta_3)\cot(2\theta_3)\right\} \\ &\quad -2\lambda_7v_1v_2\left\{\cos\theta_M-\sin\theta_M\cot(2\theta_3)\right\} \\ &\quad -\lambda\mu\frac{\eta^2}{x}\left\{\cos\theta_3-\sin\theta_3\cot(2\theta_3)\right\} \\ &\quad -\lambda_5v_1^2-\lambda_6v_2^2-2\lambda_8x^2 \\ &\quad -\frac{1}{2x}\left(\frac{\partial V^{(1)}}{\partial x}+\frac{1}{2x\sin(2\theta_3)}\frac{\partial V^{(1)}}{\partial\theta_1}\right) \end{aligned} \tag{C.9}$$

$$\begin{aligned} m_6^2 &= m_4x\frac{\sin\theta_P}{\sin\theta_{12}}-\lambda_7x^2\frac{\sin\theta_M}{\sin\theta_{12}} \\ &\quad +\frac{1}{2v_1v_2\sin\theta_{12}}\frac{\partial V^{(1)}}{\partial\theta_1} \end{aligned} \tag{C.10}$$

$$\begin{aligned} m_7^2 &= \lambda_7v_1v_2\frac{\sin\theta_M}{(2\sin\theta_3)}-\lambda\mu\frac{v_1v_2}{2x}\frac{\sin\theta_P}{(2\sin\theta_3)} \\ &\quad +m_4x\frac{v_1v_2}{2x}\frac{\sin\theta_P}{\sin(2\theta_3)}+\frac{1}{2}m_5x\frac{\sin(3\theta_3)}{\sin(2\theta_3)} \\ &\quad +\frac{1}{4x^2\sin(2\theta_3)}\frac{\partial V^{(1)}}{\partial\theta_1} \end{aligned} \tag{C.11}$$

References

[1] H. E. Haber and G. L. Kane, Phys. Rept. **117** (1985) 75.

[2] H. P. Nilles, Phys. Rept. **110** (1984) 1.

[3] R.N. Mohapatra, *Unification and Supersymmetry: The Frontiers of Quark-Lepton Physics*, Springer-Verlag, New York 1992.

[4] D. Bailin and A. Love, *Supersymmetric Gauge Field Theory and String Theory*, (Institute of Physics Publishing, Bristol England, 1994).

[5] S. P. Martin, [arXiv:hep-ph/9709356].

[6] J. F. Gunion, H. E. Haber, G. Kane, S. Dawson, *The Higgs Hunter's Guide*, Addison Wesley, 1990, errata: hep-ph/9302272.

[7] G. R. Farrar and P. Fayet, Phys. Lett. B **76** (1978) 575.

[8] S. Dimopoulos and H. Georgi, *Nucl. Phys.* **B193** (1981) 150; S. Weinberg, *Phys. Rev.* **D26** (1982) 2878; N. Sakai and T. Yanagida, *Nucl. Phys.* **B197** (1982) 533; S. Dimopoulos, S. Raby and F. Wilczek, *Phys. Rev. Lett.* **B112** (1982) 133.

[9] G. L. Kane, arXiv:hep-ph/0202185.

[10] S. A. Abel, S. Sarkar and P. L. White, Nucl. Phys. B **454** (1995) 663 [arXiv:hep-ph/9506359].

[11] J. C. Romão, Phys. Lett. B **173** (1986) 309.

[12] G. L. Kane, C. Kolda and J. D. Wells, Phys. Rev. Lett. **70** (1993) 2686 [arXiv:hep-ph/9210242].

[13] J. R. Ellis, J. F. Gunion, H. E. Haber, L. Roszkowski and F. Zwirner, Phys. Rev. D **39** (1989) 844.

[14] T. Elliot, S. F. King, P. L. White, *Phys. Rev.* **D49**, 2435 (1994).

[15] A. T. Davies, C. D. Froggatt and R. G. Moorhouse, Phys. Lett. B **372** (1996) 88 [arXiv:hep-ph/9603388].

[16] S. J. Huber and M. G. Schmidt, Eur. Phys. J. C **10** (1999) 473 [arXiv:hep-ph/9809506].

[17] J. Gunion and H. E. Haber, *Nucl. Phys.* **B272** (1986) 1.

[18] R. B. Nevzorov, M. A. Trusov, *JETP* **91**, (2000) 1079.

[19] A. Pomarol, Phys. Rev. D **47** (1993) 273 [arXiv:hep-ph/9208205].

[20] S. F. King and P. L. White, Phys. Rev. D **53** (1996) 4049 [arXiv:hep-ph/9508346].

[21] J. R. Ellis, G. Ridolfi and F. Zwirner, Phys. Lett. B **262** (1991) 477.

[22] S. F. King and P. L. White, Phys. Rev. D **52** (1995) 4183 [arXiv:hep-ph/9505326].

[23] Y. Okada, M. Yamaguchi and T. Yanagida, Phys. Lett. B **262** (1991) 54.

[24] T. Elliott, S. F. King and P. L. White, Phys. Lett. B **305** (1993) 71 [arXiv:hep-ph/9302202].

[25] M. Carena, J. R. Espinosa, M. Quiros and C. E. Wagner, Phys. Lett. B **355** (1995) 209 [arXiv:hep-ph/9504316].

[26] M. Carena, M. Quiros and C. E. Wagner, Nucl. Phys. B **461** (1996) 407 [arXiv:hep-ph/9508343].

[27] S. Heinemeyer, W. Hollik and G. Weiglein, Phys. Lett. B **440** (1998) 296 [arXiv:hep-ph/9807423]; Phys. Rev. D **58** (1998) 091701 [arXiv:hep-ph/9803277]; Eur. Phys. J. C **9** (1999) 343 [arXiv:hep-ph/9812472]; Phys. Lett. B **455** (1999) 179 [arXiv:hep-ph/9903404].

[28] G. K. Yeghiyan, *Acta Physica Slovaka* **49** (1999) 823 [arXiv:hep-ph/9904488].

[29] K. Hagiwara *et al.* [Particle Data Group Collaboration], Phys. Rev. D **66** (2002) 010001.
http://pdg.lbl.gov/

[30] U. Ellwanger and C. Hugonie, Eur. Phys. J. C **25** (2002) 297 [arXiv:hep-ph/9909260].

[31] H. Georgi and A. Pais, Phys. Rev. D **10** (1974) 1246.

[32] A. Pomarol, Phys. Lett. B **287** (1992) 331 [arXiv:hep-ph/9205247].

[33] P.G. Harris *et al.*, Phys. Rev. Lett. **82** (1999), 904; S.K. Lamoreaux and R. Golub, Phys. Rev. **D61** (2000), 51301; E.D. Commins *et al.*, Phys. Rev. **A50** (1994), 2960; M.V. Romalis, W.C. Griffith, and E.N. Fortson, Phys. Rev. Lett. **86**, 2505 (2001); J.P. Jacobs *et al.*, Phys. Rev. Lett. **71** (1993), 3782.

[34] S. Abel, S. Khalil and O. Lebedev, Nucl. Phys. B **606** (2001) 151 [arXiv:hep-ph/0103320].

[35] G. C. Branco, F. Kruger, J. C. Romao and A. M. Teixeira, JHEP **0107** (2001) 027 [arXiv:hep-ph/0012318].

[36] A. M. Teixeira, G. C. Branco, F. Kruger and J. C. Romao, arXiv:hep-ph/0110350.

[37] A. M. Teixeira, arXiv:hep-ph/0209129.

[38] A. T. Davies, C. D. Froggatt and A. Usai, Phys. Lett. B **517** (2001) 375 [arXiv:hep-ph/0105266].

[39] C. D. Froggatt, R. G. Moorhouse and I. G. Knowles, Nucl. Phys. B **386** (1992) 63.

[40] S. A. Abel and B. C. Allanach, Phys. Lett. B **431**, 339 (1998) [arXiv:hep-ph/9803476].

[41] S. Codoban, M. Jurcisin and D. Kazakov, Phys. Lett. B **477** (2000) 223 [arXiv:hep-ph/9912504].

[42] M. Jurcisin and D. I. Kazakov, Mod. Phys. Lett. A **14** (1999) 671 [arXiv:hep-ph/9902290].

[43] S. P. Martin, M. T. Vaughn, Phys.Rev. **D50** (1994) 2282.

[44] C. T. Hill, C. N. Leung and S. Rao, Nucl. Phys. B **262** (1985) 517.

[45] R. B. Nevzorov and M. A. Trusov, Phys. Atom. Nucl. **64** (2001) 1299 [Yad. Fiz. **64** (2001) 1375] [arXiv:hep-ph/0110363].

[46] M. Bastero-Gil, C. Hugonie, S. F. King, D. P. Roy and S. Vempati, Phys. Lett. B **489** (2000) 359 [arXiv:hep-ph/0006198].

[47] R. B. Nevzorov and M. A. Trusov, J. Exp. Theor. Phys. **91** (2000) 1079 [Zh. Eksp. Teor. Fiz. **91** (2000) 1251] [arXiv:hep-ph/0106351].

[48] J.-P. Derendinger, C.A. Savoy, Nucl. Phys. **B237** (1984) 307.

[49] J. A. Casas, J. R. Espinosa and H. E. Haber, Nucl. Phys. B **526** (1998) 3 [arXiv:hep-ph/9801365].

[50] G. K. Yeghian, M. Jurcisin and D. I. Kazakov, Mod. Phys. Lett. A **14** (1999) 601 [arXiv:hep-ph/9807411].

[51] V. D. Barger, M. S. Berger and P. Ohmann, Phys. Rev. D **49** (1994) 4908 [arXiv:hep-ph/9311269].

[52] M. Carena, M. Olechowski, S. Pokorski and C. E. Wagner, Nucl. Phys. B **426** (1994) 269 [arXiv:hep-ph/9402253].

[53] R. B. Nevzorov and M. A. Trusov, Phys. Atom. Nucl. **64** (2001) 1513 [Yad. Fiz. **64** (2001) 1589] [arXiv:hep-ph/0112301].